# METHODS FOR STRENGTHENING REINFORCED CONCRETE BRIDGE GIRDERS CONTAINING POORLY DETAILED FLEXURAL STEEL USING NEAR-SURFACE MOUNTED METALLICS

## Final Report

**SPR 750**

# METHODS FOR STRENGTHENING REINFORCED CONCRETE BRIDGE GIRDERS CONTAINING POORLY DETAILED FLEXURAL STEEL USING NEAR-SURFACE MOUNTED METALLICS

## Final Report

### SPR 750

by
Christopher Higgins, PhD, P.E.
Deanna Amneus, and Laura Barker
School of Civil and construction Engineering
Oregon State University
Corvallis OR 97331

for

Oregon Department of Transportation
Research Section
555 13th Street NE, Suite 1
Salem OR 97301

and

Federal Highway Administration
400 Seventh Street, SW
Washington, DC 20590-0003

**August 2015**

Technical Report Documentation Page

| | | |
|---|---|---|
| 1. Report No.<br>FHWA-OR-RD-16-02 | 2. Government Accession No. | 3. Recipient's Catalog No. |
| 4. Title and Subtitle<br>Methods for Strengthening Reinforced Concrete Bridge Girders Containing Poorly Detailed Flexural Steel Using Near-Surface Mounted Metallics | | 5. Report Date<br>-August - 2015-<br>6. Performing Organization Code |
| 7. Author(s)<br>Christopher Higgins, PhD, P.E.; Deanna Amneus, Laura Barker | | 8. Performing Organization Report No. |
| 9. Performing Organization Name and Address<br>School of civil and Construction Engineering<br>Oregon State University<br>Corvallis OR 97331 | | 10. Work Unit No. (TRAIS)<br>11. Contract or Grant No.<br>SPR 750 |
| 12. Sponsoring Agency Name and Address<br>Oregon Dept. of Transportation<br>Research Section and Federal Highway Admin.<br>555 13th Street NE, Suite 1 400 Seventh Street, SW<br>Salem, OR 97301 Washington, DC 20590-0003 | | 13. Type of Report and Period Covered<br>Final Report<br>14. Sponsoring Agency Code |
| 15. Supplementary Notes | | |

16. Abstract

Many older reinforced concrete deck girder (RCDG) bridges contain straight-bar terminations of flexural reinforcement in flexural tension zones without special detailing. Common bridge design practice of the 1950s did not consider the additional demands on the terminated bars from shear and flexure. Moreover, application of modern design code provisions and use of heavier trucks contribute to insufficient bridge load ratings when evaluating flexural anchorages in existing RCDG bridges. Replacement of bridges with poor ratings due to localized deficiencies is not economically feasible and thus strengthening methods are necessary.

The goal of this research was to investigate methods for strengthening deficient flexural steel anchorages using supplemental surface bonded metallic reinforcing bars. Full-scale reinforced concrete girder specimens with typical vintage details and materials were used as test specimens. The specimens were constructed with flexural anchorage deficiencies by terminating some of the embedded flexural bars past a 45° preformed diagonal crack. The terminated bars had only one-third of the code-prescribed development length past the diagonal crack.

A strengthening technique called near-surface mounting (NSM) was applied to the specimens. Two metallic materials were selected for the NSM reinforcement: titanium and stainless steel. These materials were chosen because of their high strength, ductility, environmental durability, and ability to form mechanical hooks at the ends of the bars. This study found that the NSM strengthening technique with metallic materials increased the deformation and load capacity of all specimens. In addition, a case study was performed to demonstrate the flexural strengthening for the Mosier Bridge overcrossing of I84 in Oregon. The case study demonstrated that the techniques and materials applied to the girder were able to achieve the required strength and provided good deformation capacity.

| | | | |
|---|---|---|---|
| 17. Key Words | 18. Distribution Statement<br>Copies available from NTIS, and online at http://www.oregon.gov/ODOT/TD/TP_RES/ | | |
| 19. Security Classification (of this report)<br>Unclassified | 20. Security Classification (of this page)<br>Unclassified | 21. No. of Pages<br>274 | 22. Price |

# SI* (MODERN METRIC) CONVERSION FACTORS

## APPROXIMATE CONVERSIONS TO SI UNITS

| Symbol | When You Know | Multiply By | To Find | Symbol |
|---|---|---|---|---|
| | | **LENGTH** | | |
| in | inches | 25.4 | millimeters | mm |
| ft | feet | 0.305 | meters | m |
| yd | yards | 0.914 | meters | m |
| mi | miles | 1.61 | kilometers | km |
| | | **AREA** | | |
| $in^2$ | square inches | 645.2 | millimeters squared | $mm^2$ |
| $ft^2$ | square feet | 0.093 | meters squared | $m^2$ |
| $yd^2$ | square yards | 0.836 | meters squared | $m^2$ |
| ac | acres | 0.405 | hectares | ha |
| $mi^2$ | square miles | 2.59 | kilometers squared | $km^2$ |
| | | **VOLUME** | | |
| fl oz | fluid ounces | 29.57 | milliliters | ml |
| gal | gallons | 3.785 | liters | L |
| $ft^3$ | cubic feet | 0.028 | meters cubed | $m^3$ |
| $yd^3$ | cubic yards | 0.765 | meters cubed | $m^3$ |
| NOTE: Volumes greater than 1000 L shall be shown in $m^3$. | | | | |
| | | **MASS** | | |
| oz | ounces | 28.35 | grams | g |
| lb | pounds | 0.454 | kilograms | kg |
| T | short tons (2000 lb) | 0.907 | megagrams | Mg |
| | | **TEMPERATURE (exact)** | | |
| °F | Fahrenheit | (F-32)/1.8 | Celsius | °C |

## APPROXIMATE CONVERSIONS FROM SI UNITS

| Symbol | When You Know | Multiply By | To Find | Symbol |
|---|---|---|---|---|
| | | **LENGTH** | | |
| mm | millimeters | 0.039 | inches | in |
| m | meters | 3.28 | feet | ft |
| m | meters | 1.09 | yards | yd |
| km | kilometers | 0.621 | miles | mi |
| | | **AREA** | | |
| $mm^2$ | millimeters squared | 0.0016 | square inches | $in^2$ |
| $m^2$ | meters squared | 10.764 | square feet | $ft^2$ |
| $m^2$ | meters squared | 1.196 | square yards | $yd^2$ |
| ha | hectares | 2.47 | acres | ac |
| $km^2$ | kilometers squared | 0.386 | square miles | $mi^2$ |
| | | **VOLUME** | | |
| ml | milliliters | 0.034 | fluid ounces | fl oz |
| L | liters | 0.264 | gallons | gal |
| $m^3$ | meters cubed | 35.315 | cubic feet | $ft^3$ |
| $m^3$ | meters cubed | 1.308 | cubic yards | $yd^3$ |
| | | **MASS** | | |
| g | grams | 0.035 | ounces | oz |
| kg | kilograms | 2.205 | pounds | lb |
| Mg | megagrams | 1.102 | short tons (2000 lb) | T |
| | | **TEMPERATURE (exact)** | | |
| °C | Celsius | 1.8C+32 | Fahrenheit | °F |

*SI is the symbol for the International System of Measurement

## ACKNOWLEDGEMENTS

The authors would like to thank the Oregon Department of Transportation (ODOT) for providing funding for this research. The support of Mr. Steven Soltesz, Dr. Tanarat Potisuk, and Mr. Norris Shippen of ODOT are gratefully acknowledged. The authors also thank Perryman Company, of California, PA for providing titanium materials and technical support. The technical and logistical support of Mr. Warren George of the Perryman Company was particularly helpful. Undergraduate research assistants Messrs. Kyle England, Brandon Zaikoski, and Caleb Lennon contributed significantly to the laboratory studies and their help is gratefully acknowledged.

## DISCLAIMER

# TABLE OF CONTENTS

## LIST OF TABLES

# LIST OF FIGURES

# LIST OF ACRONYMS

The following list of acronyms is used throughout this report.

AASHO - American Association of State Highway Officials
AASHTO - American Association of State Highway and Transportation Officials
ACI - American Concrete Institute
ASD - Allowable Stress Design
ASTM - American Society for Testing Materials (ASTM International)
CFPR – carbon-fiber reinforced polymer
FHWA - Federal Highway Administration
FRP - fiber reinforced polymer
GFRP – glass-fiber reinforced polymer
IT - Inverted T girder
LRFD – Load and Resistance Factor Design
MBE - Manual for Bridge Evaluation
NSM - near surface mount
ODOT - Oregon Department of Transportation
RCDG -reinforced concrete deck girder
R2K - Response 2000
T-T girder

# 1.0 INTRODUCTION

The expansion of the interstate highway system in the 1950s produced large numbers of short and medium span bridges with reinforced concrete deck girders (RCDG). At the same time, the advent of standardized deformed steel reinforcing bars with ASTM A-50 (*ASTM 1950*) enabled changes to American Concrete Institute (ACI) and American Association of State Highway Officials (AASHO) design specifications that dramatically changed detailing practice for flexural steel terminations. Flexural reinforcing bar terminations were permitted where steel was no longer required by calculation. The new standardized reinforcing bars were thought to provide sufficient anchorage without the need for bends or hooks. Thus the design practice employed straight-bar terminations in flexural tension regions whereas previously bends and hooks would be required. In addition, the design provisions of the time allowed higher shear stresses in the concrete than what would be permissible in modern standards, resulting in insufficient transverse reinforcing steel in the present day. Lastly, the design provisions did not recognize the additional demands in the flexural reinforcing steel from the combination of shear and flexure.

Heavier trucks and higher traffic volume on roadways today have greatly increased the service loading on these bridges. Many of these bridges exhibit diagonal cracking due to combinations of shrinkage and thermal strains, live loading, and poor detailing practices. Diagonal cracks are commonly found at locations along the span where flexural reinforcing steel terminates and are a source of concern for owners and bridge engineers. Diagonal cracking near the termination of flexural bars increase the tensile demand in the developing reinforcing steel bars. If the anchorages of the cutoff bars fail, the remaining reinforcing steel bars may not be sufficient to carry the applied loads and the member could fail.

Current load ratings of these older RCDG bridges can be controlled by the flexural anchorage deficiencies along the girders. Some RCDG bridges could have posted load limits that are controlled by the poorly detailed flexural anchorages. The ratings can be significantly reduced when the influence of shear is considered, as required by the AASHTO MBE *(AASHTO MBE 2011)*. To eliminate the need and costs required to post or replace deficient bridges, strengthening methods are necessary.

Over the last ten years, Oregon State University has conducted a large number of experimental tests on full-scale vintage RCDG bridge girder details (*Higgins et al. 2004*). These realistic girder specimens were constructed, instrumented, and tested to failure. The specimens were 26 ft (7.9 m) long beams with a 14 in. by 42 in. (356 mm x 1069 mm) stem and a 36 in. by 6 in. (914 mm x 152 mm) integral deck. Both T and Inverted-T (IT) specimens were tested, focusing on the positive and negative moment regions, respectively. The design concrete strength, concrete mixture, and transverse steel used were representative of that used in the 1950's. Some of the specimens contained straight bar terminations crossing a preformed diagonal crack in the flexural tension region combined with shear. Instrumentation focused on stresses along the reinforcement surrounding the crack and along the development length of the cutoff bars. This past research has

helped to quantify the behavior of poorly detailed flexural anchorages and demonstrated the member strength can be controlled by the anchorage failure.

The present research reported here was conducted to develop methods to strengthen RCDGs with deficient flexural anchorages. An innovative strengthening technique was developed using near-surface mounted (NSM) metallic alloys. Stainless steel and titanium alloy bars were chosen due to their environmental durability, ductility, high strength, and ability to form mechanical anchorages at the ends of the bars. For all specimens, the NSM strengthening technique increased the baseline specimen capacity and demonstrated the ability to prevent or delay flexural anchorage failures. Supplemental tests of hook ductility and bond strength of the metallic bars were also conducted. In addition to the full-scale beam specimens, a case study was conducted to demonstrate the methods for the retrofit of the Mosier Bridge 07626A, which is an overcrossing of I84 in Oregon.

The research and case study determined that stainless steel and titanium are viable materials for strengthening flexurally deficient RCDGs. Titanium offered higher strength, and greater control of the material properties which allows more optimized design. Based on this research, bridge designers should be able to economically and effectively improve vintage RCDG bridge load ratings that are controlled by deficient flexural anchorages by deploying these retrofitting techniques. This NSM retrofitting technique with metallics could ultimately help to maintain and improve the operational safety and mobility of the transportation system.

This report is organized into two (2) parts. The main report contains the experimental and analytical results from prismatic T and IT specimens and the complementary investigations of bond, pull-out, and hook ductility. A full archive of the data from these studies is reported in Appendices A, B and C. Part II, is reported in Appendix D. This contains the experimental and analytical results on bridge girders representative of Mosier Bridge #07626A.

# 2.0 BACKGROUND

This chapter surveys the archival literature on anchorage and bond for steel reinforcing and fiber reinforced polymer (FRP) bars. First, a generalized bond stress equation was derived. Then, a review of the literature was performed that summarized the literature describing the behavior of steel reinforcing bars in concrete. Next, a review of NSM bars in epoxy has been summarized. Lastly, changes in design specifications are explained with correlations to the literature.

## 2.1 ANCHORAGE OF REINFORCING BARS

Adequate anchorage is essential to obtain the full strength of a reinforcing steel bar embedded in concrete. Bridge designers prior to the 1950s commonly detailed hooked bar terminations to ensure adequate anchorage on proprietary reinforcing steel bars. This practice ceased after experimental testing on standardized deformations on reinforcing bars indicated a greatly improved bond strength. However, designers and scholars have since found that straight bar terminations in the flexural tension zone can result in cracking and premature loss of anchorage. Evidence of these early terminations can be seen from web cracking in vintage RCDG bridges.

Originally, to attain adequate anchorage of reinforcing steel, designers limited bond stress. Bond stress, μ, is the stress transferred between the reinforcing bar and the concrete and must account for the change in tension along the bar as illustrated Figure 2.1.

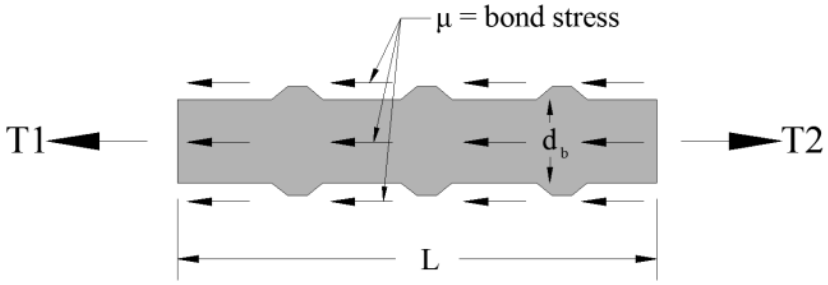


Figure 2.1: Bond stress in bar.

Bond stress is a function of the surface area and the length of bar embedded. Actual bond stress is variable over the length of the bar so $\mu$, is typically specified as $\mu_{avg}$. The bond stress of a bar is computed as:

$$\boldsymbol{\mu_{avg} = \frac{\Delta f_s d_b}{4L}} \qquad \textbf{(2.1)}$$

where $\Delta f_s$ is the change in stress over the segment, $d_b$ is the nominal bar diameter, and $L$ is the embedded length.

To design for bond stress in a full-scale beam, early literature depended on basic beam mechanics. The average bond stress in the flexural steel is found by dividing the applied shear by the area of steel multiplied by the lever arm as:

$$\mu_{avg} = \frac{V}{jd\Sigma o} \tag{2.2}$$

where $V$ is the applied shear, $jd$ is the effective distance from the centroids of the compression and tension zones, and $\Sigma o$ is the perimeter of the bar. This approach is reflected in early design specifications when detailing anchorages.

More modern research has found there are additional factors that exacerbate anchorage demands in flexural tension zones. The presence of a diagonal crack in a section with shear and flexure can place additional demands on the tension steel, as illustrated in Figure 2.2.

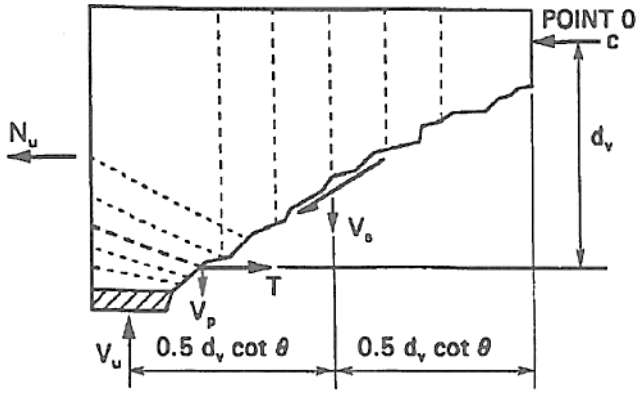


Figure 2.2: Internal forces at a diagonally cracked section *(AASHTO LRFD 2007)*.

If summed about Point 0, the tensile demand, $T$, is expressed as:

$$T = \frac{M_u}{d_v} + 0.5N_u + \left(V_u - 0.5V_s - V_p\right) * cot\theta \tag{2.3}$$

**2007 AASHTO Eq. 5.8.3.5-1**

where $M_u$ is the factored moment demand taken where the crack crosses the flexural steel, $d_v$ is the distance from the center of the compression block to the centroid of steel, $N_u$ is the applied factored axial force, $V_u$ is the applied factored shear demand, $V_s$ is the shear resistance provided by the transverse reinforcement, $V_p$ is the shear carried by the prestressing strands, and $\theta$ is the crack angle. For conventionally reinforced beams, $N_u$ and $V_p$ are not applicable. If a diagonal crack propagates in the region where the reinforcing steel bar is not fully developed, the additional demands could produce an anchorage failure.

Anchorage failures fall into two categories: slipping and splitting failures. Slipping anchorage failures usually occur if there is transverse reinforcement present to confine the flexural reinforcing steel and prevent concrete splitting. Once the bar initiates slip, the deformations of the bar engage and crush the concrete locally. The bar slowly slips through the concrete, creating a ductile response (*Triska 2010*). Splitting anchorage failure occurs when the reinforcing bar

deformations engage the concrete and create radial stresses. These stresses create cracks and split the surrounding concrete. This less ductile response commonly happens in the flanges with negative bending moment, or where there are not sufficient stirrups crossing the splitting plane (*Goodall 2010*).

## 2.2 LITERATURE REVIEW

A literature review was conducted to collect background information on anchorage of reinforcing bars embedded in concrete and epoxy. Relevant research on reinforced concrete bond and anchorage is available dating from the early 1950s to the present. However, the majority of near-surface mounted (NSM) fiber reinforced polymer (FRP) literature was written since 2000.

### 2.2.1 Steel Reinforcing Bar Bond Stress

Mylrea *(Mylrea 1948)* summarized the body of knowledge on bond stress and bar anchorage up to 1948. Generally, the pull-out test was accepted as the most common way to establish bond properties. Throughout the research, it was concluded that pull-out tests provide higher bond stresses than were apparent in a full-scale beam. It was established that bond stress is not uniformly distributed over the bar and increases non-linearly with movement of the bar. Furthermore, the highest bond stress achieved in beam tests is always the stress prior to the first slip. After initial concrete crushing or slipping, it is easier to propagate cracks and create more bar slip. Bond stress from plain bars in pull-out tests ranged from 200-400 psi (1.38-2.76 MPa).

Clark *(Clark 1949)* investigated the bond stresses in several proprietary bars in reinforced concrete. The study proposed and tested a larger deformation pattern on reinforcing steel. The experiment used scaled beam tests with varying embedment length, bar type, and depth. The beam end specimens were 8 x 8 x 78 in. (0.2 x 0.2 x 1.98 m) concrete prisms with various reinforcement lengths and depths. The beam specimens had a loading point directly over the termination of the bar cutoff. The specimens failed by bond slippage if the bar had a short embedment length, or by diagonal tension and bond failure with a longer embedment length. In general, the loaded end bars experienced larger slips at lower bond stresses; while the free ends experienced high bond stresses before any significant slipping. Clark reported a mean average bond stress of 300-400 psi (2.07-2.76 MPa) for #7 (22M) bars in the beam end test after slipping. The results confirmed that more deformed reinforcing bars created a stronger bond. Furthermore, the specimens with the newly proposed deformation pattern achieved the greatest bond stress, thus contributing to the adoption of ASTM A305-47T into ACI 318.

Mains *(Mains 1951)* measured the distribution of bond stresses along reinforcing bars using a method that would not affect bond between bars and concrete. The reinforcing bars of interest were cut at two sections and had strain gages placed inside a groove cut into the bar near the neutral axis. Several beam and pull-out specimens were tested with plain and deformed bars. Previous code requirements assumed even distribution of bond stress over the bar. Mains' new technique showed that measured bond stress was consistently higher than calculated bond stress. This demonstrated that the assumption of even bond stress distribution in the previous code requirements was inaccurate. A straight embedment of deformed bars in pull-out specimens attained 770 psi (5.31 MPa) at the highest test load. Beam specimens with deformed bar straight terminations achieved bond stresses ranging from 540-815 psi (3.72-5.62 MPa) at the highest test

loads. All bars in the beam tests failed by fracture rather than bond. Evidence was presented that cracking in the beam increased the local stresses along the reinforcing bars. When the beam specimen was subjected to combined shear and moment, the tensile forces in the bars exceeded the calculated tensile demand.

Ferguson and Breen *(Ferguson and Breen 1965)* considered lap splice length in a constant moment region. Tests were conducted on rectangular full scale beams with four bars of flexural reinforcement and no transverse reinforcement. A lap splice was embedded at length, *L*, at midspan under a constant moment region. Ferguson and Breen found that lap splices could be 5-6 in. (127-152 mm) apart and still be effective. Bond stress decreased as the splice length increased. The larger #11 (36M) bars had a greater bond stress than the #8 (25M) bars. The #11 (36M) bars had an average bond stress ranging from 350-475 psi (2.41-3.27 MPa) with increasing splice lengths. Specimens with stirrups increased the average bond stress to 560 psi (3.86 MPa). Other conclusions were that concrete strength did not significantly affect splitting failures, steel strains had little influence in bond strength in a splice, and the presence of transverse steel increased the lap splice strengths.

Orangun et al. *(Orangun et al. 1977)* reevaluated previous data on development length and splices. An equation for determining development length was proposed based on a nonlinear regression of previous beam tests. A bond stress formula was calculated using tangential forces from the longitudinal bond stress and radial forces from deformations on the bar. However, since the angle of the radial stress is difficult to quantify, an empirical method to determine development length was used. Based on previous data, the proposed development length equation reflects the length, cover, spacing, bar diameter, and transverse reinforcement.

$$l_d = \frac{10200 d_b}{\sqrt{f'_c}\left(1 + \frac{2.5C}{d_b} + K_{tr}\right)} \quad \textbf{(2.4)}$$

where $d_b$ is the bar diameter, $f'_c$ is the compressive strength of concrete in psi, $C$ is the lesser of the clear cover or half the clear spacing, and $K_{tr}$ is as follows:

$$K_{tr} = \frac{A_{tr} f_{yt}}{600 s d_b} \leq 2.5 \quad \textbf{(2.5)}$$

where $A_{tr}$ is the area of transverse reinforcement, $f_{yt}$ is the yield strength of stirrups, and $s$ is the stirrup spacing. All units are in English and $f'_c$ is in psi. This equation accounted for stress transfer between reinforcing bars in concrete. Furthermore, Orangun *et al.* concluded that for the same bar diameter, clear spacing, cover and concrete strength the values for development length and lap splice length were interchangeable. Furthermore, the new equation required an increase of anchorage length from 10-25% from current ACI 318-71 provisions (*Orangun et al. 1977*). However, the presence of transverse reinforcement may reduce the anchorage lengths.

Darwin *(Darwin 1996)* tested a large array of splice and development length specimens investigating the influence of transverse reinforcement, concrete strength, and rib area. Similar to previous studies, Darwin found that the development length and bond forces were linear, but not proportional. To accurately calculate bond, the number and size of transverse reinforcing bars present over the developing length should be used. Larger relative rib areas on steel may decrease development and splice lengths. It was also found that reducing the contribution from concrete strength would more accurately represent bond stress. Furthermore, variability in splice and development length design calculations implies that the code safety factors may need to be altered. The expression formulated for the steel reinforcing bar development length incorporated a reliability-based strength reduction factor:

$$\frac{\boldsymbol{l_d}}{\boldsymbol{d_b}} = \frac{\frac{\boldsymbol{f_y}}{\boldsymbol{f_c'^{1/4}}} - \mathbf{1900}}{\mathbf{72}\left(\frac{\boldsymbol{c + K_{tr}}}{\boldsymbol{d_b}}\right)} \tag{2.6}$$

where the variables are defined previously. This equation is a simplification of the proposed detailed design equation. A $\phi$ factor of 0.9 is incorporated as well as simplifying a cover ratio to 1.

McLean and Smith *(McLean and Smith 1997)* investigated non-contact lap splices in panels and column shaft connections. Two dimensional and three dimensional models were used to predict behavior of the specimens respectively. Experimental tests were done on near full-scale panel specimens and on 1/4-scale column-shaft specimens under monotonic and cyclic loading. The offset splice spacing in the panels ranged from 6-15 in. (152-381 mm). Three preliminary specimens did not have transverse reinforcement. A discrepancy in the relation of bond stresses and non-contact lap splices arose from using either an effective lap length or an overall lap length. The proposed overall splice length is composed of the effective length plus the length added from the bar spacing and crack angle. All the preliminary specimens without transverse reinforcement failed as a result of tension cracking of the concrete perpendicular to the spliced bars. The failure loads were only 40-60% of the bar yielding force. The greater the offset spacing, the greater the amount and extent of cracking occurred in the tests. A strut and tie methodology could be used for design: the transverse reinforcement acts as a tie and the concrete compression strut acts between diagonal cracks between bars. After testing, McLean and Smith recommended longer embedment length and less conservative splice length if splicing two different bars.

Darwin *(Darwin 2005)* surveyed current design provisions and compared experimental data to calculated results. Because of high variability in bond stress, Darwin suggested that an adequate splice length be recommended instead of a maximum bond stress. Furthermore, yielding of the steel reinforcing bar did not significantly affect bond strength. Darwin confirmed bond strength is a function of several factors: the development length, the side and bottom cover, spacing of the reinforcing bar, transverse reinforcement, the top bar factor, the bar surface condition, and the concrete strength. Development and splice length were compared in the following codes: AASHTO, ACI 318, ACI Committee 408, CEB-FIB Model Code 1990, and Eurocode 2. Of those codes, Darwin found that ACI 408 provided the best match with test results for both

developed and spliced bars. The ACI 408 equation for development length was derived from work by Zuo and Darwin *(Zuo and Darwin 1998)* as:

$$l_d = \frac{\left(\frac{f_y}{f'^{1/4}_c} - 48\omega\right)\alpha\beta\lambda}{1.5\left(\frac{c\omega + K_{tr}}{d_b}\right)} d_b \quad \textbf{(2.7)}$$

where $c=c_{min}+0.5d_b$, $\omega=0.1(c_{max}/c_{min})+0.9\leq 1.25$, $c_{max}$ and $c_{min}$ are the maximum and minimum of $c_b$ (the bottom cover) and $c_s$ (the side cover). $\alpha$, $\beta$, and $\lambda$ are terms for excess reinforcement.

Triska (*2010*) constructed and tested four full scale vintage T beam specimens. The specimens reflected previous work simulating vintage RCDG details performed by Higgins *et al.* (*2004*). The typical specimen was 26 ft (7.92 m) long, with a 14 x 42 in. (356 x 1067 mm) web, and a 6 x 36 in. (152 x 914 mm) deck. Vintage concrete mixtures with strengths around 3300 psi (22.75 MPa) were used. Lower-strength shear reinforcing bars were used to simulate in-situ bridge strength. The specimens had three or four #11 (36M) bars with a built-in anchorage deficiency. Two flexural steel reinforcing bars were terminated one-third of the specified development length past a preformed diagonal crack to simulate an anchorage deficiency. The angle of the preformed diagonal crack varied from 0, 45, and 60 degrees. Reinforcing bar strain and cutoff bar slip was monitored to verify the design and analysis. All specimens failed in shear-tension due to anchorage slip of the cutoff bar. Stirrups confined the cutoff bar and created a ductile slipping anchorage failure. The average cutoff bar bond stress was 851 psi (5.87 MPa). Average bond stress for the anchored bars was 284 psi (1.96 MPa). All bond stress values were measured from the intersection of the preformed crack to the end of the cutoff bar. Triska determined that the AASHTO LRFD specifications for tensile demand are adequate at failure. The preformed diagonal crack did not dictate the failure crack and may not significantly weaken the structure at service loads. Lastly, chevron cracks were found to propagate along the cutoff bar close to failure.

Similarly, Goodall *(Goodall 2010)* investigated the influence of diagonal cracks on the flexural anchorage performance in negative moment regions of full-size RCDG specimens. Similar to previous specimens constructed by Higgins et al. *(Higgins et al. 2004)*, the specimens were 26 ft (7.92 m) long with a 14 x 42 in. (356 x 1067 mm) web, and a 6 x 36 in. (152 x 914 mm) deck. Goodall tested four RCDG IT-beam specimens containing diagonal cracks that interacted with the cutoffs of flexural steel reinforcing bars. Specimens were designed to replicate vintage RCDG members. To do this, concrete mixtures were used with target strengths of 3300 psi (22.8 MPa) and Grade 40 (Grade 280) stirrups were used. The specimens were constructed with a preformed diagonal crack at an angle of 45º or 60º to prevent aggregate interlock and had either five or six Grade 60 (Grade 420) flexural reinforcing bars. The specimens were constructed with bars cutoff before they were fully developed. The cutoff bars extended approximately one-half of the minimum development length, determined by ACI 318-08, past where they intersected with the preformed crack. The tests had bond stresses in the developed bars that exceeded the amount predicted by current specifications, therefore a more accurate estimate of bond stress is necessary. Specimen behavior at failure was found to be independent of the initial diagonal preformed crack.

Various bond stresses reported in the literature are shown in Table 2.1.

**Figure 2.3: Summary of bond stress in steel reinforcing bars from literature.**

| Author | Bar Type | Bar Diameter (in) [mm] | Bar Embedment (in) [mm] | Test Type | Average Bond Stress (psi) [MPa] |
|---|---|---|---|---|---|
| *Mylrea (1948)* | Plain Bar | 1.00 [25.4] | 10 [254] | Pull-out | 400 [2.76] |
| *Clark (1949)* | Deformed Proprietary | 0.875 [22.2] | 8 – 16 [203-406] | Beam End | 300 – 400 [2.07-2.76] |
| *Mains (1951)* | Deformed | 0.875 [22.2] | 21 [533] | Pull-out | 770 [5.31] |
| | Deformed | 0.875 [22.2] | 78 [1981] | Beam | 540 – 815 [3.72-5.62] |
| *Ferguson and Breen (1965)* | Deformed | 1.41 [35.8] | Fully Anchored | Beam | 560 [3.86] |
| | Deformed | 1.41 [35.8] | 30 – 80 [762-2032] | Beam | 350 - 475 [2.41-3.27] |
| *Triska (2010)* | Deformed | 1.41 [35.8] | Fully Anchored | T Beam | 284 [1.96] |
| | Deformed | 1.41 [35.8] | Cutoff 1/3 ld | T Beam | 851 [5.87] |

## 2.2.2 Near-surface Mounting Technique

The near-surface mounting technique (NSM )of retrofitting has emerged as a potential solution for strengthening infrastructure in the past three decades. A literature review was conducted to briefly identify trends in testing, analysis, and design. The purpose, testing methodology, and conclusions are summarized. Specific data are listed if the literature included relevant bond stress or load deformation responses. The development of code specifications can be seen in the gradual presentation of analytical methods. Articles commonly focused on carbon-fiber reinforced polymer (CFRP) reinforcement and short bond lengths.

Rizkalla et al. *(Rizkalla et al. 2003)* wrote an overview of the history, properties, and use of FRP in strengthening concrete structures. FRP emerged in the mid-1950s but did not become a commercially recognized material until the late 1970s. Mechanical properties are dependent on the resin modulus, failure strain in the fiber, and the bond between the resin and fiber. Currently, ASTM D3039-08 (ASTM 2008) is used for tensile testing of polymer matrix composite

materials. In many cases, serviceability criteria, fatigue, and creep rupture endurance limits may control the design because of its linear elastic behavior and tendency for sudden failures. Specifically, near-surface mounted FRP systems can strengthen regions where external reinforcement would be subject to damage. In addition, the NSM rods have shown a greater anchoring capacity compared to the surface bonded FRP. Failure modes of NSM strips include epoxy split failure (can be avoided with increasing epoxy thickness), or concrete split failure where the tensile strength of the epoxy exceeds the concrete (widening the groove can minimize the induced tensile stresses).

DeLorenzis et al. *(DeLorenzis et al. 2000)* discussed the advantages and bond strength of NSM FRP strengthening in concrete. Direct pull-out and a beam pull-out tests were used to measure bond stress in the FRP material. The experimental variables included the bonded length, diameter of rod, type of material (glass fiber reinforced polymer (GRFP) or CFRP), surface configuration, and size of groove. In general, deformed CFRP bars appeared to be more efficient and achieved higher bond strengths. Furthermore, increasing the groove size led to higher bond strength and decreased the failure by splitting of the epoxy cover. Ultimate load increased with an increased embedded length; however, the average bond strength was decreased as the bonded length increased, similar to reinforcing bar concrete bond stress behavior. A #4 (13M) CFRP bar embedded 6 in. (152.4 mm) had an average bond strength of 1078 psi (7.43 MPa). With a 12 in. (304.8 mm) embedment, the #4 (13M) CFRP bar had an average bond strength of 620 psi (4.27 MPa). Several large scale T-specimens were cast and retrofit with FRP. The specimens had two # 7 (22M) bars as flexural reinforcement and were tested with four point bending. The NSM retrofit consisted of two #4 (13M) CFRP bars and increased the capacity of the baseline specimen by 44.3%. The baseline specimen had a capacity of 35.2 kips (157 kN) with a deflection of approximately 1.6 in. (40.6 mm). The strengthened specimen had a capacity of 50.79 kips (226 kN) with a deflection of approximately 1.1 in. (27.9 mm). The retrofitted beam had a much stiffer load displacement response and decreased the ductility from the control specimen.

After prior studies, DeLorenzis and Nanni *(DeLorenzis and Nanni 2001)* discussed a design procedure for flexural and shear strengthening of reinforced concrete beams with NSM FRP reinforcement. The proposed design procedure for flexure consisted of obtaining the local bond strength of NSM bars from literature or bond tests, $u_f$, computing the minimum stabilized crack spacing, $l_{min}$, computing the delamination stress, $\sigma_{fdelmax}$, computing the nominal ultimate moment using conventional reinforced concrete theory, and finally computing the design ultimate moment by applying reduction factors. A critical component in this design is the delamination stress where $\sigma_{fdel}$ is equal to:

$$\boldsymbol{\sigma_{fdel} = \frac{2bL_p l}{3n\pi d_b^2 h'} f_{ct}} \qquad \textbf{(2.8)}$$

where $b$ is the width of the beam, $L_p$ is the effective length of the NSM bars in the shear span, $l$ is the crack spacing, $n$ is the number of NSM bars, $d_b$ is the bar diameter, $h'$ is the distance from the top of the section to the centroid of NSM, and $f_{ct}$ is the concrete tensile strength. This equation would govern the available tensile stress for strengthening. However, this equation was not incorporated into the code, and a different empirical equation for delamination strain was used.

De Lorenzis also proposed a development length equation calculated based on minimum crack distances in the concrete, $l_{min}$. The minimum crack distance is based on the area of concrete in tension, the concrete tensile strength, and bond strength between the concrete-reinforcing bar interface and the NSM bar-epoxy interface. This method is similar to techniques described by McLean and Smith *(McLean and Smith 1997)* for bars in concrete but was not adopted into the ACI 440 specifications.

De Lorenzis *(DeLorenzis 2002)* investigated modified pull-out or bond tests for NSM FRP rods. Failure modes of the pull-out tests are often governed by the distance from the concrete edge and the short bonded length. Since these behaviors may not occur in full-scale specimens, a modified approach was necessary. The test specimens were "C" shaped concrete blocks with a pre-formed groove for the FRP. The variables tested were the groove filling material, groove size, and rod surface (sandblasted, spirally wound, and ribbed). The epoxy-concrete was the critical interface. A #4 (13M) spirally wound CFRP bar embedded in epoxy a length of four times the bar diameter had an average bond strength of 1637 psi (11.29 MPa). The average bond strength at the epoxy-concrete interface $\tau_{av1u}$ was expressed as:

$$\boldsymbol{\tau_{av1u} = \frac{P_{max}}{3 d_g l_b}} \qquad \textbf{(2.9)}$$

where $P_{max}$ is the ultimate load, $d_g$ is the groove size, and $l_b$ is the bonded length. De Lorenzis used Equation (2.9), obtained peak stresses, and used a Bertero-Popov-Eligehausen (BPE) relationship to fit the experimental data. From this, De Lorenzis determined a generalized bond stress relationship between concrete-epoxy and epoxy-bar interfaces. However, this method must be calibrated using experimental results before being used to develop the required embedment length. Other conclusions recommended saw cutting of grooves, and observing that the average bond stress decreases as the groove size and embedment length increases.

Hassan *(Hassan 2003)* conducted an experimental study of the bond of NSM FRP strips. Small scale T-specimens were constructed and designed to fail in flexure. Each beam was strengthened with one 0.05 x 1.97 in. (1.2 x 50 mm) strip of CFRP that extended varying lengths from 5.9 in. to 47.2 in. (150 mm to 1,200 mm) on each side of midspan. The specimens were tested with 3 point loading. A significant strength increase was associated with embedment lengths over 5.9 in. (150 mm). However, debonding was prevalent until the embedment lengths reached 33.5 in. (850mm). This indicated the full composite action was not developed due to anchorage concerns. The control specimen had a capacity of 11.7 kip (52 kN) and a deflection of approximately 2.56 in. (65 mm). The shortest fully composite beam used a 33.5 in. (850 mm) development length and reached a load of 17.6 kip (79 kN) with approximately 1.1 in. (28 mm) of deflection. The NSM retrofit response was much stiffer and increased the baseline capacity by 52% but decreased the deformation capacity by 57%. Furthermore, Hassan found that the load required to debond the NSM FRM material generally increased with embedment length, concrete strength, and groove width. Lastly, greater internal reinforcing steel ratios increased the required development length by shifting the neutral axis and increased the load required to debond the NSM FRP.

DeLorenzis *(DeLorenzis 2004)* continued research on developing an anchorage length for NSM FRP based on analytical modeling. An analytical model was calibrated to experimental results and used to compute the bond failure load as a function of the anchorage length. Primarily, short bond lengths were used. The service level anchorage length was determined by $l_m$, the embedment length at which the bar does not slip. This equation was described in previous work by DeLorenzis *(DeLorenzis 2002)* and calculated as:

$$\boldsymbol{l_m = \sqrt{\frac{2 * s_m}{\chi * \tau_m} * \frac{(1+\alpha)}{(1-\alpha)^2}}} \quad \textbf{(2.10)}$$

where $\alpha$ is the parameter influencing the shape of the ascending branch of the bond slip curve and is calculated by the area under curve until the peak bond stress, $\tau_m$. $s_m$ is the slip at peak bond stress. The cross section parameter, $\chi$, is calculated for the rod–epoxy interface and epoxy-concrete respectively as:

$$\boldsymbol{\chi = \frac{4}{E_b * d_b} \quad or \quad \chi = \frac{3 d_g}{E_e * A_{om}}} \quad \textbf{(2.11)}$$

where $E_b$ and $E_e$ are the elastic moduli of bar and groove filler respectively. $A_{om}$ is the cross-sectional area of the groove-filling constituents, and $d_b$ and $d_g$ are the diameter of the bar and depth of the square groove. Using this analytical approach, the experimental results agreed with the predicted development length and maximum load.

Novidis *(Novidis 2008)* summarized the results of 45 short-anchorage eccentric pull-out concrete specimens with NSM FRP. The study investigated the size and surface roughness of the groove, the embedment length, the surface finish of the bars, and isolated the pull-out section with vertical foam sheets. The foam sheet pull-out specimen, called the novel specimen, avoided axial compression in the concrete surrounding the bar. The anchorage lengths ranged from 3, 4, and 10 bar diameters from the top of the block. A 0.47 in. (12 mm) diameter CFRP bar was embedded 10 bar diameters and failed at the concrete epoxy interface achieving a bond strength of 654 psi (4.51 MPa). In general, the capacity increased with the length of embedment, but the bond stress decreases after a critical value. The bar stiffness and deformation pattern played a significant role in determining the amount of bond that may be mobilized in the NSM setup. The bond strengths are compared with others in the literature in Table 2.2.

Bournas and Triantafillou (Bournas and Triantafillou 2009) presented results of a large scale program focusing on the flexural strengthening of columns with several NSM techniques and materials. Although this study was focused on columns, a majority of the experimental results could be applicable to beams. The specimens were strengthened with CFRP strips, GFRP bars, and stainless steel bars. Specimens with less internal (or existing) steel reinforcement experienced larger strength increases with the application of the NSM CFRP material. The addition of CFRP strips to a constant internal reinforcing steel ratio also almost linearly increased the strength of the column. The NSM reinforcement selection was based on equal tensile strength. The stainless steel NSM strengthened column was significantly stiffer than the other NSM strengthened columns. All specimens failed in flexure, as per design calculations.

Buckling of the longitudinal reinforcing steel bars always occurred immediately after the failure of the NSM reinforcement. Load cycling may indicate a detrimental effect on the tensile strength of CFRP. Partial debonding reduced the lateral restraint of the NSM materials and made the NSM materials more vulnerable to compressive stresses. Overall, strengthening with the stainless steel NSM bars resulted in a substantial increase in stiffness and dissipated energy. In this application, stainless steel and GFRP outperformed CFRP by 25%. An average bond stress along the bonded length was found for most specimens. The specimen with CFRP strips had an average bond stress of 590 psi (4.07 MPa), while the stainless steel NSM had an average bond stress of 873 psi (6.02 MPa) along the instrumented length.

Al-Mahmoud et al. *(Al-Mahmoud et al. 2009)* considered the global behavior of several reinforced concrete beam specimens with CFRP NSM retrofitting techniques. The experimental variables included the concrete strength, embedment length, bond materials, and CFRP diameter. The specimens were 118 in. (3 m) long beam with a 59 x 110 in. (150 x 280 cm) cross section. They were retrofit with one or two CFRP rods. The specimen was tested with a monotonic increasing four point load. The control specimen had two 0.47 in. (12 mm) diameter steel reinforcing bars as flexural reinforcement. The moment capacity of the control specimen was approximately 19.9 kip-ft (27 kN-m), with 2.36 in. (60 mm) of deflection. The specimen retrofitted with one 0.47 in. (12 mm) diameter CFRP bar with 4.4 ksi (30 MPa) concrete strength demonstrated a 126% increase in capacity. The strengthened specimen achieved an ultimate capacity of 48.2 kip-ft (65.4 kN-m) with 1.73 in. (44 mm) of deflection. The CFRP diameter greatly influenced the strength and stiffness of the beam. The specimens with one 0.47 in. (12 mm) diameter bar (instead of two bars) increased the stiffness of the beam which encouraged the displacement of the reinforcing steel yielding threshold. The ultimate loads of the specimens with the 0.47 in. (12 mm) diameter NSM CFRP bar were higher than those with the 0.24 in. (6 mm) specimen with a similar failure mechanism. Furthermore, Al-Mahmoud concluded that concrete strength does not influence the load-carrying capacity of the strengthened beam when failure occurs by the NSM system failure. Figure 2.3 shows the capacity and ductility of the specimens strengthened with CFRP rods.

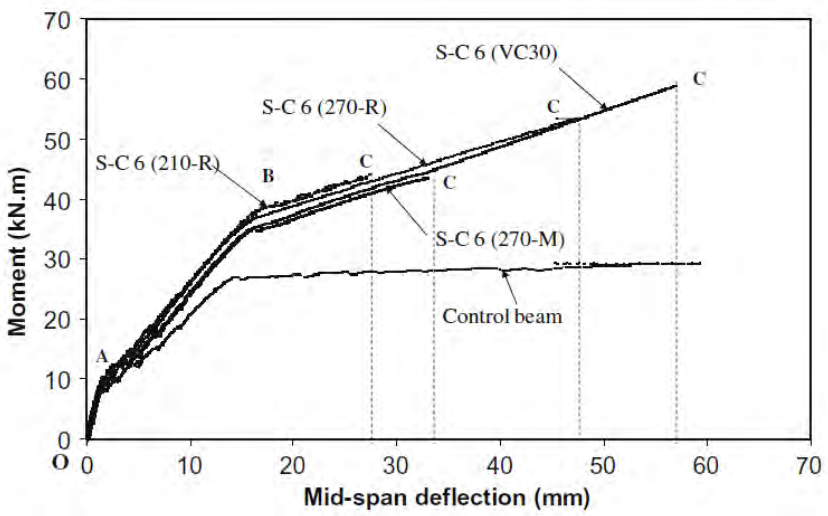


Figure 2.4: Midspan moment and deflection for CFRP strengthened specimen (*Al-Mahmoud et al. 2009*).

Al-Mahmoud et al. *(Al-Mahmoud et al. 2010)* investigated the anchorage and tension-stiffening effect between NSM CFRP and concrete. A pull-out test and direct tension member test was performed with varying concrete strengths, groove dimensions, and bond materials. The pull-out and tension member specimens were concrete blocks with dimensions of 19.7 in. (500 mm) in length with a 3.93 x 3.93 in. (100 x 100 mm) cross section. Both specimens used a 0.47 in. (12 mm) diameter sand coated CFRP rod embedded 2.36 in. (60 mm). The pull-out specimen was contained in a steel box to minimize loading eccentricity. These tests determined an optimal groove width to rod diameter ratio between 1.7- 2.5. The maximum load for the pull-out test with resin was 7.78 kip (34.6 kN). The direct tension test embedded the NSM CFRP fully along the length and applied a load at each end. This test found that the active bond length was less than 3.93 in. (100 mm) (before the first gage) because the strains at each location were equal until cracking.

**Figure 2.5: Reported NSM bond stresses in literature.**

| Author | Bar Type | Bar Diameter (in.) [mm] | Bar Embedment (in.) [mm] | Test Type | Average Bond Stress (psi) [MPa] |
|---|---|---|---|---|---|
| *DeLorenzis (2000)* | CFRP | 0.5 [12.7] | 6 [152] | Pull-out | 1078 [7.43] |
| | CFRP | 0.5 [12.7] | 12 [305] | Pull-out | 620 [4.27] |
| *DeLorenzis (2002)* | CFRP (Spiral wound) | 0.5 [12.7] | 2 [50.8] | Modified Pull-out | 1637 [11.29] |
| *Novidis (2008)* | CFRP | 0.5 [12.7] | 4.7 [120] | Modified Pull-out | 654 [4.51] |
| *Bournas and Triantafillou (2009)* | CFRP (Strip) | 0.63 x 0.08 [16 x 2] | 2.75 [70.0]* | Column | 590 [4.07] |
| | Stainless Steel | 0.47 [12] | 2.75 [70.0]* | Column | 873 [6.02] |

*Length between strain gages, fully embedded along the column

## 2.3 DESIGN SPECIFICATION REVIEW

Over time, design codes and specifications have formed to influence bridge design. Research on reinforced concrete has improved the understanding of the of bond and stress behavior of reinforcing steel bars in concrete. This section reviews changes in AASHTO and ACI specifications regarding bond stress and development length for steel reinforcing bars and NSM bars. All equations shown use standard English units.

### 2.3.1 AASHO Allowable Stress Design

A compilation of standards and specifications for bridge design began in 1921 with the formation of the American Association of State Highway Officials. The first edition of the AASHO

standards was published in 1931. In the 1953 edition, several assumptions were used in reinforced concrete design. These assumptions included that concrete has negligible tensile strength and the bond between concrete and reinforcing steel bars remain intact within the working or service stress range. From 1953 through 1973, AASHO codes recommended using allowable stress design. That was, structures were designed to a specified stress limit chosen at service level loads. The 1953 edition provided typical reinforced concrete design equations assuming plane sections remain plane. The tensile unit stress in longitudinal reinforcement, $f_s$, is seen below:

$$f_s = \frac{M}{A_s jd} \qquad \textbf{1953 AASHO Sec. 3.7.3.b (2.12)}$$

where $M$ is the applied moment, $A_s$ is the area of steel, and $jd$ is the distance between the compression and tension resultants. From Eq. [2.12] above, bond stress per unit area $u$ is calculated below:

$$u = \frac{V}{Zojd} \qquad \textbf{1953 AASHTO Sec. 3.7.3.c (2.13)}$$

Equation (2.13) represents the stress on the surface between the steel reinforcing bar and concrete. $Zo$ is the sum of perimeters of bars in the area considered, $V$ is the total shear applied. The steel reinforcing bars should be detailed and extended in a manner to develop the tension in the straight steel reinforcing bar without exceeding the maximum working bond stress $u_{max}$:

$$u_{max} = 0.10 * f'_c \leq 350 \qquad \textbf{1953 AASHO Sec. 3.4.12 (2.14)}$$

where $f'_c$ is the compressive strength of concrete. Other anchorage requirements include extending a bar at least 15 diameters, but not less than 1/20 of the span length past where calculations indicate the bar is no longer needed in a simply supported beam.

The 1957 AASHO Specifications for Highway Bridges had similar bond requirements. It was assumed that there was no slip in service level conditions and had the same bar termination requirements. This version of the code also required new reinforcing bar standards such as ASTM A 305-53T *(ASTM 1953)*.

## 2.3.2 AASHO Load Factor Bridge Design Specifications

The 1973 AASHO specifications observed a shift in analysis and design of reinforced concrete bridges. The code was split to allowable stress design and load factor design. The calculated bond stress was equivalent to Equation (2.13) but had different stress limits. The allowable stress design specified a limit for working bond stress for a bottom size #3-#11 steel reinforcing bar as shown:

$$u_{max} = \frac{4.8\sqrt{f'_c}}{D} \leq 500 \qquad \textbf{1973 AASHO Sec. 1.5.1.D.1 (2.15)}$$

where $D$ is the diameter of the steel reinforcing bar and $f'_c$ is defined in the equation above. Anchorage requirements from the 1953 code were still applicable with some additions for beam end requirements. For example, in restrained or continuous beams, at least 1/4 of the positive moment reinforcement shall extend beyond the face of supports. Additionally, steel reinforcing bars were more likely to be Gr. 60 (Gr. 420) or Gr. 40 (Gr. 280) and conform to ASTM A 615-73. No formal development length equations were listed but the development bond stress was computed. The bond stress for a developing steel reinforcing bar was calculated as the bar forces divided by the perimeters of bars multiplied by the embedment length.

Load factor design required consideration for several limit states: strength, service, and fatigue. To design for strength, the concrete strain is limited at a maximum value of 0.003 (concrete crushing strain), and the stress in the reinforcing steel bars is set at yield. The 1973 AASHO specifications included an expanded section pertaining to the development of reinforcement. The AASHO load factor design code had more stringent requirements and states that reinforcement shall extend a distance equal to the effective depth $d$ of the member or 12 bar diameters, whichever is greater. Also, flexural reinforcement shall not be terminated in a tension zone and a development length equation was accepted. For #11 (36M) bars or smaller the development length can be taken as:

$$L_d = \frac{0.04 a_s f_y}{\sqrt{f'c}} > 0.0004 D f_y \qquad \textbf{1973 AASHO Sec. 1.5.29.E.1 (2.16)}$$

where $a_s$ is the individual area of the bar, $f_y$ is the yield strength, and all other variables are defined previously. After equating $L_d$, the value was multiplied by applicable modification factors to obtain the required development length.

### 2.3.3 AASHTO-LRFD Bridge Design Specifications

After years of development, American Association of State Highway Transportation Officials (AASHTO, formerly AASHO) fully incorporated Load Factored Resistance Design (LRFD) into the specifications. The 4th edition, (*AASHTO 2007*), is the edition used in this report for design calculations. Some updates to current specifications include considering additional demands on tension steel from shear and cracks, calculated as the tensile demand in the steel reinforcing bars as:

$$A_s f_y \geq \frac{|M_u|}{d_v \varphi_f} + 0.5 \frac{N_u}{\varphi_c} + \left( \left| \frac{V_u}{\varphi_v} \right| - 0.5 V_s \right) cot\theta \qquad \textbf{2007 AASHTO Eq. 5.8.3.5-1 (2.17)}$$

where $d_v$ is the distance from compression to tension centroids (formerly $jd$), $N_u$ is the applied axial force, $V_u$ is the applied factored shear, $V_s$ is the shear capacity of stirrups, $\Theta$ is the angle of the crack, and $\varphi_f, \varphi_c, \varphi_v$, are resistance factors for moment, axial force, and shear force. A simplified version of this equation is described previously.

AASHTO LRFD 2007 development length, $l_{d,}$ can be taken for #11 (36M) steel reinforcing bars and smaller as:

$$l_d = \frac{1.25 A_b f_y}{\sqrt{f'_c}} \qquad \textbf{2007 AASHTO Sec. 5.11.2.1.1 (2.18)}$$

where $A_b$ is area of bar or wire, and all other variables are defined previously. Additionally, this equation is multiplied by applicable modification factors. Similar flexural bar termination requirements are maintained as the 1973 code.

### 2.3.4 ACI 318 Building Code for Structural Concrete

In 1956, the American Concrete Institute published the Building Code Requirements for Reinforced Concrete (ACI 318-56). During this time, allowable stress design was permitted for reinforced concrete structures. The bond stress calculation similar to Equation (2.13) and maintained allowable stress requirements as described in Equation (2.14). Similar to current AASHTO standards, bar termination requirements required the steel reinforcing bar must extend at least 12 bar diameters past the theoretical cutoff point.

Like AASHTO specifications, ACI adopted LRFD. The calculations in this paper are based off the current code ACI code (ACI 318-11). Since allowable stress is not used to design for bond stresses, ACI created a general and detailed equation to determine development length given a bar size. ACI 318-11 equates straight development length, $l_d$, of #7 bars and larger as:

$$l_d = \left( \frac{f_y \psi_t \psi_e}{20 \lambda \sqrt{f'_c}} \right) d_b \qquad \textbf{2011 ACI 318 Sec. 12.2.2 (2.19)}$$

where $\psi_t$ and $\psi_e$ are modification factors for the location of bar and coating of the bar respectively. $\lambda$ is the lightweight concrete factor and all other variables are defined in equations above. The more detailed equation recognizes the contribution of the transverse reinforcement and cover of the bar, thus providing a more accurate development length shown as:

$$l_d = \left( \frac{3}{40\lambda} \frac{f_y}{\sqrt{f'_c}} \frac{\psi_t \psi_e \psi_s}{\frac{c_b + K_{tr}}{d_b}} \right) d_b \qquad \textbf{2011 ACI 318 Eq. 12-1 (2.20)}$$

where $\psi_t$ is the size factor for the bar, $c_b$ is either the smallest of the side or top cover, or half the center to center spacing between the bars. $K_{tr}$ is the contribution of confining reinforcement and is calculated by:

$$K_{tr} = \frac{40 A_{tr}}{sn} \qquad \textbf{2011 ACI 318 Eq. 12-2 (2.21)}$$

where $A_{tr}$ is the area of transverse reinforcement across the splitting plane, s is the spacing of stirrups, and n is the number of bars being developed. $K_{tr}$ may be taken as zero for a conservative design. General requirements for the development of flexural reinforcement include extending a distance $d$ or $12d_b$ past the point where reinforcement is no longer required.

### 2.3.5 ACI 440 Guide for Design of Externally Bonded FRP Systems

ACI created a committee focused on the design and construction for strengthening reinforced concrete using external fiber reinforced polymer (FRP) systems. The two systems described include FRP laminate sheets and FRP rods and strips used for a near-surface mounted (NSM) application. The majority of the code is based on behavior of reinforced concrete sections strengthened with FRP laminate. NSM strengthening guidelines include groove spacing, depth, effective strain and required development length.

To determine the strength of the cross section retrofitted with NSM materials the effective strain in NSM material was calculated. The effective strain in the NSM material was taken as the lesser of the concrete crushing or debonding strain in the NSM material shown as:

$$\boldsymbol{\varepsilon_{fe} = 0.003\left(\frac{d_f - c}{c}\right) - \varepsilon_{bi} < \varepsilon_{fd}} \qquad \textbf{ACI 440 Eq. (10-3) (2.22)}$$

where $d_f$ is the distance from the extreme compression fiber to the centroid of the NSM reinforcement, $c$, is the distance from the extreme compression fiber to the neutral axis, and $\varepsilon_{bi}$ is the existing strain in the reinforcement calculated from the dead load. The advantage of a mechanical anchorage decreases the probability of a bond failure so the bond depended coefficient may be less stringent for the NSM titanium and stainless steel near hooked bar terminations. The debonding strain ($\varepsilon_{fd}$) for the NSM material is calculated as:

$$\boldsymbol{\varepsilon_{fd} = \kappa_m \varepsilon_{fu}} \qquad \textbf{ACI 440 Eq. (10-2) (2.23)}$$

where $\kappa_m$ is the bond depended coefficient for the NSM material provided by the manufacturer taken as 0.7. The 70% reduction in ultimate strain is due to concrete dilation and tendency to debond after cracking. $\varepsilon_{fu}$ is the ultimate strain of the NSM material.

The development length, $l_{db}$, for straight circular FRP bars is calculated as:

$$\boldsymbol{l_{db} = \frac{d_b}{4\tau_b} f_{fd}} \qquad \textbf{ACI 440 Eq. (13-3) (2.24)}$$

where $\tau_b$ is the average bond stress, taken as 1000 psi, and $f_{fd}$ is the debonding stress of FRP, based on the debonding strain of the section. Essentially, Eq. [2.24] is equivalent to Eq. [2.1] but uses FRP debonding stress instead of yield stress.

Minimal guidance is given on termination of NSM bars. However, ACI 440 recommends extending the FRP a distance from the maximum moment to at least 6 in. past the location of the first cracking moment or the development length, whichever is greater to minimize debonding failures.

## 2.4 CONCLUSIONS

Based on a review of the literature and design specifications, several conclusions on bond and behavior of steel reinforcing bars in concrete and NSM FRP bars have been made.

- Bond strengths from pull-out tests are not representative of those observed in beam tests. Furthermore, there is limited research on large-size specimens.
- The development length of steel reinforcing bars in concrete is based on bar strength, diameter, placement, covering, spacing, transverse reinforcement, and concrete strength.
- Reported average bond stresses in steel reinforced concrete beam tests range from 540-815 psi (3.72-5.62 MPa).
- Strengthening with NSM FRP bars significantly increases the strength and stiffness of the beam, but reduces ductility.
- Shorter NSM bond lengths produce higher average bond stresses and the concrete-epoxy bond is the most critical interface.
- Anchorage of NSM bars limits the effective design stress in FRP systems.

Reported average bond stresses in NSM FRP pull-out tests range widely from 620-1637 psi (4.27-11.3 MPa).

## 2.5 RESEARCH OBJECTIVES

Current load ratings for RCDG bridges from the 1950's can be controlled by flexural anchorage deficiencies in the girders. In order to mitigate posting or replacement of these RCDG bridges, methods for strengthening existing girders are necessary. A retrofitting technique using near-surface mounted (NSM) carbon fiber reinforced polymer (CFRP) bars has been shown to increase the strength of deficient RC specimens. The CFRP materials show no ductility, rarely achieve their full material strength due to issues in bond and anchorage, and while specimens with NSM-CFRP exhibit higher strength, they have reduced deformations and ductility at failure. At the same time, there is limited prior research using metallics in NSM applications. Based on these observations, environmentally insensitive metallics with high strength, ductility, and the ability to fabricate mechanical anchorages were studied in the present work. Stainless steel and titanium alloy bars were selected for the research program. No prior research has been conducted using titanium alloy bars for strengthening civil infrastructure, and thus additional emphasis was placed on this material.

The main objectives of this research were to:

- Characterize the mechanical properties of the metallic NSM bars.

- Develop NSM methods using metallic bars to strengthen poorly detailed flexural anchorages in existing reinforced concrete deck girders in negative and positive moment regions.

- Assess bond stresses and strength of the metallic NSM bars.

- Use experimental findings to develop design guidance for use of metallic NSM bars to strengthen deficient flexural anchorage details in existing RC bridge girders.

# 3.0 EXPERIMENTAL SETUP

An experimental program was developed to investigate full-scale reinforced concrete girders typical of 1950's vintage RCDG bridges with anchorage deficiencies in the positive and negative moment regions that were strengthened with NSM titanium and stainless steel bars. This chapter describes the design, details, construction, instrumentation, and testing protocols used in the experimental program.

## 3.1 SPECIMEN DESIGN

In a typical RCDG, three likely failure modes are: diagonal-tension failure due to lack for shear reinforcement, diagonal-tension failure due to inadequate flexural steel anchorage, and flexural failure. The intent of this study was to strengthen specimens that would otherwise fail due to anchorage deficiencies. A survey was conducted prior to this experimental work to characterize typical vintage concrete deck girders. The survey provided the geometry and reinforcing steel details of vintage girders *(Higgins et al. 2004)*. All specimens in this program were 26 ft (7.92 m) long, with a 14 in. (356 mm) thick web, 42 in. (1067 mm) tall stem, 36 in. (914 mm) wide flange, and a 6 in. (152 mm) thick deck. T and IT beams were used to study the positive and negative moment regions, respectively. Eleven specimens were tested in this program, three (3) T and four (4) IT specimens, as well as three (3) specimens designed to replicate an actual in-service girder and reported in greater detail in Appendix D. Each of the T and IT specimens is described below.

Reinforcing steel bars #11 (36M) were used as flexural tension and flexural compression steel. In each of the specimens, some of the flexural tension steel bars were continuous and well anchored while others were terminated in the flexural tension zone to mimic the features of an in situ girder. A preformed diagonal crack was used to control the demands on the developing cutoff bars and allowed placement of sensors to capture the stresses in the flexural and transverse reinforcing steel at the highest demand location a priori. Similar large-sized specimens from previous research studies by Triska *(Triska 2010)* and Goodall *(Goodall 2010)* were used as control specimens to compare with the present NSM strengthened specimens. The specimens are designated with an SPR in front of the name and also detail the number of #11 flexural bars used in the member (5 or 6) at the end of the name.

The naming convention used in this study is shown in Figure 3.1 and Table 3.1 lists the specimens considered in this study.

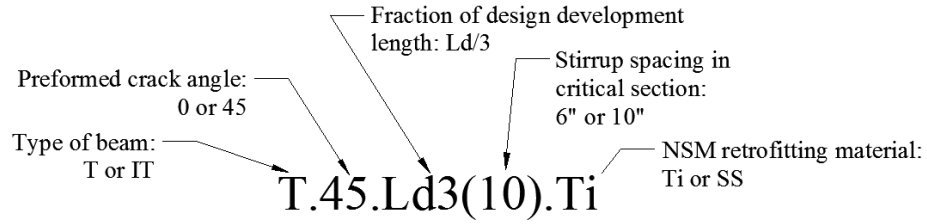


Figure 3.1: Specimen naming convention (Note an SPR designation before the type of beam indicates a comparison specimen tested by previous researchers).

**Table 3.1: Specimen summary and year tested**

| Specimen ID | Retrofitting Material | Year Tested |
|---|---|---|
| SPR T.45.Ld3(10) | - | 2010 |
| T.45.Ld3(10).Ti | Titanium | 2014 |
| T.45.Ld3(6).Ti | Titanium | 2014 |
| T.45.Ld3(6).SS | Stainless Steel | 2014 |
| SPR IT.45.Ld2(10).(5) | - | 2010 |
| SPR IT.45.Ld2(10).(6) | - | 2010 |
| SPR IT.0.0(10).(5) | - | 2010 |
| IT.45.Ld3(10).Ti | Titanium | 2014 |
| IT.45.Ld3(6).Ti | Titanium | 2014 |
| IT.45.Ld3(6).SS | Stainless Steel | 2014 |
| IT.0.0(6).Ti | Titanium | 2014 |

To design the specimens with an anchorage deficiency, the development length of a #11 (36M) reinforcing steel bar was estimated based on expected steel and concrete material properties. The minimum development length of the mild reinforcing steel bars was determined using the AASHTO LRFD and ACI 318-11 specifications. The smallest and least conservative value was chosen for the development length. Calculations were performed with an expected yield stress of 68.5 ksi (472 MPa) for the flexural steel, and expected yield stress of 50.7 ksi (350 MPa) for transverse steel. The nominal concrete strength used was 3500 psi (24.1 MPa), which is typical of bridges in the 1950s. Development lengths from the ACI and AASHTO methods are shown in Table 3.2. A stirrup spacing of 10 in. (254 mm) and value of $c_b$ of 2.02 in. (51 mm) was used in the detailed ACI 318 equation. As seen in Table 3.2, the smallest permissible length to develop the #11 (36M) Gr. 60 (Gr. 420) bar was 61.2 in. (1554 mm).

**Table 3.2: Summary of expected development lengths of #11 (36M) steel reinforcing bars**

| Method | AASHTO LFRD (in.) [mm] | ACI 318-11 (in.) [mm] |
|---|---|---|
| Straight Bar | 71.4 [1813] | 61.2 [1554] |
| Straight Bar Simplified | - | 81.6 [2072] |
| Hooked Bar | 28.6 [726] | 32.6 [828] |

Tests by Triska and Goodall *(Triska and Goodall 2010)* demonstrated that anchorage failures occurred when around ½ to 1/3 of the specified embedment length was used. Therefore, the strengthened specimens in this study were designed to have the cutoff bars extend 20.4 in. (518 mm) past the preformed diagonal crack (around 1/3 of the specified embedment length).

## 3.2 SPECIMEN DETAILS

This section describes the internal reinforcing steel details, specimen construction, and NSM details and installation.

### 3.2.1 Reinforcing Steel and NSM Details for T-Specimens

The transverse reinforcing steel consisted of open leg #4 (13M) stirrups. Two straight #11 (36M) bars make up the compression steel. The flexural reinforcement consisted of five #11 bars (36M) in two layers. Three #11 (36M) bars were fully anchored on the bottom layer of flexural reinforcement. The top layer of reinforcement consisted of two cutoff steel reinforcing bars. The cutoff steel reinforcing bars were embedded 20.4 in. (118 mm) past the preformed diagonal crack. The cross section and elevation of the specimens can be seen in Figure 3.2 through Figure 3.8.

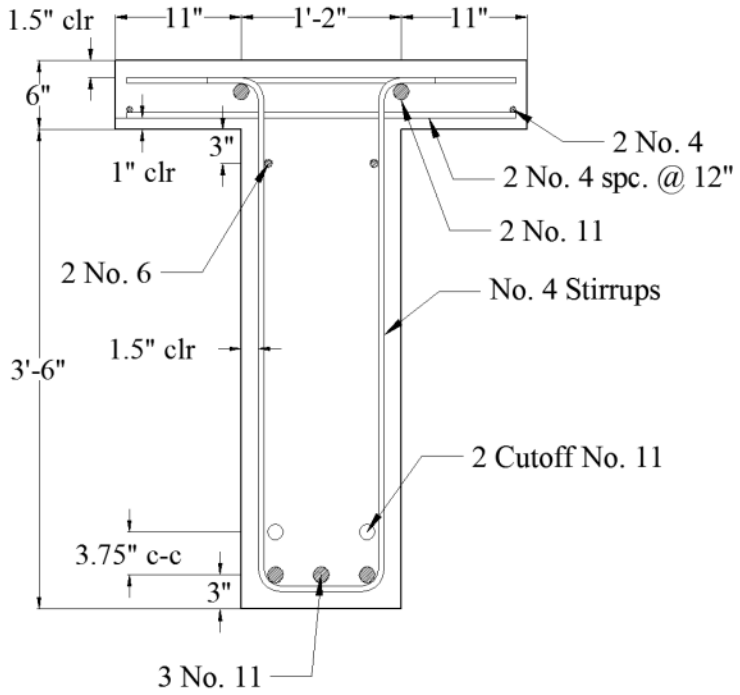


Figure 3.2: Cross section of SPR T.45.Ld3(10).

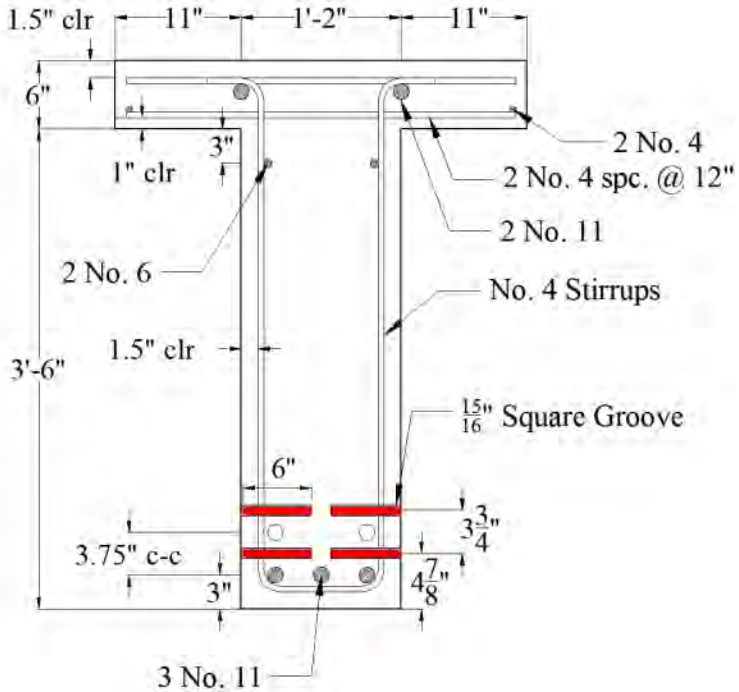


Figure 3.3: Cross section of T.45.Ld3(10).Ti and T.45.Ld3(6).Ti.

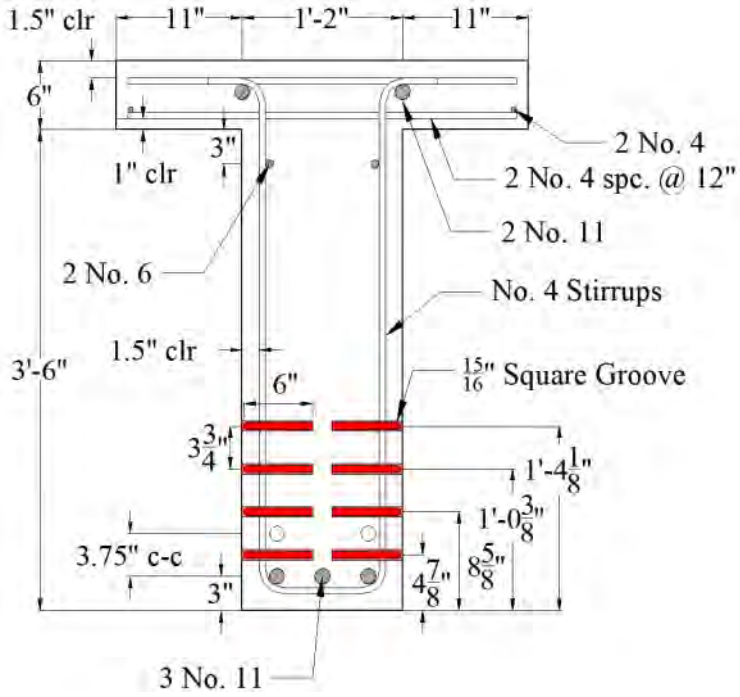

Figure 3.4: Cross section for specimen T.45.Ld3(6).SS.

Figure 3.3 and Figure 3.4, show the hooked termination detail of the NSM material in red. Between the terminations, a small square groove was cut into the section's concrete cover. The NSM retrofit location and extent is also shown as the red lines on the Figure 3.6 through Figure 3.8. The metallic NSM retrofit bars were 12.5 ft (3.81 m) long (out-to-out) with a 90° hook at the ends with a length of 6 in. (152 mm) (out-to-out). The titanium strengthened specimens had four 5/8 in. (16 mm) (nominal) diameter bars bonded into the square saw-cut grooves, two on each side of the web. Stainless steel specimens had eight 5/8 in. (16 mm) diameter bars bonded into the square saw-cut grooves, four on each side of the web. The baseline specimen elevation is shown in Figure 3.5.

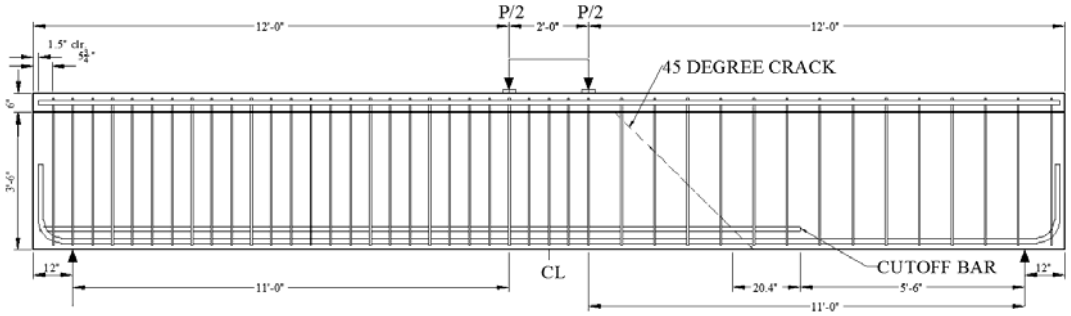


Figure 3.5: Elevation of baseline specimen SPR T.45.Ld3(10).

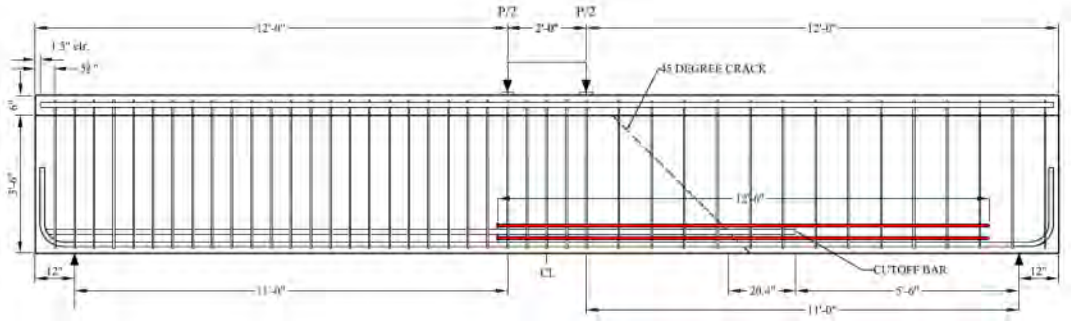


Figure 3.6: Elevation of specimen T.45.Ld3(10).Ti.

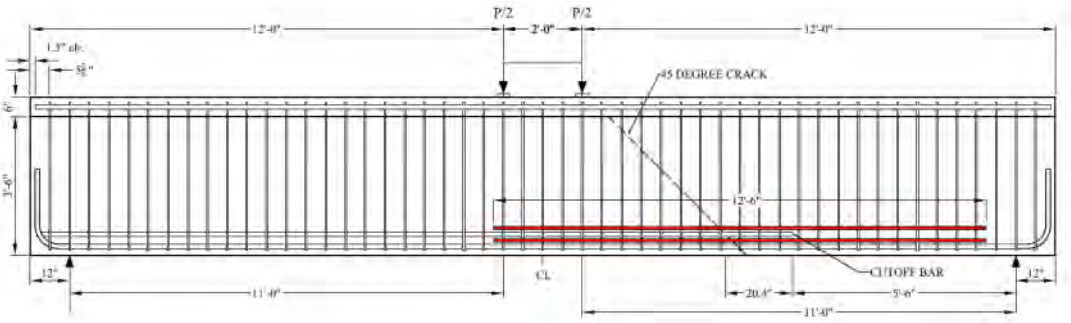


Figure 3.7: Elevation of specimen T.45.Ld3(6).Ti.

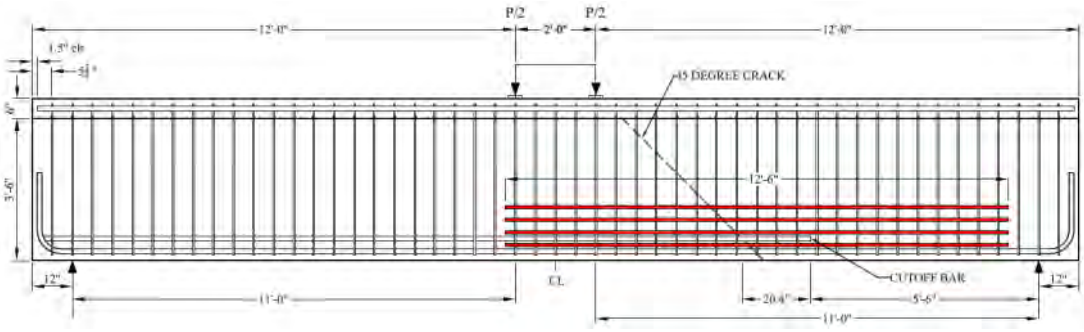


Figure 3.8: Elevation of specimen T.45.Ld3(6).SS.

All specimens utilized a tight stirrup spacing of 6 in. (152 mm) on the half of the specimen with fully anchored reinforcing steel. The control specimen and the T.45.Ld3(10).Ti specimen had a 10 in. (254 mm) stirrup spacing on the half with a predicted anchorage deficiency. T.45.Ld3(6).Ti and T.45.Ld3(6).SS both had 6 in. (154 mm) stirrup spacing throughout the full length to preclude the possibility of a shear-tension failure on the strengthened half.

### 3.2.2 Reinforcing Steel and NSM Details for IT-Specimens

Three of the IT specimens (IT.45.Ld3(10).Ti, IT.45.Ld3(6).Ti, and IT.45.Ld3(6).SS) had one layer consisting of five straight #11 (M36) flexural steel bars located in the flange. These specimens also contained a 1/16 in. (1.6 mm) polycarbonate preformed diagonal crack oriented at a 45° angle. The three interior flexural bars were continuous throughout the entire length of the specimen and hooked at the ends. The two exterior flexural bars were fully anchored on one end and cutoff past the preformed crack at 1/3 of their theoretical development length. In order to ensure failure on the half of the specimen where the cutoff bar, retrofit, and instrumentation were located, the opposite half of the beam was over-reinforced with #4 (M13) stirrups spaced at 6 in. (152 mm). Beginning at the closest load point, the under-reinforced half of this specimen contained 10 in. (245 mm) stirrup spacing. The other two specimens contained 6 in. (152 mm) stirrup spacing throughout the entire length of the beams. Two of these specimens were retrofitted with NSM-titanium and the third with NSM-stainless steel. Four titanium and eight stainless steel 5/8 in. (16 mm) diameter round bars were used as NSM reinforcement for their respective specimens. The NSM materials had a 12.5 ft (3.81 m) out-to-out length.

The fourth specimen consisted of three hooked #11 (M36) flexural bars located in the flange. These bars were cut, leaving a 2 in. (51 mm) gap in the center of the beam. This specimen did not contain a preformed crack. Stirrups were spaced at 6

in. (152 mm) throughout the length of the beam. Four titanium 5/8 in. (16 mm) round bars were used as the NSM retrofit material. The two interior NSM bars had a 12.5 ft (3.81 m) out to out length. The exterior two titanium bars were 11.5 ft (3.51 m) out-to-out.

The baseline specimens were used for comparison. Specimen SPR IT.45.Ld2(10).(5) was identical to IT.45.Ld3(10).Ti except the two cutoff bars extended 1/2 of their theoretical development length past the preformed crack. Specimen SPR IT.45.Ld2(10).(6) was similar, but had four fully anchored flexural bars and two cutoff bars for a total of six #11 (M36) flexural reinforcing bars. Lastly, specimen SPR IT.0.0(10).(5) had five fully anchored #11 (M36) flexural reinforcing bars. This specimen did not contain a preformed crack or any cutoff bars. Elevations and cross-sections for each of the retrofitted and baseline specimens are shown in Figure 3.9 to Figure 3.19.

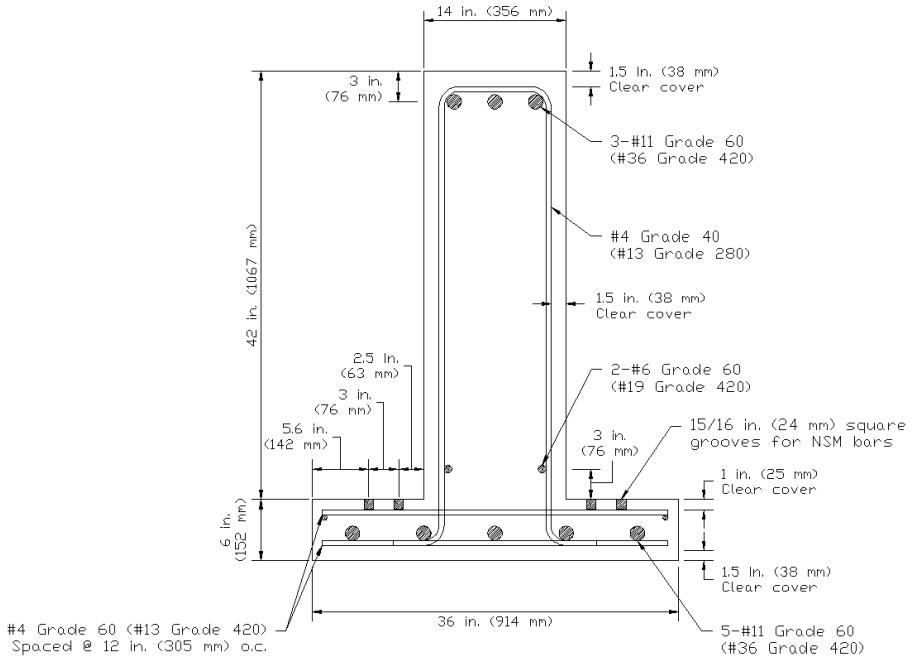


Figure 3.9: Specimens IT.45.Ld3(10).Ti and IT.45.Ld3(6).Ti cross-sections.

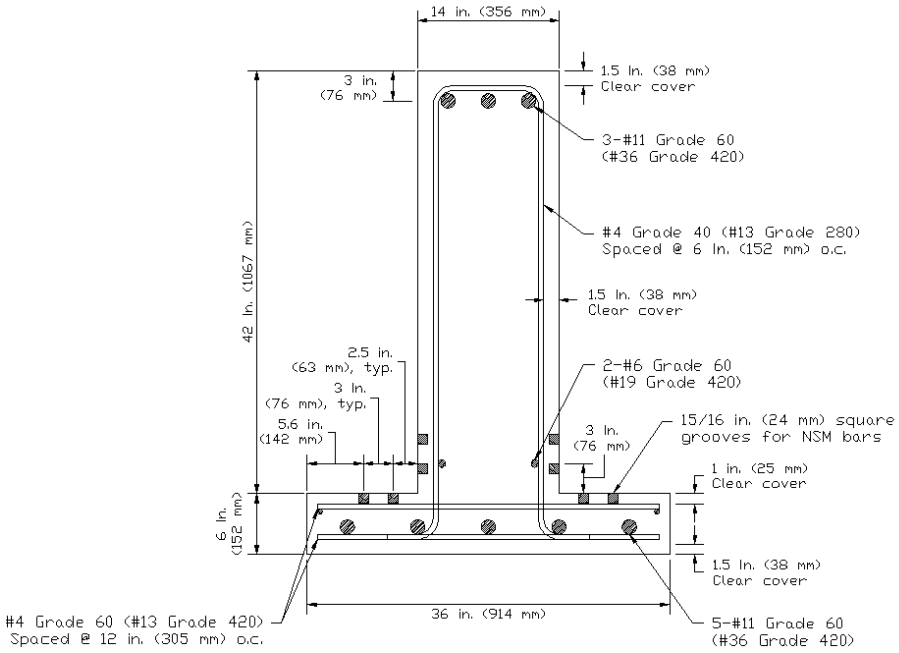


Figure 3.10: Specimen IT.45.Ld3(6).SS cross-section.

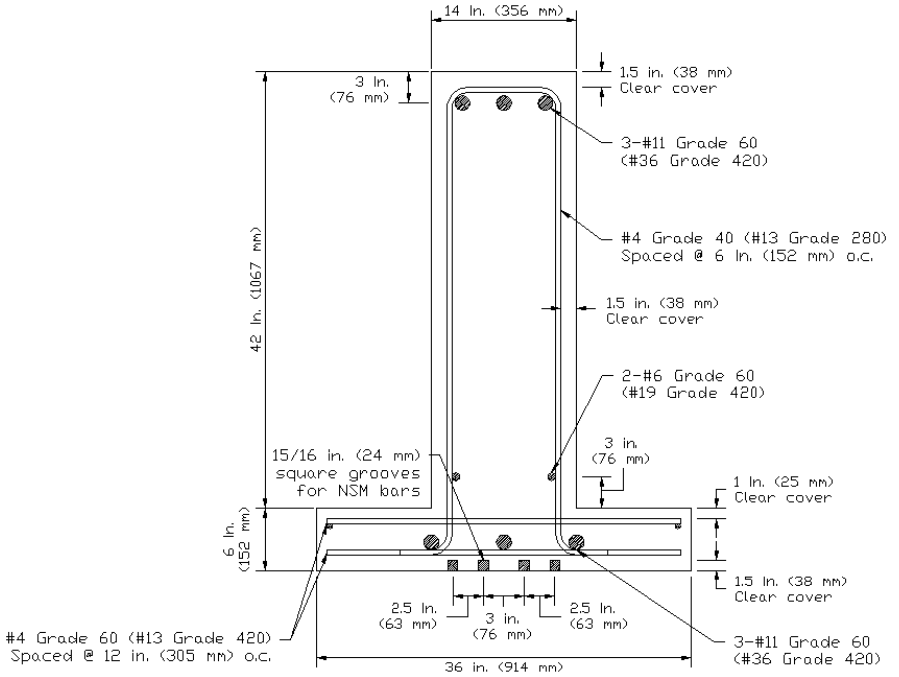


Figure 3.11: Specimen IT.0.0(6).Ti cross-section.

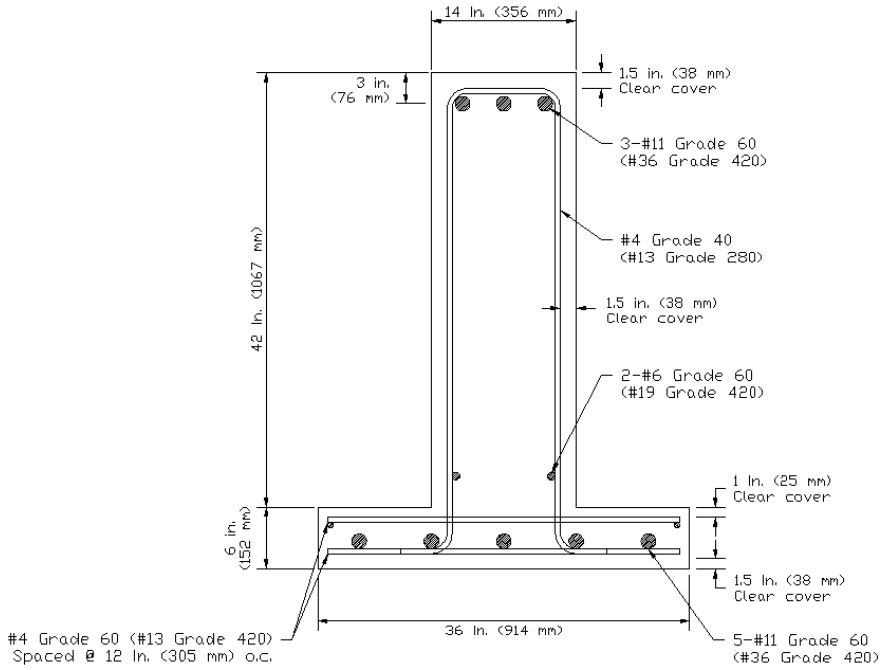


Figure 3.12: Specimens SPR IT.45.Ld2(10).(5) and SPR IT.0.0(10).(5) cross-sections.

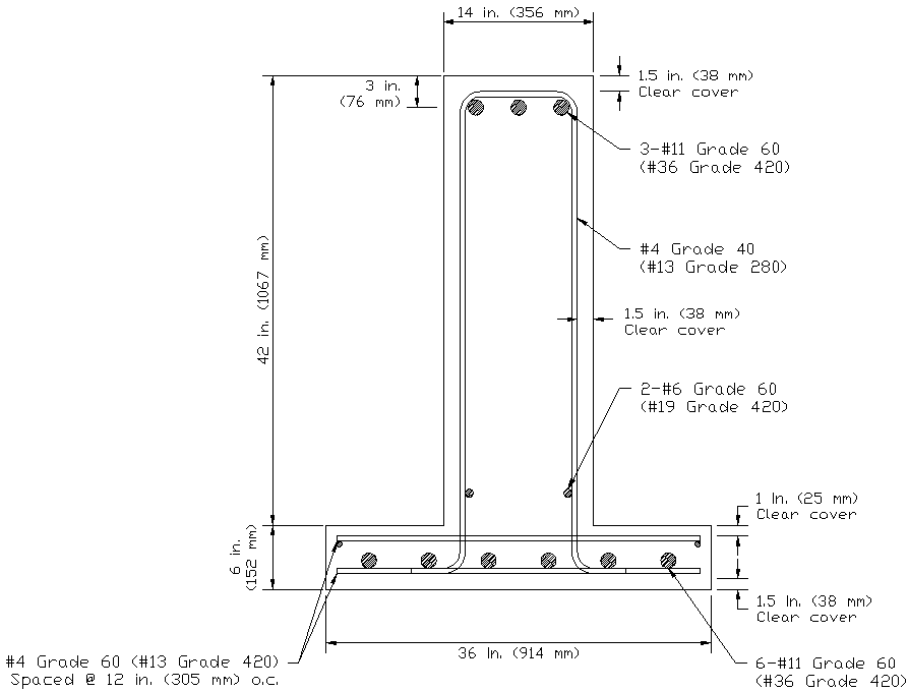


Figure 3.13: Specimen SPR IT.45.Ld2(10).(6) cross-section.

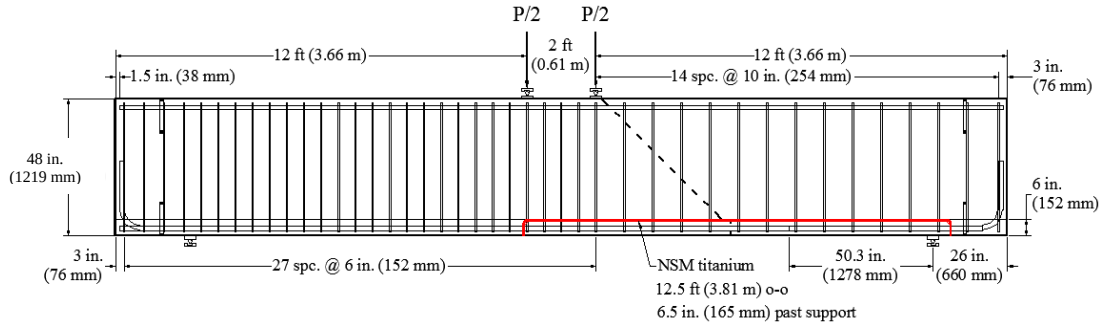


Figure 3.14: Elevation of specimen IT.45.Ld3(10).Ti.

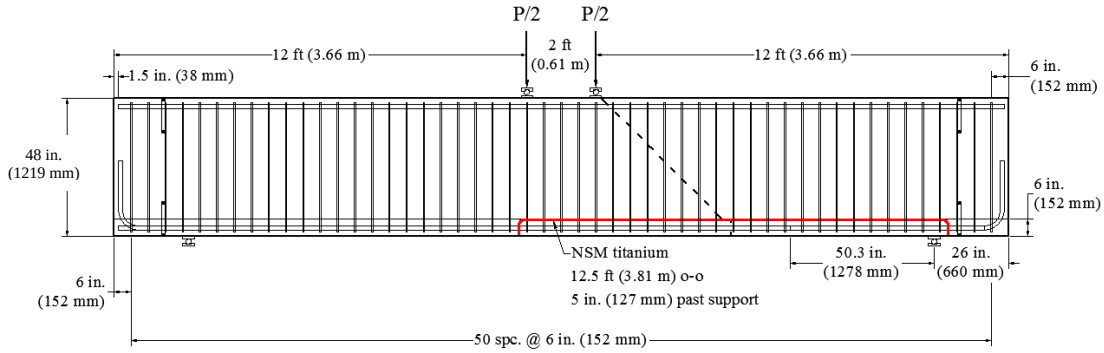


Figure 3.15: Elevation of specimen IT.45.Ld3(6).Ti.

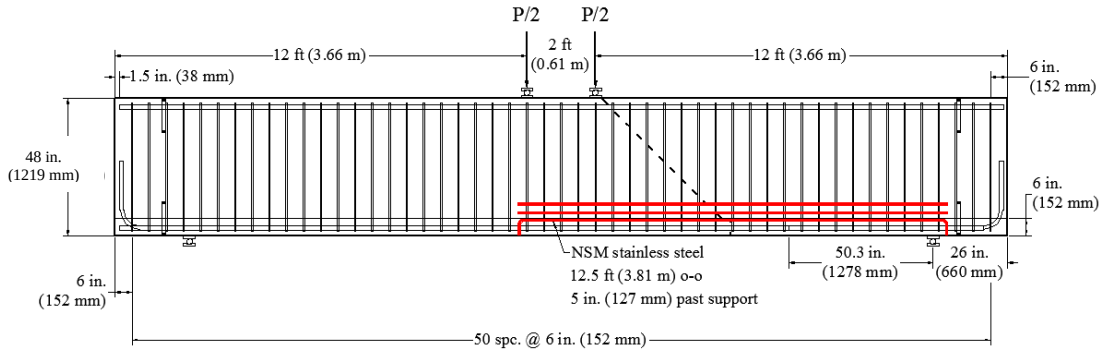


Figure 3.16: Elevation of specimen IT.45.Ld3(6).SS.

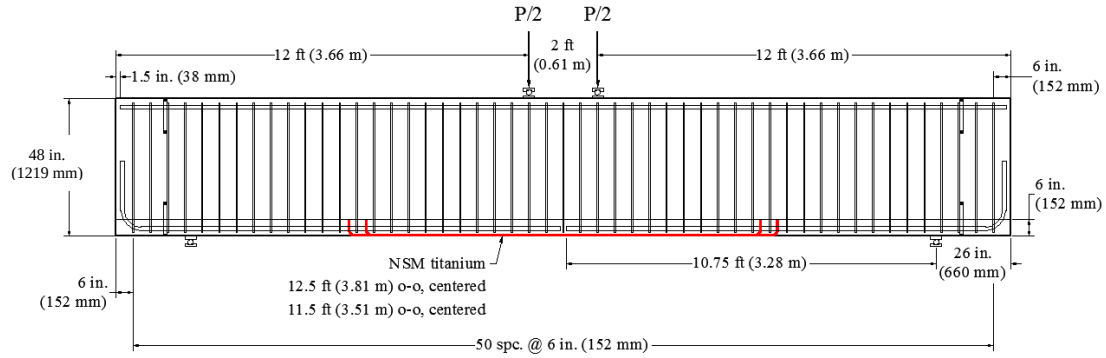


Figure 3.17: Elevation of specimen IT.0.0(6).Ti.

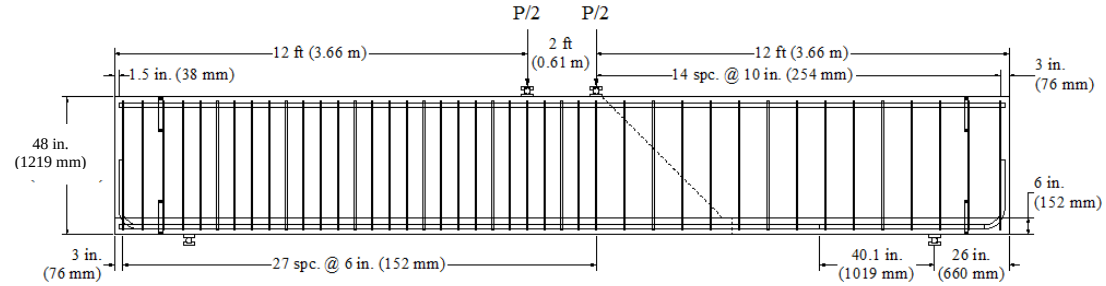


Figure 3.18: Elevation of specimens SPR IT.45.Ld2(10).(5) and SPR IT.45.Ld2(10).(6).

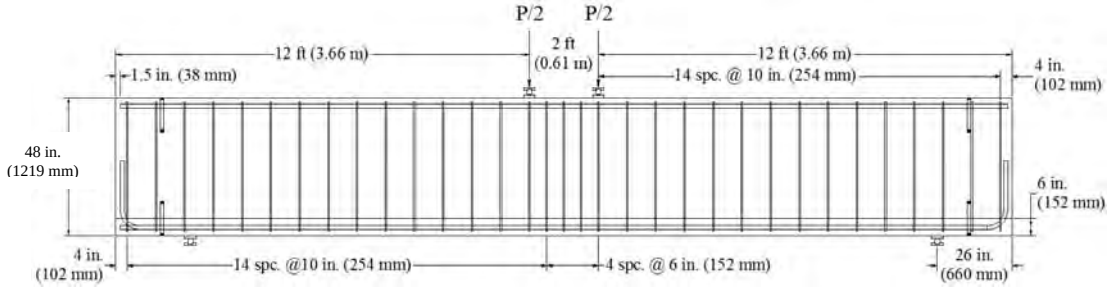


Figure 3.19: Elevation of specimen SPR IT.0.0(10).(5).

### 3.2.3 Specimen Construction

Before building each reinforcing steel cage, selected transverse and flexural reinforcing bars were instrumented with strain gages at specified locations along the bar lengths. IT specimen reinforcing cages were constructed in a T beam configuration for ease of construction. The steel reinforcing cages were fabricated using conventional rebar tying methods to maintain dimensional stability of the reinforcing cage. The two longitudinal cutoff bars were saw-cut to the required length using a band saw prior to installation in the cage. These bars extended 1/3 of

their development length past the preformed diagonal crack. Foam blockouts were installed at the ends of the cutoff bars in all IT specimens and in two of the T specimens (T.45.Ld3(10) and T.45.Ld3(10).Ti), to allow displacement sensors to measure slip of the cutoff bars during testing. While testing T.45.Ld3(10).Ti, it was observed that the blockout reduced dowel action and produced bending stresses in the titanium bars and lower layer of reinforcing steel. To maintain the dowel action in the titanium bars and reinforcing steel, a small diameter side port was used to measure end slip of the cutoff bar. A nut was welded to the side of the cutoff steel reinforcing bar and was enclosed by a piece of polyvinyl chloride (PVC) pipe tapered to the bar. Once cast, the circular end of the PVC pipe was exposed and a threaded rod was inserted into the nut. The displacement sensor was attached to the nearby concrete with an epoxied steel dowel and reacted against the threaded rod anchored to the cutoff reinforcing steel bar. These different techniques are shown in Figure 3.20.

Figure 3.20: Cutoff bar slip sensor ports (left), and block-out box (right).

Coil thread anchors were installed on both ends of the specimens to enable lifting the specimens after concrete casting and curing. The coil anchors were fastened to the center longitudinal bars and to a nearby piece of deck steel or stirrup. A finished reinforcing cage can be seen in Figure 3.21.

Figure 3.21: Finished rebar cage.

Double leg open stirrups were hung from the top flexural bars and tied in place, and longitudinal compression steel was tied in the web to the interior bottom of the stirrups. The top layer of transverse deck steel was tied to the top of the tension bars in the flange. The bottom layer was a “floating” layer created by placing the transverse steel on top of the longitudinal #6 (M19) bars and the transverse steel to two longitudinal #4 (M13) bars. On the fully anchored end of the beam, one stirrup that had been bent outward to a “W” shape was tied to the regular stirrups on each side of the cage to help provide cage stability for both moving the cage and during casting.

#### *3.2.3.1 Clear Cover*

Clear cover dimensions on the web and flange were achieved by using spacers as shown in Figure 3.22. The bottom layer of deck steel “floated” to the correct placement with the correct cover once placed in the formwork using chairs. Metal chairs were tied diagonally to the bottom of the cage to provide the clear cover depth and to support the cage when it was placed in the formwork.

Figure 3.22: Chair used to ensure cover concrete.

#### *3.2.3.2 Preformed Diagonal Crack*

A preformed diagonal crack was used to investigate the influence of an existing diagonal crack and NSM material demands. The approach is similar to that by Goodall and Triska *(Goodall and Triska 2010)*. The common assumption of shear-dominated beam behavior results in an idealized 45˚ diagonal crack. For the specimens, a 45˚ diagonal crack angle projected up to be coincident with the edge of the beam loading plate, and extended from depth of the theoretical compression zone down to the flexural tension steel. To produce a simulated diagonal crack, a 1/16 in. (1.6 mm) thick polycarbonate sheet was placed between the stirrups legs within the web and extended toward the bottom of the theoretical compression zone and around the flexural bars in the flange as seen in Figure 3.23. Small holes were drilled in the polycarbonate sheet at locations where it crossed the internal reinforcing steel to allow attachment of the plastic to the cage thereby restricting movement during concrete casting.

Figure 3.23: Preformed crack placement (IT specimen).

#### *3.2.3.3 Cage Placement and Concrete Casting*

After construction, the reinforcing cage was placed into the formwork using an overhead bridge crane as seen in Figure 3.24.

Figure 3.24: Typical cage lifting process.

Concrete casting was done with a 2 $yd^3$ (1.53 $m^3$) clamshell bucket (Figure 3.25a). The concrete was placed into the forms and consolidated using a mechanical vibrator (Figure 3.25b). Concrete was carefully placed around the preformed diagonal crack to balance the pressure on both faces of the polycarbonate sheet in the stem. After placement, the concrete was screeded and the surface was finished using hand trowels. Specimens were covered with wet burlap and plastic sheeting and cured for at least seven days in the formwork.

a)  b) 

Figure 3.25: a) Clamshell bucket carrying concrete and b) consolidating concrete.

After curing, the specimens were removed from the formwork. The IT specimens were carefully rotated into the testing configuration as illustrated in Figure 3.26. Specimens were moved onto the laboratory floor for NSM installation and testing.

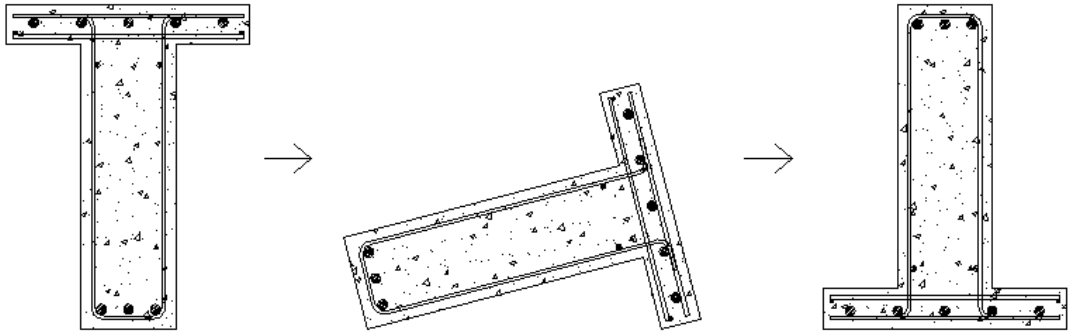

Figure 3.26: Rotation progression for IT specimens.

### 3.2.4 NSM Material Details

The design intent of the metallic NSM strengthening was to retrofit anchorage deficiencies in RCDGs. To accomplish this, the NSM material had to effectively increase the strength of the girder at the cut off location of the flexural reinforcing steel. To determine the locations to terminate the NSM materials, the demand on flexural reinforcing steel from the combined shear and moment contributions was compared to the available anchorage capacity provided at the cross section using AASHTO methods. Where the demand exceeded the capacity, an anchorage failure would be expected unless the deficiency was remediated with the NSM materials. Typical flexural tension demands and capacity for a T-specimen at failure is shown in Figure 3.27. As seen here, the drop in capacity of the original base specimen is due to the cutoff flexural reinforcing bars. NSM materials were selected to develop sufficient force and increase the member strength locally over the deficient region. The starting and ending locations of the NSM materials were selected based on these analyses.

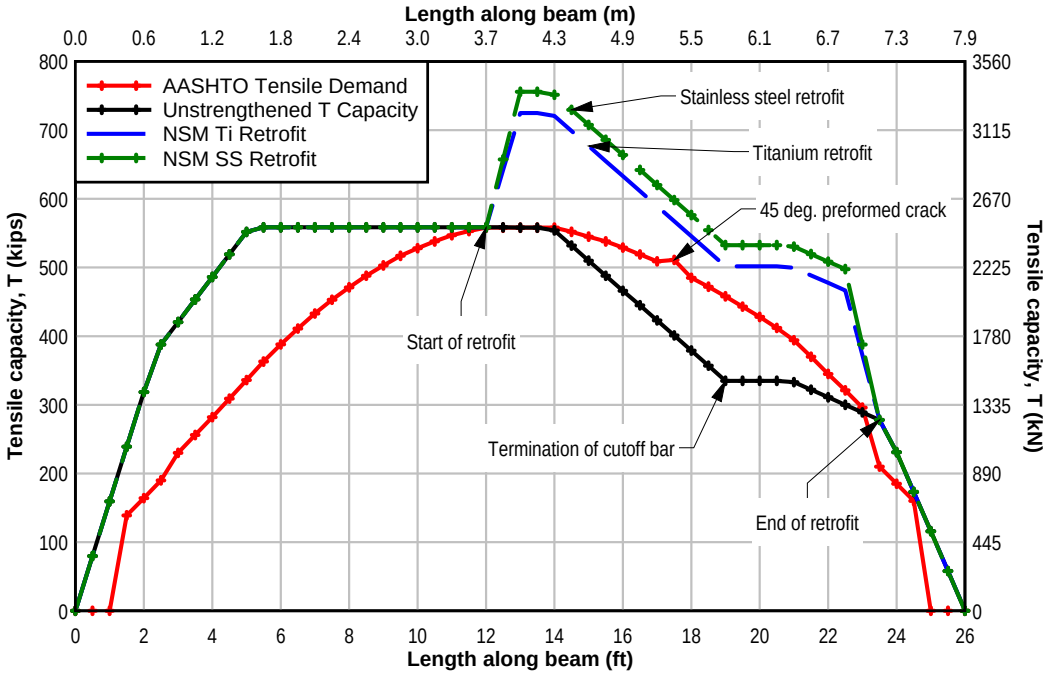


Figure 3.27: Flexural tension capacity and demand along the length of typical T-specimen at failure load.

### *3.2.4.1 NSM Dimensions and Installation*

The methodology used to design the metallic NSM retrofit systems followed that prescribed by ACI 440.2R-08, which was developed for FRP systems. ACI 440 provides guidelines for groove width, depth, and spacing. For circular bars, groove widths and depths are prescribed to be greater than or equal to 1.5 times the diameter of the bar, $d_b$. To avoid overlapping of the tensile stresses around the NSM bars, the minimum clear spacing between grooves should be greater than twice the groove depth. A clear distance between a groove and the edge of the concrete should be provided at a minimum distance of four times the groove depth in order to minimize likelihood of premature failure due to debonding at the edges. These guidelines are summarized in Figure 3.28.

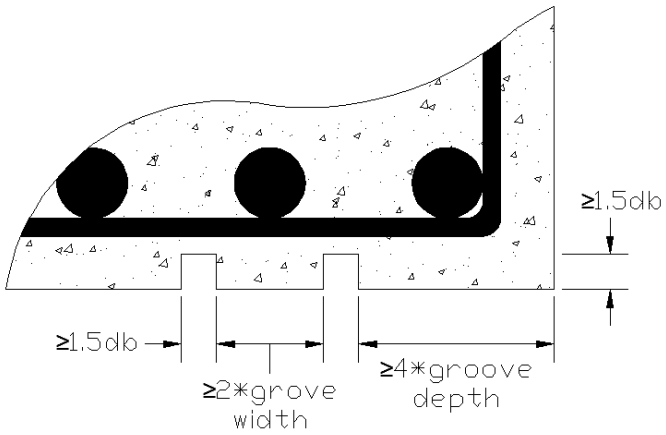


Figure 3.28: ACI 440 groove spacing and dimension guidelines.

The stainless steel and titanium bars were 0.625 in. (15.9 mm) diameter corresponding to #5 (M16) bars and are shown in Figure 3.29. Based on the given bar diameters, 15/16 in. (24 mm) square grooves were used. The grooves were spaced 2 in. (51 mm) apart and at least 4 in. (102 mm) from the edge of the concrete.

Figure 3.29: Stainless steel (top) and titanium alloy bar (bottom).

The grooves were cut into the specimens by a local concrete cutting company. Grooves were cut by making three passes with a hand-held circular saw with a diamond blade. The remaining conrete was chipped out by a rotohammer. Each of the NSM bars contained a 5.5 in. (138 mm) 90° hook at each end. This length was sufficient to prevent drilling through the relatively thin concrete deck. To accommodate the hooks, a 3/4 in. (19 mm) hole was drilled into each groove end. The diameter of the hole was based on the typical diameter for a post-installed anchor bolt. The holes were intended to be drilled at approximately a 5.75 in. (146 mm) depth. In specimens IT.45.Ld3(10).Ti, IT.45.Ld3(6).Ti and IT.45.Ld3(6).SS due to the thin amount of deck left at this depth, the drill created a spall on the bottom of the flange. To account for the NSM bar bend radius, the intersection between the hole and the groove was manually chipped away using a chisel or hammer drill.

The stainless steel hooks were cold bent around a 2 in. (51 mm) bending pin in a conventional rebar bending machine. The titanium hooks were heated in order to bend the materials around a 2 in. (51 mm) pin.  Heating was performed using an oxy-acetylene

torch or a two-burner forge (IT.45.Ld3(6).Ti). Color indication was used to identify the temperature in the bars (Figure 3.30). The titanium NSM bars for IT.45.Ld3(10).Ti and IT.45.Ld3(6).Ti were bent at approximately 900 ˚F (482 ˚C) while the bars for IT.0.0(6).Ti were bent at approximately 1250 ˚F (677 ˚C). After heating to the specified temperature, the bars were inserted into the rebar bending machine and bent around a 2 in. (51 mm) diameter bending pin. Both the stainless steel and the titanium experienced springback while bending; therefore, the bars were over-bent in order to produce a 90° end result.

a) 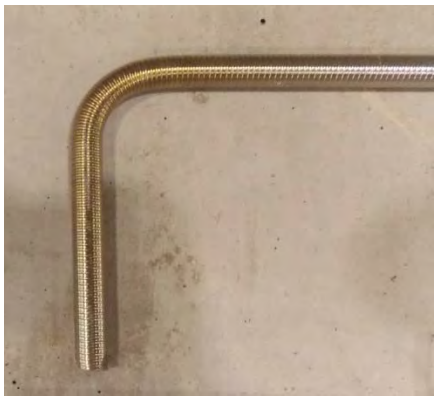 b) 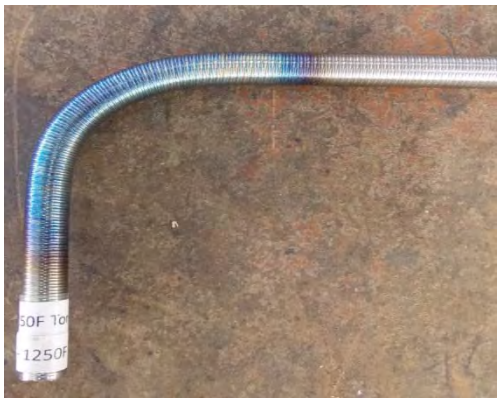

Figure 3.30: Color indication at a) 900 ˚F (482 ˚C) and b) 1250 ˚F (677 ˚C). Note: the bar in the right image is only for demonstration of color reference.

After concrete cutting, the grooves were cleaned with water and a brush and then given sufficient time to dry. Then the NSM materials were installed. To enable a clean surface finish, duct tape was used to line the concrete surface at the edges of the cut grooves. Installation consisted of placing epoxy in the holes and a pass of the epoxy groove, pushing the NSM bar into the groove with the hooks extending into the holes, and placing a second layer of epoxy over the bar. The NSM bars were centered in the grooves during the epoxy placement. The epoxy was finished flush with the surface of the concrete. In order to prevent the epoxy from sagging, the least amount of finishing necessary was done. Installation photos of the epoxy into the grooves and finished surface are shown in Figure 3.31a and b.

a)  b) 

Figure 3.31: a) First epoxy layer and b) finished NSM installation.

IT specimens that had spalled concrete on the bottom of the flange were duct taped underneath and had wood clamped next to the tape to prevent the epoxy from dripping out of the hole. The epoxy was allowed to cure for a minimum of seven days between the manufacturer's recommended curing temperatures of 60 ˚F to 80 ˚F. The curing temperatures were monitored and recorded hourly over the 7 day curing period to ensure the requirements were met. Installation during the winter was performed using heat tent placed around the specimens consisting of tarps and electric space heaters. Note that the NSM installation for specimen IT.0.0(6).Ti occurred while it was still in the formwork in the T configuration.

## 3.3 MATERIAL PROPERTIES

### 3.3.1 Concrete

Each specimen required approximately 6 $yd^3$ (4.59 $m^3$) of concrete. Concrete was provided by a local ready-mix supplier. The concrete mix design was based the AASHO "Class A" 3,000 psi (21 MPa) mixture used for vintage concrete bridges. Actual compression strengths are more likely higher due to in-situ strength gain over time. This design is congruent with previous research on similar sized specimens at Oregon State University. Standard slump tests were conducted and water added where necessary to achieve a 5 in. (127 mm) slump. The actual concrete compressive and tensile strengths tests were performed in accordance with ASTM C39/C39M-09 and ASTM C496/C496M-11, respectively. Cylinders were field cured next to the girder specimens before testing. Average test-day concrete cylinder compressive and tensile strengths are reported in Table 3.3. Specimens had a test-day minimum compressive strength target of 3300 psi (22.8 MPa) not to exceed 4100 psi (28.3 MPa).

**Table 3.3: Test-day concrete compressive and tensile strengths (3 replicates).**

| Specimen | Concrete Age (days) | Avg. $f_c'$ | Standard Deviation $f_c'$ | Avg. $f_{ct}$ | Standard Deviation $f_{ct}$ |
|---|---|---|---|---|---|
| | | (psi) [MPa] | (psi) [MPa] | psi [MPa] | psi [MPa] |
| T.45.Ld3(10).Ti | 36 | 3712 [25.6] | 169 [1.17] | 418 [2.9] | 17.8 [0.12] |
| T.45.Ld3(6).Ti | 30 | 3823 [26.4] | 65.0 [0.45] | 363 [2.5] | 7.3 [0.05] |
| T.45.Ld3(6).SS | 40 | 3206 [22.1] | 190 [1.31] | 416 [2.9] | 38.9 [0.27] |
| IT.45.Ld3(10).Ti | 44 | 4056 [28.0] | 371 [2.56] | 476 [3.3] | 36.7 [0.25] |
| IT.45.Ld3(6).Ti | 35 | 3734 [25.7] | 38.0 [0.26] | 385 [2.7] | 59.6 [0.41] |
| IT.45.Ld3(6).SS | 42 | 3525 [24.3] | 76.3 [0.53] | 394 [2.7] | 35.7 [0.25] |
| IT.0.0(6).Ti | 59 | 3397 [23.4] | 263 [1.81] | 429 [3.0] | 42.6 [0.29] |

### 3.3.2 Internal Reinforcing Steel

All reinforcing steel was provided by local rebar fabricators. The transverse reinforcing bars were ASTM A615 (2009) Gr. 40, #4 (Grade 280, M13) and were made from a steel heat with the lowest available yield stress at the time of purchase. The longitudinal reinforcement was ASTM A706 (2009) Gr. 60, #11 (Grade 420, M36). The material properties for all the steel reinforcement were determined in accordance with ASTM E8/E8M-13a. The average measured material properties from three replicate samples are reported in Table 3.4. The transverse reinforcing steel used in the specimens was a reasonable approximation of ASTM A305 (1950) Gr. 40 (Grade 276) steel available in the 1950's. Regrettably, Gr. 40 (Grade 276) #11 (M36) bars are not commercially available and Gr. 60 (Grade 420) bars were used as a substitute. These should provide conservative results due to larger bond demands and lower dowel action, compared to the lower grade bars for similar member strength.

**Table 3.4: Average reinforcing steel properties (three replicates)**

| Type | Bar Size | Grade (ksi) [MPa] | $f_y$ (ksi) [MPa] | $\sigma$, $f_y$ (ksi) [MPa] | $f_u$ (ksi) [MPa] | $\sigma$, $f_u$ (ksi) [MPa] |
|---|---|---|---|---|---|---|
| Transverse | #4 [M13] | 40 [280] | 50.2 [346] | 0.12 [0.83] | 79.6 [549] | 0.17 [1.17] |
| Construction | #6 [M19] | 60 [280] | 72.2 [498] | 0.14 [0.96] | 107 [735] | 0.06 [0.41] |
| Longitudinal | #11 [M36] | 60 [420] | 71.6 [494] | 1.26 [8.69] | 107 [738] | 0.93 [6.41] |

### 3.3.3 NSM Materials

Two NSM materials were used in the test program: titanium and stainless steel. Material tests were conducted in accordance with ASTM E8/E8M-13a. For both materials, 2 in. (50 mm) gage lengths were used on the tensile coupons.

The stainless alloy used was Enduramet 32. The alloy was chosen for its high strength, ductility, and its work hardening characteristics. Enduramet 32 is a "low-nickel, nitrogen strengthened austenitic stainless steel" (Carpenter Technology Corporation, 2006). The alloy is recommended for use in bridge deck repair, retaining walls, and coastal infrastructure. Enduramet 32 meets or exceeds the requirements for ASTM A955 with a nominal yield strength of 75 ksi (517 MPa). The unit weight of the stainless steel alloy is 483 lb/ft$^3$ (7747 kg/m$^3$), slightly lower than mild steel. Generally, stainless steel does not have a well-defined yield plateau. The average measured yield stress was 83 ksi (572 MPa) with 0.82% COV, the average ultimate stress was 127 ksi with

0.28% COV, and the average elongation was 49% with a 9.05% COV. Table 3.5 describes the NSM material properties.

**Table 3.5: NSM reinforcing bar properties (three replicates).**

| Reinforcement Type | Bar Size | Bar Area ($in^2$) [$mm^2$] | Grade (ksi) [MPa] | Avg. $f_y$ (ksi) [MPa] | StDev., $f_y$ (ksi) [MPa] | Avg. $f_u$ (ksi) [MPa] | StDev., $f_u$ (ksi) [MPa] |
|---|---|---|---|---|---|---|---|
| Stainless Steel | #5 | 0.31 | 75 | 83.0 | 0.68 | 127.3 | 0.35 |
| | [M16] | [7.9] | [520] | [572] | [4.69] | [878] | [2.41] |
| Titanium Alloy | 5/8 in. | 0.2975 | n/a | 145.4 | 1.56 | 158.1 | 1.39 |
| | [M16] | [7.6] | | [1002] | [10.75] | [1090] | [9.58] |

Titanium is not commonly used in civil infrastructure applications. The majority of titanium is used in medical and aerospace industries. The titanium manufacturer follows strict material and dimensional tolerances required for the aerospace industry, thus, the titanium used in this study exhibited remarkably small coefficients of variation (COV). The titanium alloy contains 6% aluminum and 4% vanadium (Ti-6Al-4V), and meets ASTM B348 specifications. Titanium has a low coefficient of thermal expansion of around 4.78 μin/in °F (8.6 μm/m °C), and is impervious to environmental deterioration in common structural engineering applications. The unit weight of titanium is around half that of steel. Titanium has a unit weight of 276 $lb/ft^3$ (4419$kg/m^3$), much less than the unit weight steel of 490 $lb/ft^3$ (7846 $kg/m^3$). The titanium was fabricated with a unique surface treatment in lieu of the standard rebar deformation pattern in order to enhance bond at the titanium and epoxy interface, as illustrated in Fig. 3.32.

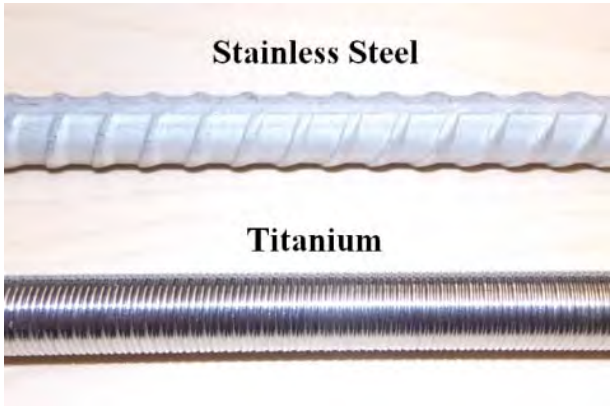


Figure 3.32: Deformation patterns on stainless steel (top) and titanium (bottom).

Stress-strain curves show that the titanium exhibited almost ideal elasto-plastic behavior, as shown in Figure 3.33. Because neither material exhibited a well-defined yield plateau, the yield stress was found using a 0.2% strain offset. The titanium bars had a yield stress of 145.2 ksi (1000 MPa) with 1.01% COV, an ultimate stress of 158.1 ksi (10,090 MPa) with 0.88% COV, and elongation of 11.3% with a 2.66% COV. The nominal modulus of elasticity for titanium is

15,500 ksi (106,800 MPa), while the average measured modulus was computed as 15,120 ksi (104,200 MPa). The stiffness of titanium is approximately half that of steel.

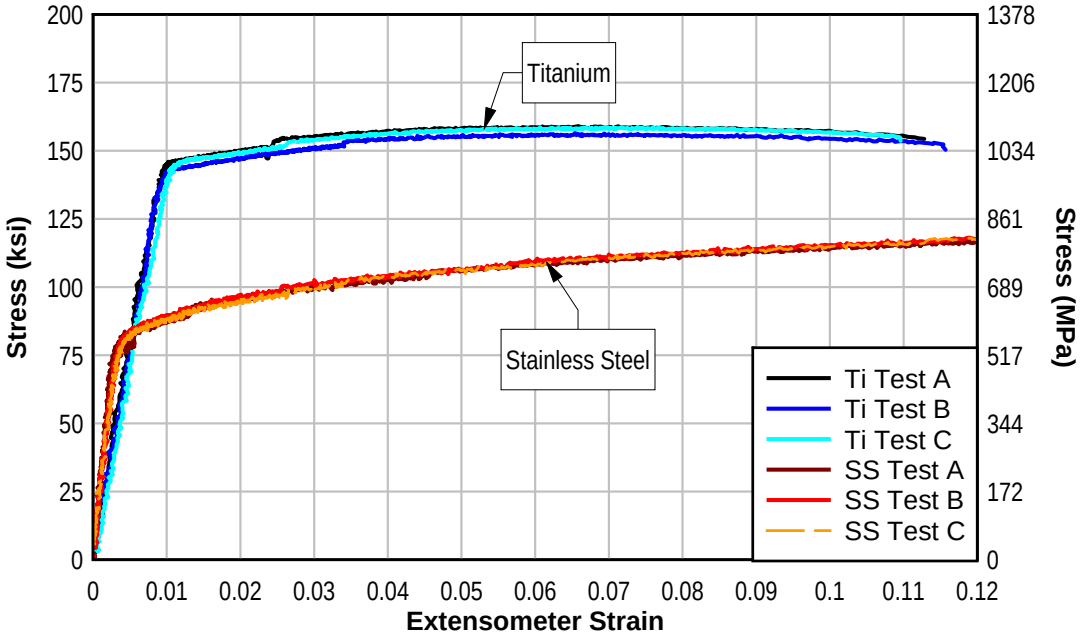


Figure 3.33: Stress-strain relationships for the titanium alloy and stainless steel bars.

The stainless steel and titanium alloy bars were bonded in the concrete grooves using a commercially available general purpose gel epoxy adhesive (CONCRESIVE 1420). This is a non-sag epoxy widely used for bonding to concrete. The manufacturer reported material properties for the epoxy were tensile strength of 4 ksi (27.6 MPa), elongation at break of 1.0%, compressive yield strength of 12.5 ksi (86.2 MPa), and 2-day cure bond strength greater than 2 ksi (13.8 MPa).

## 3.4 INSTRUMENTATION

To collect data necessary for analysis, internal and external sensors were applied prior to testing. Data from all sensors were sampled at 5 Hz or 0.20 sec. intervals. Details and labeling conventions for the internal and external sensor arrays are described in Appendices A and B for the IT and T specimens, respectively.

### 3.4.1 Internal Sensor Array

Bondable foil strain gages were used for the internal sensor array. The strain gages were general purpose linear strain gages and had 0.062 in. (1.6 mm) gage length with a 120 Ω resistance. The output of the collected data was in units of microstrain.

The steel reinforcing bars were instrumented with strain gages prior to tying the reinforcing bar cage shown previously. The process of applying a strain gage is summarized in Figure 3.34. The bar deformations and mill scale were removed by grinding. The area was smoothed with a fine

grit sand paper. The area was cleaned using an acidic solution followed by a neutralizer as per recommendations by the strain gage manufacturer. The strain gage was adhered to the surface with cyanoacrylate adhesive. The strain gage was soldered to wire leads, tested for resistance, and covered with several protective layers. A water-proof electrical insulation coating was applied first, then, a rubber mastic, and finally, aluminum tape to protect the strain gages during concrete placement.


Figure 3.34: Application of strain gage on reinforcing bar.

Instrumentation at each critical section included a strain gage on the hooked and cutoff reinforcing steel bars as well as the metallic NSM bars, as illustrated in Figure 3.35. Due to symmetry, instrumentation was only applied to a quarter of each specimen. The locations of the longitudinal and transverse strain gages were similar to the baseline specimens to enable comparisons.

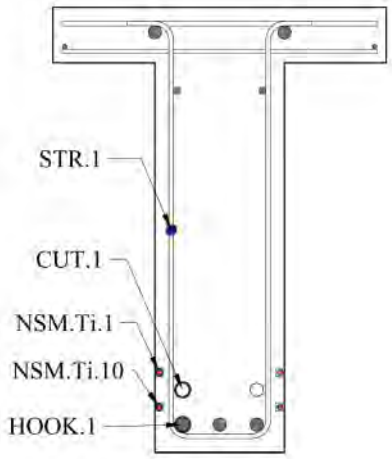


Figure 3.35: Typical titanium strengthened specimen cross section with labeled internal sensors for T-specimen.

Longitudinal instrumentation was specifically focused around the termination of the cutoff bar and NSM reinforcement. At each section of interest, at least three strain gages were placed 6.5 in (165 mm) apart. A series of strain gages along the termination of the cutoff internal flexural bar was implemented to assess bond stresses. Figures 3.36 and 3.37 identify the strain gages in their relative positions along the length of typical T and IT specimens, respectively. Complete details of the placements of all strain gauges are shown in Appendices A and B for all specimens. The unique details of Specimen IT.0.0(6).Ti required a different strain gauge pattern is illustrated in Figure 3.38.

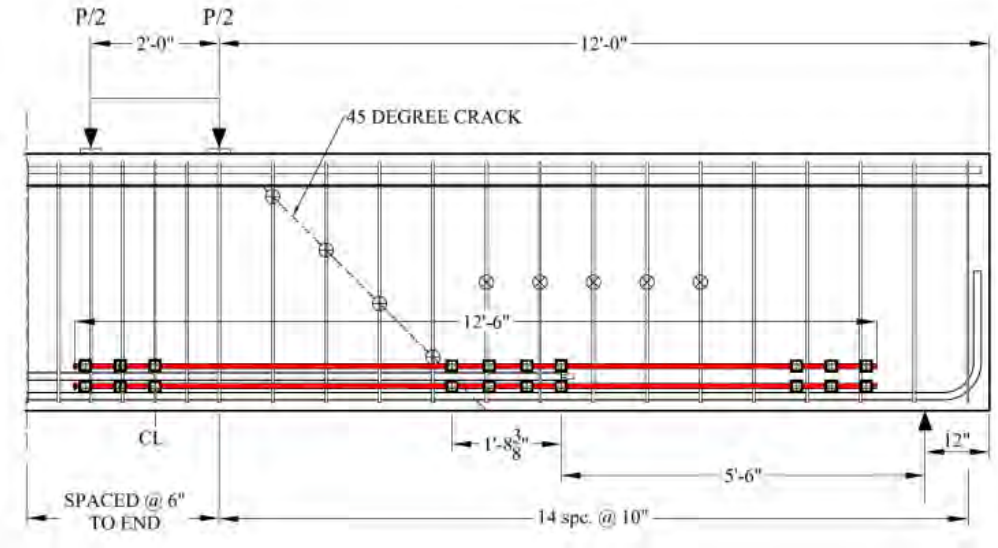


Figure 3.36: Typical internal sensor array for T specimens (10 in. stirrup spacing).

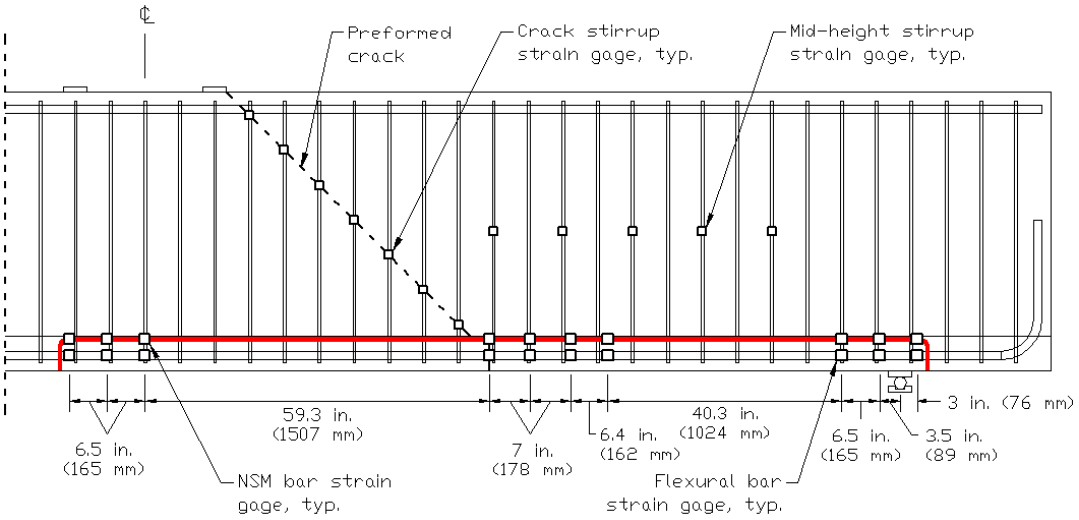


Figure 3.37: Typical internal sensor array for IT specimens (6 in. stirrup spacing).

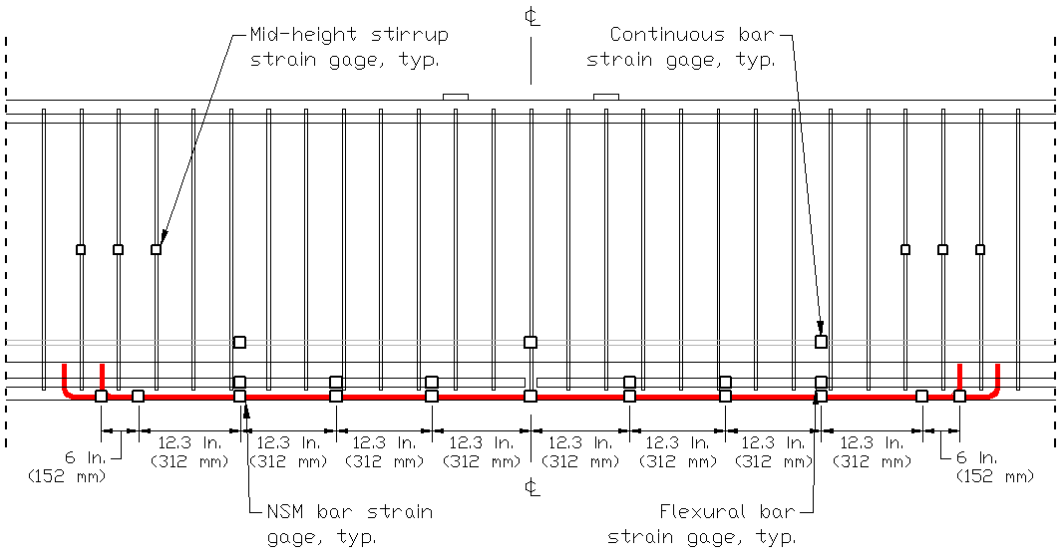


Figure 3.38: Specimen IT.0.0(6).Ti strain gage locations.

To assess the shear force in the stirrups, strain gages were bonded to one leg of the transverse reinforcing steel. Four stirrups intersecting the preformed-diagonal crack were instrumented with strain gages for specimens with 10 in. (254 mm) stirrup spacing and six stirrups were instrumented for specimens with 6 in. (152 mm) stirrup spacing. Other stirrups along the specimen which instrumented at mid-height.

Strain gages were placed on the NSM titanium alloy bars at locations coincident with those of the cutoff and hooked bar strain gages. The stainless steel bar instrumentation pattern differed somewhat due to the increased number of bars. The stainless steel reinforcing bars with the largest and smallest distance (top and bottom) from the compression zone had coincident strain gages as the hooked steel. The remaining stainless steel bars had strain gages at the end of the bar and along the diagonal crack location. Appendices A and B provide detailed information about strain gage labeling and locations.

### 3.4.2 External Sensor Array

Several other types of sensors were used to monitor the overall response of the specimens: load cell, string potentiometers, displacement sensors, and tilt sensors. All displacement sensors had units of inches and the tilt sensors measured in units of degrees, loads were measured in units of kips.

Four potentiometers were used to measure the net deflection of the specimen, two at each side of midspan, and two support locations. The midspan displacement was monitored with two 10 in. (254 mm) stroke string potentiometers. Displacement on each side of the web was measured to calculate the average midspan displacement. Each string potentiometer was attached to a steel dowel bonded into a hammer-drilled hole in the stem. An example of a string potentiometer used to measure midspan displacement is shown in Figure 3.39a.

Support settlements were measured with two 1.5 in. (38.1 mm) displacement sensors. The sensor was clamped to a metal stand and reacted off of an aluminum angle bonded to the web of the

beam. Measured north and south settlements were averaged and subtracted from the measured midspan displacement for the true midspan displacement. A typical support displacement sensor is shown on the right in Figure 3.39b.

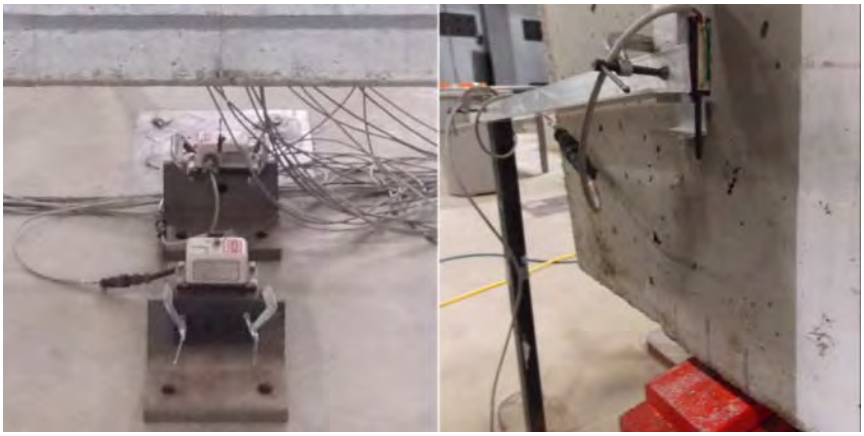

a) b)

Figure 3.39: Midspan displacement (a) and support settlement (b).

Two 1 in. (25.4 mm) stroke displacement sensors were used to measure slip of the cutoff steel reinforcing bars relative to the surrounding concrete. Blockouts were used at the ends of the cutoff bars for the T and IT specimens to enable placement of the instrumentation, as illustrated in Fig. 3.40a. In later tests for T specimens (T.45.Ld3(6)Ti and T.45.Ld3(6)SS) a different approach was devised as illustrated in Figure 3.40b. Here a PVC port method is shown which eliminated the need for a larger block-out.

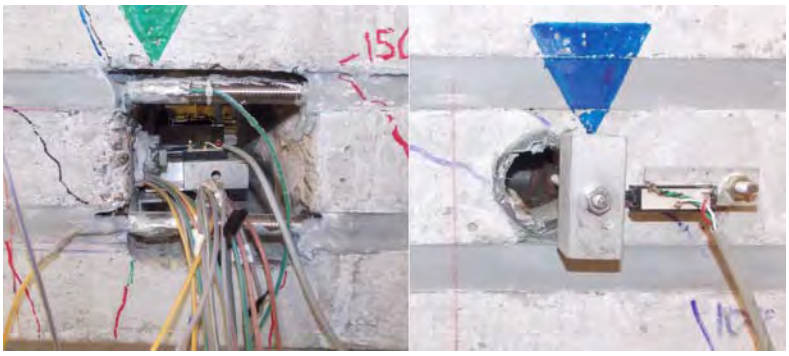

a) b)

Figure 3.40: Slip displacement sensor configurations a) blockout in T and IT specimens, and b) PVC port used in later T specimens.

Tilt sensors were attached to one side of the web over each support. The sensors measured the end rotation of each end of the specimen during testing.

Pairs of diagonal displacement sensors were used to measure crack initiation and propagation over regions of the beam. Each displacement sensor had a range of 1 in. (25.4 mm). The diagonal

displacement sensors were attached to small threaded rods epoxied in the concrete web. The configuration of a typical diagonal displacement setup is illustrated in Figures 3.41 and 3.42 for the T and IT specimens, respectively. Diagonal displacement configurations for each specimen can be found in Appendices A and B.

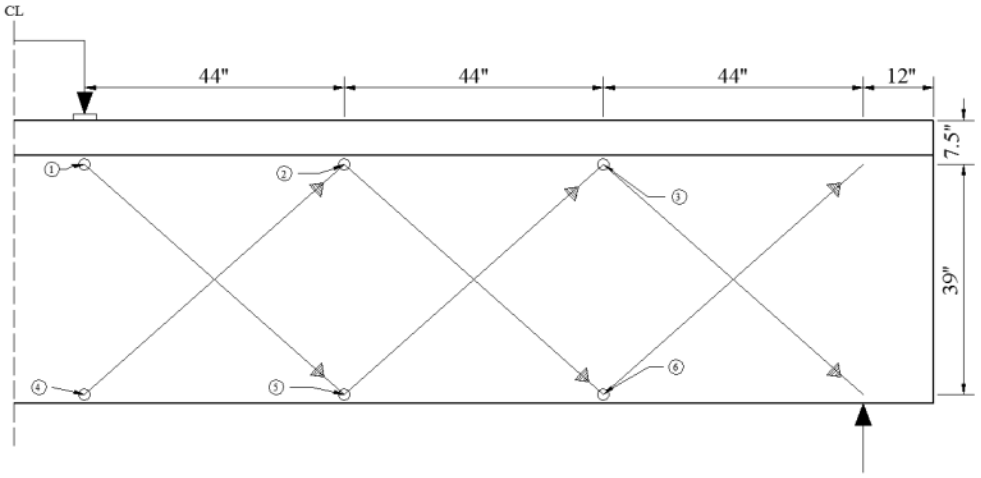


Figure 3.41: Typical location of diagonal displacement sensors for T specimens.

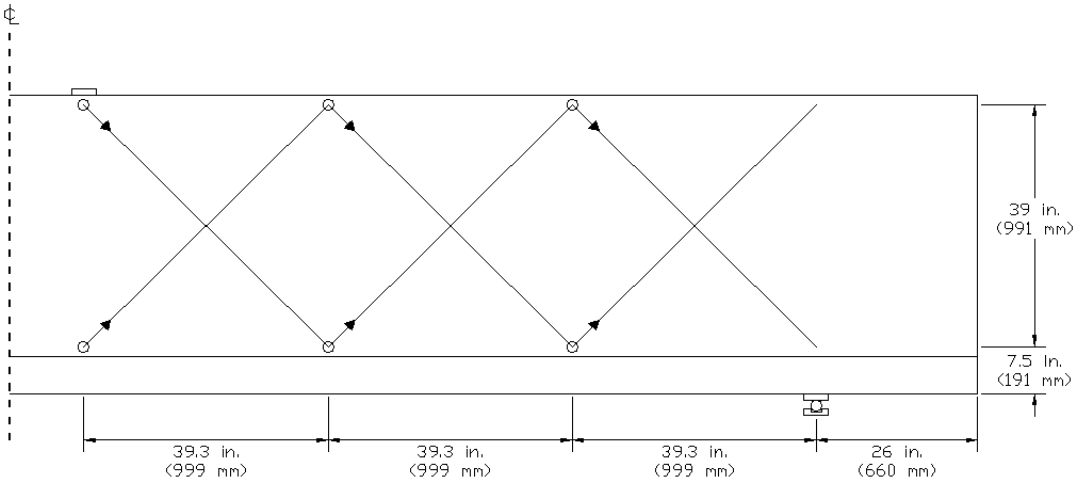


Figure 3.42: Typical specimen diagonal displacement sensor layout for IT specimens.

## 3.5 TEST PROTOCOLS

All specimens were tested in the Structural Engineering Research Laboratory at Oregon State University. A reaction frame was built to apply four-point loading to the specimens. The reaction frame was anchored into the strong floor and held a servo-hydraulic load-controlled actuator. The actuator had a 500 kip (2224 kN) capacity and a 30 in. (762 mm) stroke. All specimens were simply supported. The T-specimens had a span length of 24 ft (7.32 m) between centerlines of supports and the IT-specimens had a span length of 21.7 ft (6.60 m) between centerlines of supports. The actuator force was distributed through a spreader beam creating a 2 ft (610 mm) constant moment region at midspan. All reaction points distributed the load from a 4 in. (101.6

mm) plate on a 2 in. (50.8 mm) diameter captive roller. Loading plates at midspan were leveled with a high-strength grout. Prior to testing, the actuator was plumbed, and loading plates were shimmed where necessary. The loading setup is illustrated in Figure 3.43.

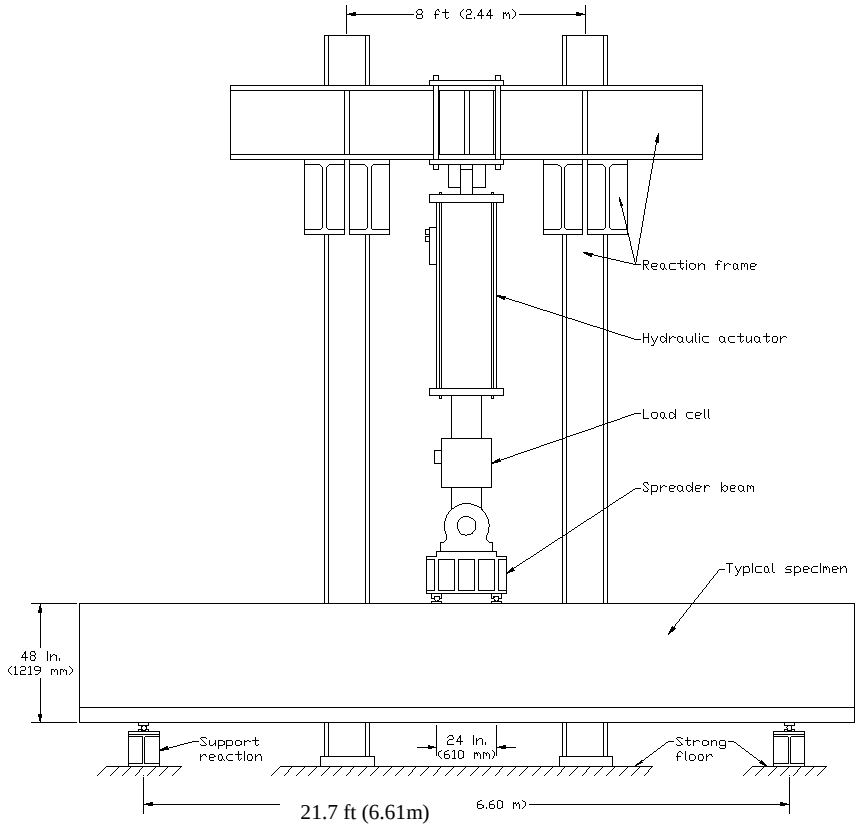


Figure 3.43: Test setup shown with IT-girder test span.

The load was increasingly applied in 50 kip (222 kN) increments followed by unloading to a minimum load of 5 kips (22.2 kN) and continued until specimen failure. The loading rate was pseudo-static at 1 kip/sec (4.4 kN/sec). After reaching each target load step, the load was reduced by 25 kips (111 kN) then held to minimize creep effects while cracks were identified, marked, and photographs were taken.

## 3.6 SUPPLEMENTAL TESTS OF BOND, PULLOUT, AND HOOK DUCTILITY

In parallel with the full-size girder tests, three other characterization tests were performed. A bond strength study was performed on the titanium and stainless bars to investigate the bond stress transfer between the epoxy-bar and epoxy-concrete interfaces. Pull-out tests and hook ductility tests were also conducted on the NSM titanium bars to assess ductility of alternative details and bond strength of different surface treatments.

### 3.6.1 Bond Stress Tests

An adaptation of ASTM A944-10 (2010) was used to characterize the bond of titanium alloy bars in a NSM configuration. Six 9x12x24 in. (229x305x610 mm) concrete blocks were constructed with two Gr. 60 (Gr. 420) #4 (13M) internal reinforcement bars. Each specimen had a saw-cut 15/16 in. (24 mm) square groove cut into the top of the block. Three specimens embedded the NSM material in epoxy for 4 in. (101.6 mm) and three specimens embedded the NSM material in epoxy for 12 in. (305 mm). The concrete had a compressive strength of 4443 psi (30.6 MPa) and a tensile strength of 389 psi (2.68 MPa) from three replicate cylinder tests.

Three displacement sensors monitored the elongation and slip of the NSM reinforcing bar. One was placed inside the groove to measure the slip at the stress-free end (also called the embedded end) of the bar. Another sensor was placed at the end of the block to measure the loaded end elongation. A vertical sensor was placed at the free end of the embedded NSM bar to measure any vertical movement.

The specimens with 12 in. (305 mm) embedment length were instrumented with three strain gages distributed along the bond length. The strain gages were located at 3 in. (76.2 mm), 6 in. (152.4 mm), and 9 in. (228.6 mm) from the stress-free end of the bar. The design intent of the 12 in. embedded length was to measure the active bond length and characterize a stress transfer. All data were collected at a sampling rate of 10 Hz.

The NSM material was epoxied into the groove and a 55 kip (245 kN) servo-hydraulic actuator was used to pull the NSM material (loaded end) out of the block. The loading rate was 0.002 in/sec (0.051 mm/sec) and the block reacted off of an angle bolted to the loading apparatus. Any upward eccentricity was counteracted with a tensioned plate reacting off the unloaded end of the specimen illustrated in Figure 3.44. The typical reinforcing cage is shown in Figure 3.45, and the loading setup is pictured in Figure 3.46.

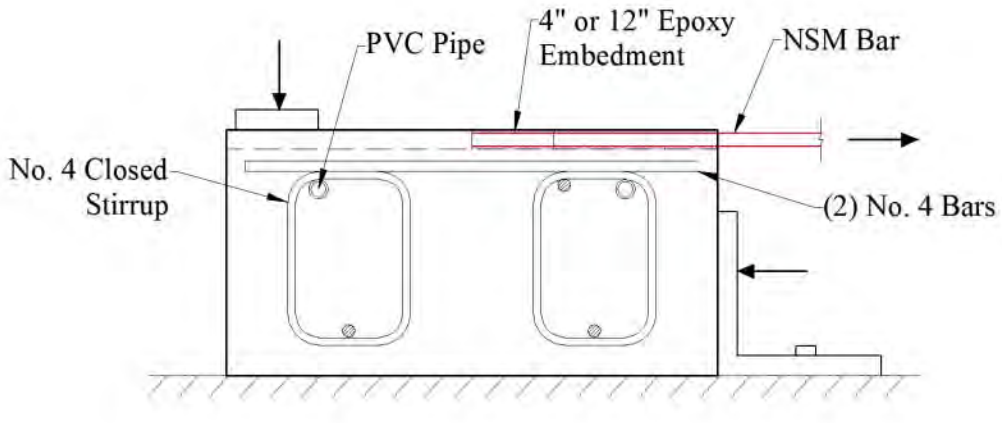


Figure 3.44: Schematic of bond length specimen.

Figure 3.45: Reinforcing cage for bond length specimens.

Figure 3.46: Loading setup for bond length specimens.

### 3.6.2 Pullout Tests

Pullout tests were performed to evaluate the strength of the titanium-epoxy interface. Titanium bars are typically fabricated to be smooth and without defects. Therefore, the manufacturer developed five alternative surface finishes to enhance bond along the bar surface including: surface blasted, rough finish, light turn, light turn blasted, and heavy turn. Examples are shown in Figure 3.47. Tensile tests were performed on each bar type. One bar of each surface roughness was used for pullout testing. After testing, the heavy turn finish was selected for use in NSM strengthening of the girder specimens. Three additional pullout tests were performed on the heavy turn finished titanium alloy bars.

Figure 3.47: Initial surface roughness samples (top to bottom: surface blasted, rough finish, light turn blasted, light turn, and heavy turn).

Four additional tests were performed on titanium alloy bars with a “bulb” end. Two of these tests used the light turn bars while the other two used the surface blasted bars. Three of the bars were taken to a blacksmith and forged using conventional forging techniques. Of these, one light turn bar was fabricated with a bulb on the end and the blasted bars were fabricated with an end bulb on one and the other with a bulb in the middle of the length to be embedded for the pullout test. The other light turn bar was fabricated by heating with an oxy-acetylene torch and the end was hammered by hand into a bulb shape. The method of hammering by hand was not effective. Examples of the fabricated “bulbs” can be seen in Figure 3.48.

Figure 3.48: Bulb end samples for pullout testing.

For the pullout tests, 0.75 in. (19 mm) diameter holes were drilled to a depth of 5 in. (127 mm) into concrete blocks. The holes were filled approximately halfway with a general purpose gel epoxy adhesive that is widely used for bonding to concrete (Concresive 1420). A bar specimen was inserted into the hole and pushed through the epoxy until it reached the bottom of the hole. The bar was centered in the hole and set perpendicular to the concrete face. Excess epoxy above the hole was removed and the epoxy was finished flush with the concrete. The epoxy was then allowed to cure for a minimum of seven days before testing.

The pullout test setup used a large plate with a 2 in. (51 mm) diameter hole that was placed over the bar that reacted the pullout force against the concrete surface very close to the embedded bar. This purposely confined the concrete to prevent a pullout cone failure that could otherwise occur

given the shallow embedment length. A hollow-core hydraulic jack was positioned on top of the plate. The jack was connected to a hydraulic hand pump. Two additional plates were placed on top of the jack. These plates allotted for full bearing between the hydraulic jack and a donut load cell. On top of the load cell, a prestressing chuck was leveled by spherical washers. Lastly, a 1.5 in. (38 mm) vertical displacement sensor was placed on the tip of the bar specimen to measure the vertical movement during loading. Figure 3.49 shows the setup for pullout tests.


Figure 3.49: Pullout test setup and hydraulic hand pump.

Tests were performed manually by increasing the hydraulic pressure to the jack by a hand pump. Tests concluded after failure of a cone of concrete and epoxy or the bar specimen sheared through the epoxy. Additional loading only provided the sliding friction required to drag the cone or bar specimen through the concrete or epoxy, respectively.

### 3.6.3 Hook Ductility Tests

Hook ductility tests were performed to assess the load capacity and ductility of the mechanical hooks at the ends of the titanium bars. Tests were performed on the heavy turn titanium alloy bars bent into180˚ hooks to assess the hook ductility at various bending temperatures and diameters. A testing apparatus was designed and fabricated to test the hooks by transversely pulling on both legs of the hooks.

The hooks were heated in a forge using color indication to identify the temperature of the bar. After heating, the bars were inserted into a rebar bending machine and bent around a bending pin. A total of 12 samples were fabricated. Three sets of (3) replicates were heated to 900 ˚F (482 ˚C) and bent around 2 in. (51 mm), 3 in. (76 mm), and 4.5 in. (114 mm) diameter bending pins, respectively. An additional three samples were heated to 1250 ˚F (677 ˚C) and bent around the 2 in. (51 mm) diameter bending pin. An example of each set can be seen in Figure 3.50. Due to springback in the titanium alloy, the samples that were bent around the 4.5 in. (114 mm) bending

pin ended up with final an inner diameter of 5.0 in. (127 mm). The inner diameters of all the other samples matched the pin they were bent around.

Figure 3.50: 180˚ hook specimen examples.

Testing was performed using a 110 kip (489 kN) universal testing machine (UTM). The hooks were inserted through 0.6875 in. (17.5 mm) diameter drilled holes in A572 Grade 50 (Grade 340) steel plates. After placing the hook through the steel plates, a prestressing chuck was inserted over each leg to prevent the titanium from pulling out during testing. The plates were gripped by the UTM machine and pulled at a rate of 0.01 kip/sec (0.254 kN/sec). A typical experimental setup is shown in Figure 3.51 and the dimensions are illustrated in Fig. 3.52. Two displacement sensors were used to measure opening displacement of the hook (separation of the plates). To ensure repeatability of the hook tests, the distance, *e*, from the bearing plates to the outside of the hook as shown in Figure 3.53 was established as:

$$e = 2 + \left( \frac{Ø - 2}{2} \right) \tag{4.3}$$

where *Ø* is the inside hook diameter (in.).

Figure 3.51: Sample 180˚ hook in test setup.

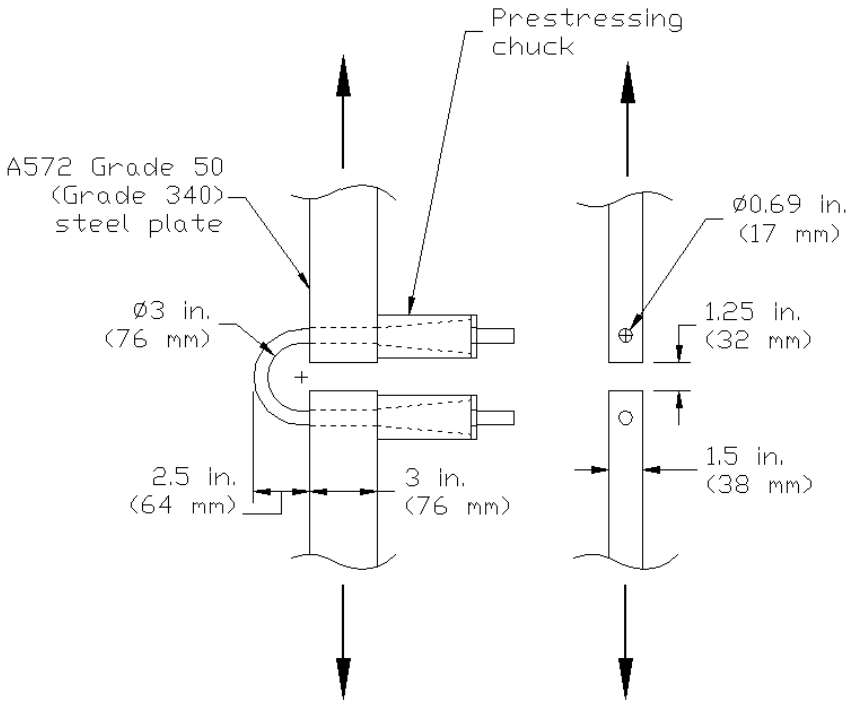


Figure 3.52: Plan and elevation of 3 in. (76 mm) diameter hook specimen test setup.

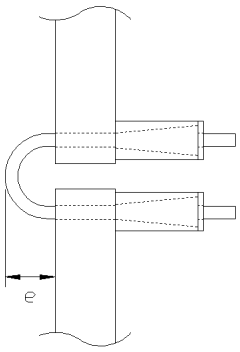


Figure 3.53: Distance from outside of hook to bearing plate.

# 4.0 EXPERIMENTAL RESULTS

This chapter describes the experimental results of the T and IT girder specimens tested in this research program. The tested specimens were compared to similar specimens from Triska and Goodall *(Triska and Goodall 2010)*. The reported data include the overall member response, tension strains and distributions in the internal reinforcing steel and NSM bars, and bond stress of the full-scale specimens. Also reported in this section are the results of the sub-assemblage bond tests, pullout tests, and hook ductility tests. Comprehensive data sets for all specimens and tests are reported in Appendices A and B.

## 4.1 GIRDER SPECIMEN RESPONSE

All of the NSM-strengthened T and IT girder specimens were tested to failure. The loads were converted into shear force on failed section using statics and the geometry of the simply supported span of the test specimens. The shear force applied by the actuator ($V_{APP}$), dead load shear ($V_{DL}$), total shear ($V_{EXP}$), midspan displacement, and observed failure crack angle are reported in Table 4.1. The reported midspan displacement corresponds to the peak load. The total shear is the applied shear from the actuator plus the dead load shear acting across the failure crack plane. Dead load shear was calculated from the self-weight of the concrete (using a unit weight of 150 pcf (23.6 kN/m$^3$)) acting across the failure plane.

**Table 4.1: Summary of specimen capacity and midspan displacement.**

| Specimen | Applied Load | $V_{APP}$ | $V_{DL}$ | $V_{EXP}$ | Midspan Disp. | Failure Crack Angle |
|---|---|---|---|---|---|---|
| | kips [MN] | kips [kN] | kips [kN] | kips [kN] | in. [mm] | degree |
| SPRT.45.Ld3(10) | 299.5 | 149.8 | 3.1 | 152.9 | 1.14 | 33 |
| | [1.33] | [665] | [14] | [679] | [29] | |
| T.45.Ld3(10).Ti | 392.9 | 196.5 | 3.5 | 200.0 | 2.11 | 33 |
| | [1.75] | [874] | [16] | [890] | [54] | |
| T.45.Ld3(6).Ti | 430.7 | 215.4 | 1.0 | 216.4 | 3.12 | 90 |
| | [1.92] | [958] | [4.0] | [963] | [79] | |
| T.45.Ld3(6).SS | 429.3 | 214.7 | 1.0 | 215.7 | 2.59 | 90 |
| | [1.91] | [955] | [4.0] | [959] | [66] | |
| IT.45.Ld3(10).Ti | 420.5 | 210.2 | 3.6 | 213.8 | 1.12 | 36 |
| | [1.87] | [935] | [16] | [951] | [28] | |
| IT.45.Ld3(6).Ti | 448.0 | 224.0 | 0 | 224.0 | 1.06 | 90 |
| | [1.99] | [996] | [0] | [996] | [27] | |
| IT.45.Ld3(6).SS | 500.0 | 250.0 | 0 | 250.0 | 1.15 | 90 |
| | [2.22] | [1112] | [0] | [1112] | [29] | |
| IT.0.0(6).Ti` | 191.3 | 95.7 | 0 | 95.7 | 1.48 | 90 |
| | [0.85] | [426] | [0] | [426] | [38] | |
| SPR IT.45.Ld2(10).(5) | 358.9 | 179.5 | 4.8 | 184.3 | 0.98 | 44 |
| | [1.60] | [798] | [26] | [820] | [25] | |
| SPR IT.45.Ld2(10).(6) | 450.8 | 225.4 | 3.4 | 228.8 | 0.97 | 32 |
| | [2.01] | [1003] | [19] | [1018] | [25] | |
| SPR IT.0.0(10).(5) | 401.4 | 200.7 | 4.6 | 205.3 | 1.20 | 30 |
| | [1.79] | [893] | [20] | [913] | [30] | |

Specimens IT.45.Ld3(6).Ti and IT.45.Ld3(6).SS both failed in flexure at the ends of the NSM bars near midspan. No anchorage failures were observed for these specimens. Specimen IT.45.Ld3(10).Ti failed in shear which subsequently resulted in pullout of the anchorage. The specimen with discontinuous reinforcement at midspan (IT.0.0(6).Ti) failed in flexure with the titanium alloy bars eventually debonding, resulting in one of the hooks pulling out of the specimen. Specimen T.45.Ld3(10).Ti failed in shear subsequently resulted in pullout of the

anchorage. Specimens T.45.Ld3(6).Ti and T.45.Ld3(6).SS both failed in flexure, with no observed anchorage failures.

Comparison of the failure loads with comparable baseline specimens tested by Triska and Goodall (2010) (the SPR specimens) showed the NSM-strengthened specimens achieved substantially greater capacity than the similar baseline specimens. The NSM-strengthened specimens exhibited larger deformation capacity at failure and also displayed more distributed cracking with manifest signs of distress prior to failure. For the T specimens, specimen T.45.Ld3(10).Ti delayed the onset of an anchorage slip. Specimens T.45.Ld3(6).Ti and SS eliminated anchorage shear-tension failures (specimens failed in flexure).

The specimen T.45.Ld3(10).Ti exhibited increased load capacity of 31% and increased midspan displacement of 85% compared with the baseline specimen SPRT.45.Ld3(10). Specimens T.45.Ld3(6).Ti and T.45.Ld3(6).SS both failed in flexure with a failure crack close to 90 degrees near midspan. Specimen T.45.Ld3(6).Ti increased the capacity by 44% and deformation by 174%, while specimen T.45.Ld3(6).SS increased capacity by 43% and deformation by 127% compared to the unretrofitted baseline specimen. It should be noted that for specimens T.45.Ld3(6).Ti and T.45.Ld3(6).SS, had increased numbers of stirrups over the development length of the cutoff bars which contributed to the increase in strength and deformation capacity. . . For IT specimens, the closest comparison of the NSM strengthened specimen IT.45.Ld3(10).Ti was to SPR IT.45.Ld2(10).(5). The NSM strengthened specimen showed a 17% increase in strength and 14% increase in deformation, even though it contained a shorter anchorage length for the cutoff bar. This specimen also exhibited larger capacity than SPR IT.0.0(10).(5), which had no flexural cutoff bars (all bars were well anchored). Specimens IT.45.Ld3(6).Ti and IT.45.Ld3(6).SS produced flexural failures which were not comparable to baseline specimens. However, these illustrated that the approach can effectively change the failure mode from anchorage/shear to flexure, which can take full advantage of the existing flexural steel.

### 4.1.1 Load-Deformation Response of Girder Specimens

The load and deformation response describes the overall behavior of the specimens. Load deformation responses for T-specimens are shown in Figure 4.1 and for the IT specimens in Figures 4.2 to 4.6. Each specimen was loaded in 50 kip increments, unloaded, and then preceded to the next load step until eventual failure. If the specimen was close to failure the load cycle was extended until the maximum capacity was reached.

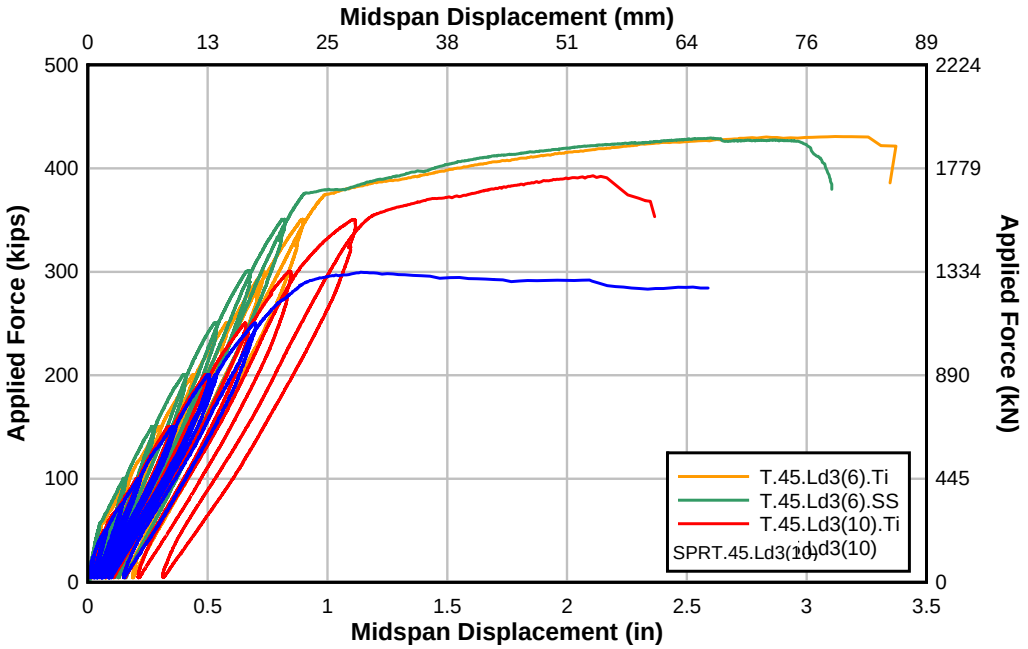


Figure 4.1: Overall load-displacement response at midspan for T specimens.

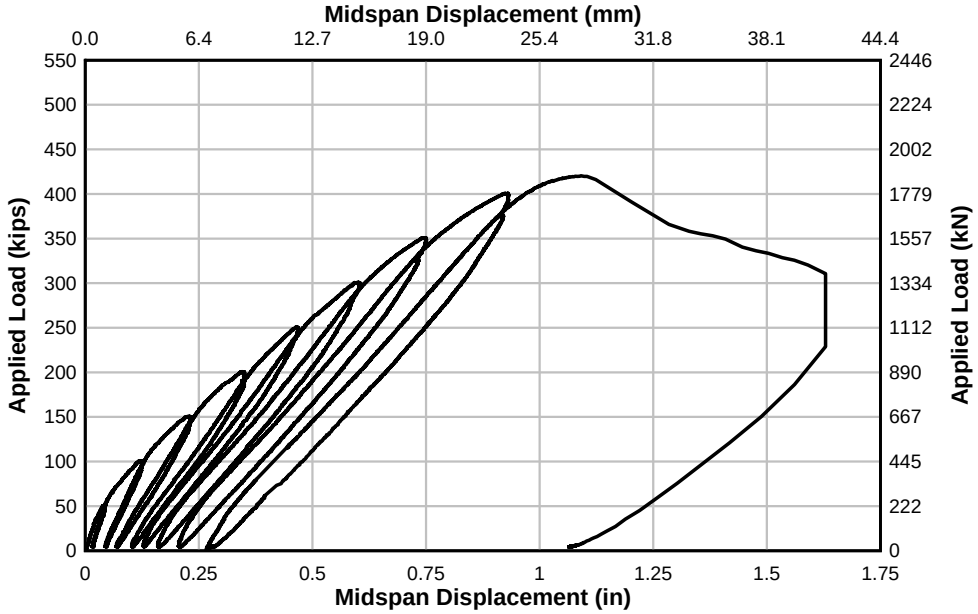


Figure 4.2: Specimen IT.45.Ld3(10).Ti load-displacement response at midspan.

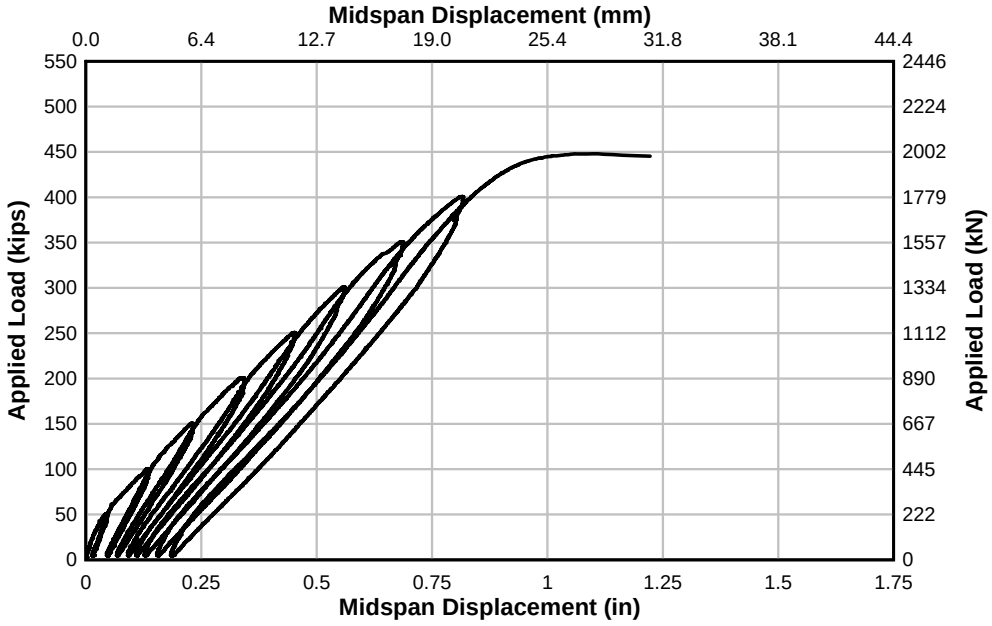


Figure 4.3: Specimen IT.45.Ld3(6).Ti load-displacement response at midspan.

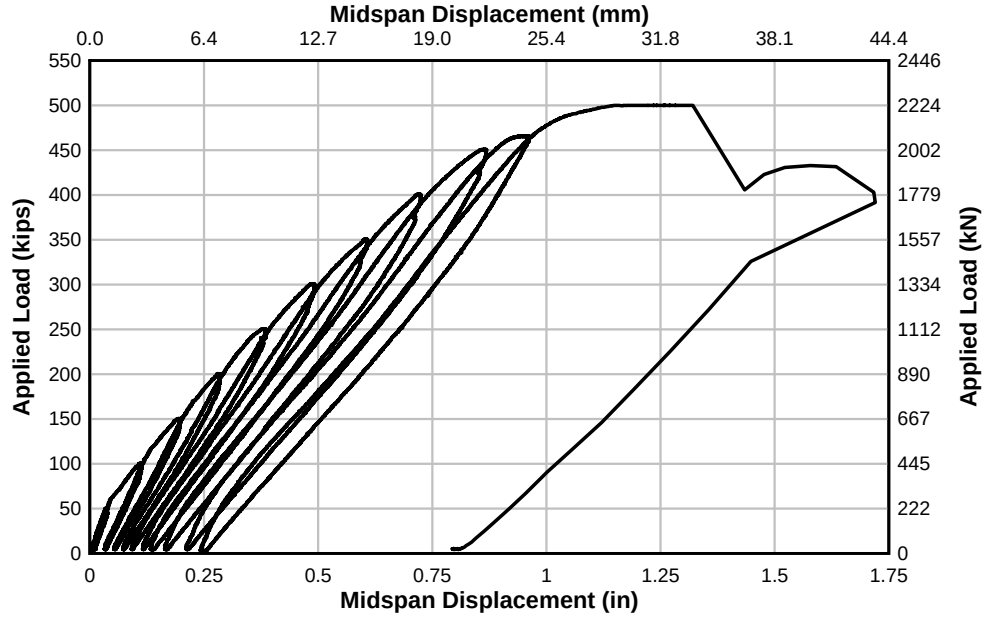


Figure 4.4: Specimen IT.45.Ld3(6).SS load-displacement response at midspan.

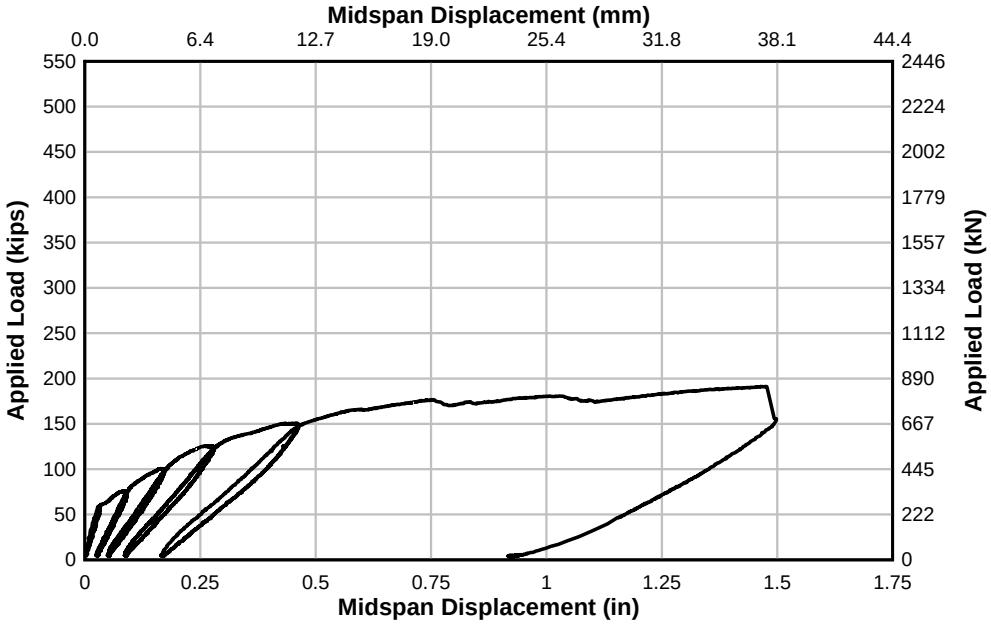


Figure 4.5: Specimen IT.0.0(6).Ti load-displacement response at midspan.

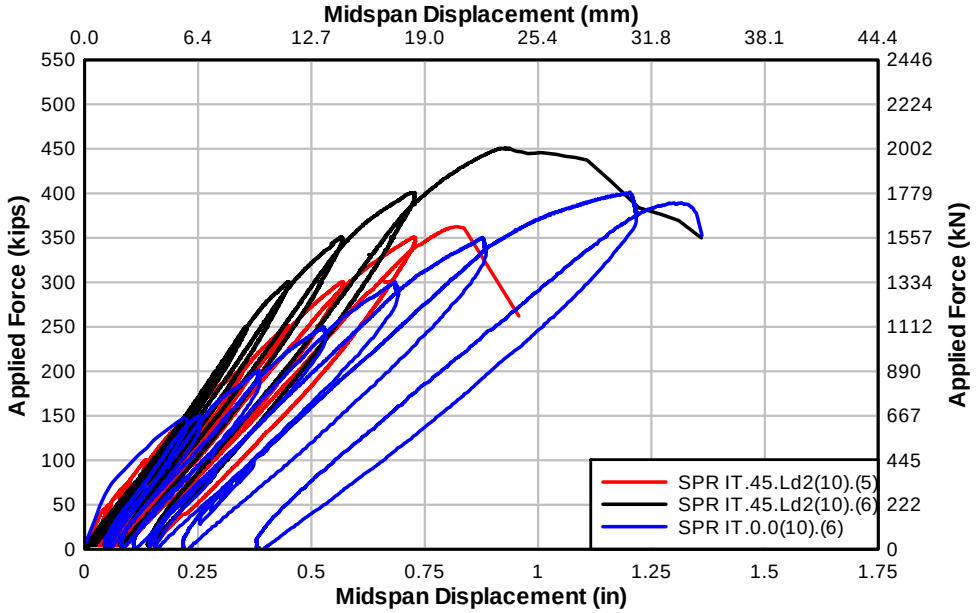


Figure 4.6: Comparison SPR IT specimen load-displacement responses at midspan.

As illustrated in the above figures, the T specimens have greater deformation capacity and ductility compared to IT specimens. Specimens T.45.Ld3(6).Ti and T.45.Ld3(6).SS failed in flexure and had very similar load deformation plots. Both specimens used 6 in. (152 mm) spacing for shear reinforcement and achieved higher loads and provided more ductility than the specimens with the 10 in. (254 mm) stirrup spacing. Specimen T.45.Ld3(6).SS had a stiffer ascending branch than T.45.Ld3(6).Ti due to the higher modulus of elasticity of the stainless

steel NSM bars and the higher amount of stainless steel reinforcing bars compared to the NSM titanium alloy specimens. After the specimen became inelastic, at a load of around 375 kips (1664 kN), T.45.Ld3(6).Ti and T.45.Ld3(6).SS had similar load deformation responses and failed in flexure just after the termination of the NSM reinforcement at midspan. Specimen T.45.Ld3(6).Ti provided the largest overall deformation capacity. The NSM titanium strengthened specimens did not significantly change the initial stiffness of the IT specimens. Specimen IT.45.Ld3(6).SS had a higher stiffness than IT.45.Ld3(6).Ti due to the use of twice the material having twice the axial stiffness (4 times the stiffness compared to the titanium bars). Specimen IT.45.Ld3(6).SS achieved higher capacity than IT.45.Ld3(6).Ti due to overstrength and higher stiffness of the stainless steel bars. Also, specimen IT.45.Ld3(6).Ti exhibited nonuniform slip of the cutoff fleuxral bars on the two sides of the flange which produced out-of-plane bending of the specimen thereby failing the compression zone on one side of the web. The failure occurred at the nominal flexural capacity of the specimens.

### 4.1.2 Crack Maps for Girder Specimens

Concrete crack initiation and propagation was monitored throughout the test for all specimens. After each peak load cycle was achieved, the load was decreased by 25 kips (111 kN) and then held to minimize creep effects. During this hold time, the specimens were inspected and cracks were measured and highlighted. Digital pictures were taken at each load step to record the cracked condition. The crack patterns at failure are shown in Figure 4.7 for each specimen.

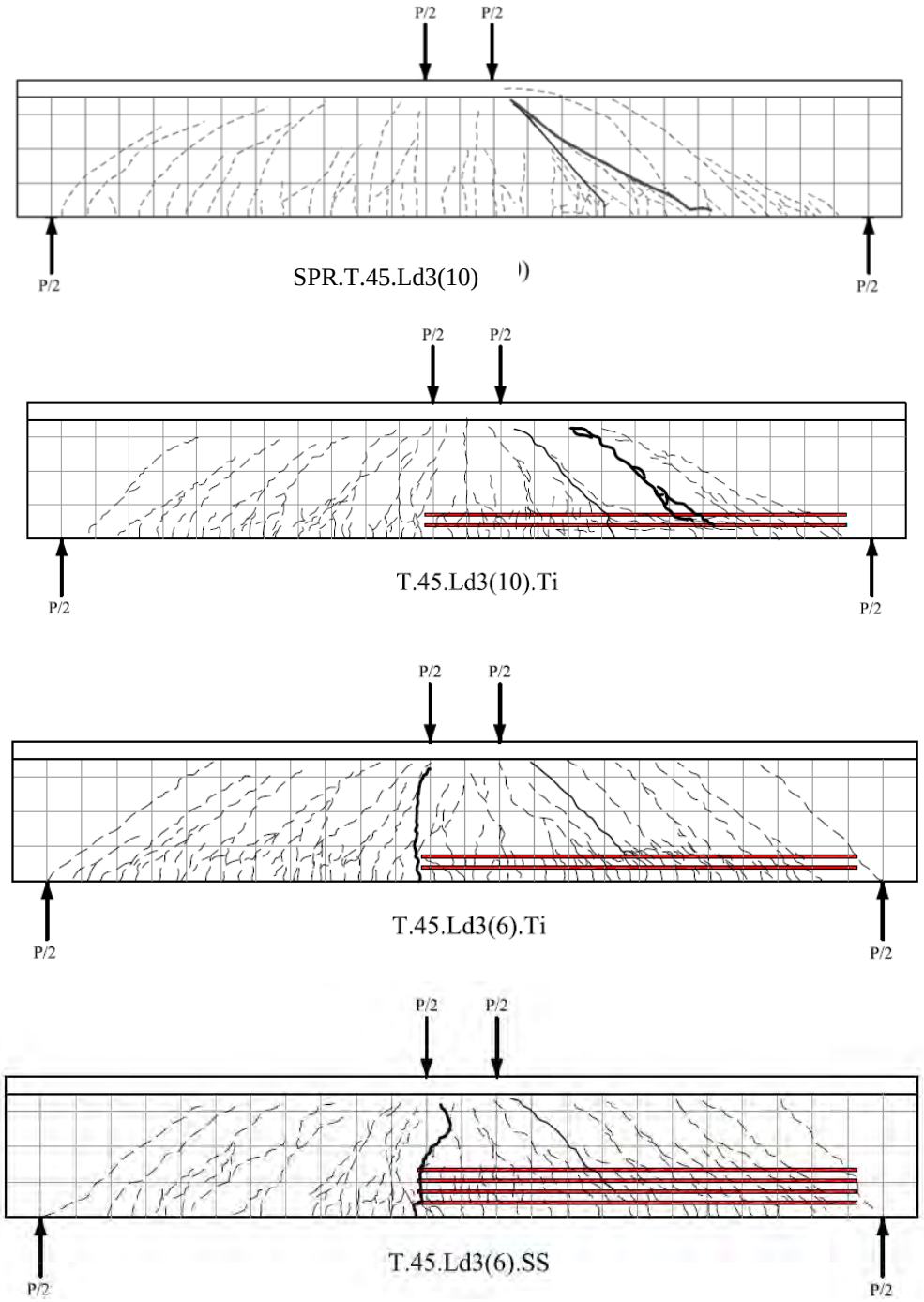


Figure 4.7: Specimen crack mapping with highlighted failure cracks.

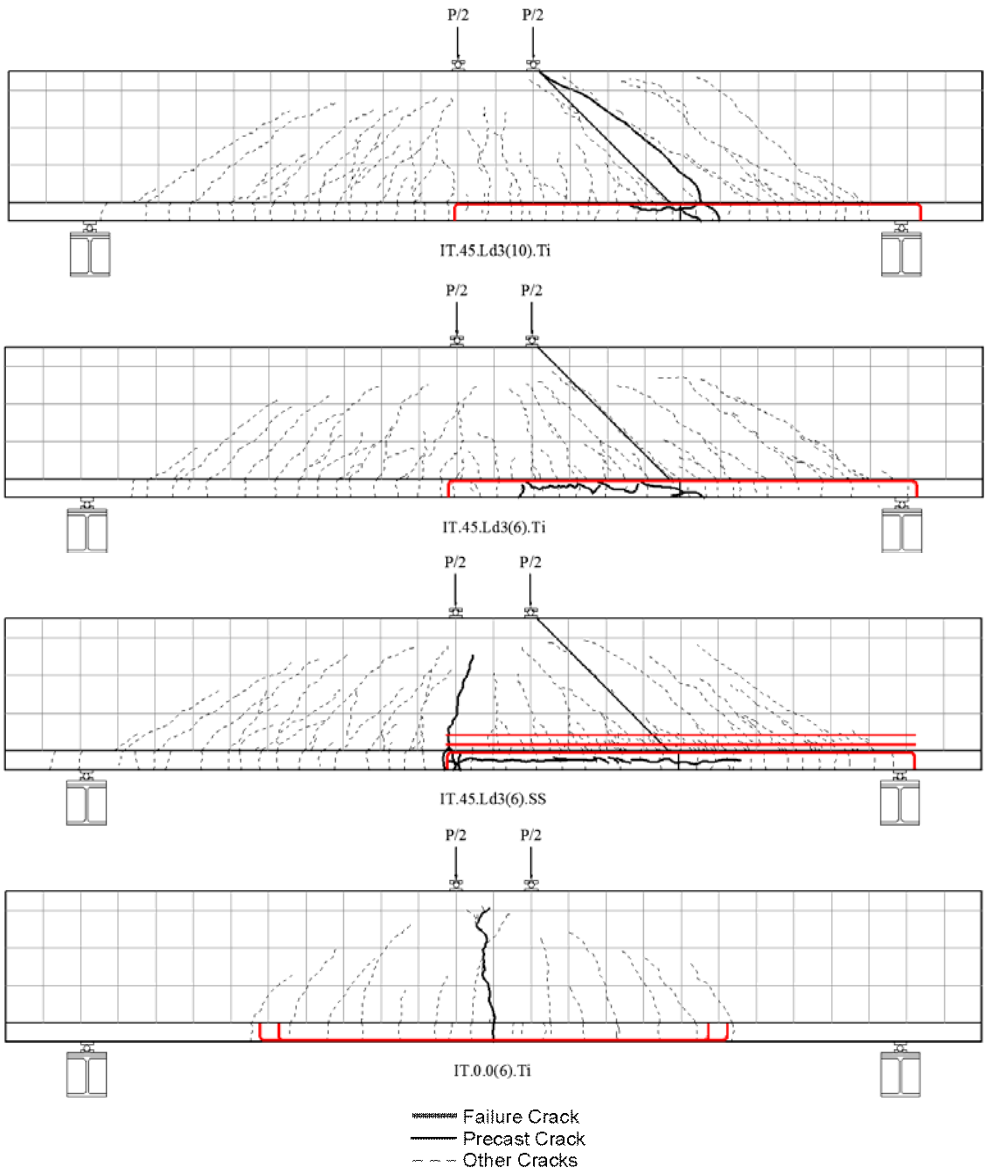


Figure 4.7: Continued

Specimen SPR T.45.Ld3(10) and the corresponding NSM-titanium retrofitted counterpart, T.45.Ld3(10).Ti, failed in a similar manner with the failure crack extending from the edge of the loading plate to the end of the cutoff reinforcing steel bars. This was also true of Specimen SPRIT.45.Ld2(10) and the corresponding NSM-titanium retrofitted counterpart, IT.45.Ld3(10).Ti. Specimens T.45.Ld3(6).Ti and SS, as well as IT.45.Ld3.Ti and SS shifted the failure location to near midspan. The failure cracks for T and IT 45.Ld3(6).Ti and SS specimens initiated just outside the constant moment region, traveled around the end of the hooks then curved towards the middle of the constant moment region. For simplification, the failure crack of the specimens with 6 in. (152.4 mm) stirrup spacing was estimated to be 90°. Chevron cracks, typical of anchorage failures, appeared near failure in the NSM specimens. In all cases, the preformed diagonal crack did not dictate the failure location. The NSM retrofitted specimens displayed distributed cracking over the length of the specimens. Vertical cracks did not

propagate through the epoxy until near failure loads and longitudinal splitting cracks in the epoxy were seen only at failure. The widespread extent of macrocracking in the concrete and around the epoxy provided visual indication of distress prior to failure. Digital photos of each specimen after failure are shown in Figure 4.8 and Figure 4.9 for the T and IT specimens, respectively.


Figure 4.8: Failure photographs of T specimens (front and back sides).

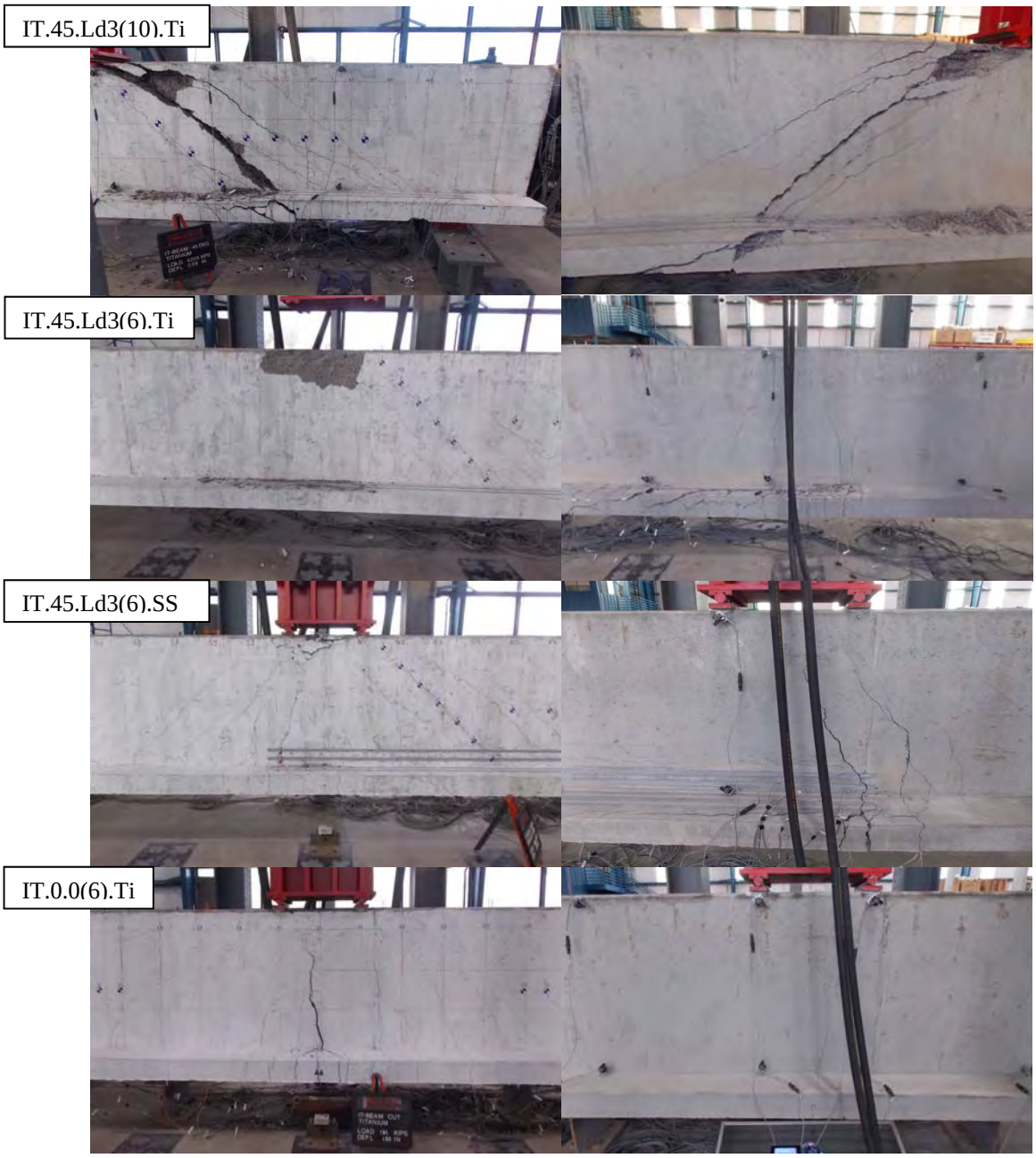


Figure 4.9: Failure photographs of IT specimens (front and back sides).

### 4.1.3 Anchorage Slip Response in Girder Specimens

The applied load-slip responses are shown in Fig. 4.10 for the T-specimens and Figures 4.11 to 4.13 for the IT specimens. As the load increased, the embedded steel cutoff bars exhibited slip early in the loading history, around the time of diagonal cracking. As the applied load increased towards failure, residual slip was observed for all specimens. Towards failure of the IT specimens, one of the cutoff bars slipped more on one side of the stem than the other. Anchorage loss occurred on the side of the specimen that exhibited the larger slip value. Specimens IT.45.Ld3(6).Ti and IT.45.Ld3(6).SS had greater shear capacities over the cutoff bars which

decreased the demand in the flexural steel from shear. Specimen IT.45.Ld3(6).Ti showed significantly more slip on the west side, which eventually led to out-of-plane bending and failure of one side of the compression zone for the specimen. The slip of the T-specimens was more balanced between the east and west sides due to stirrups crossing the splitting plane. The responses are similar to the overall load-midspan displacement responses. The load-slip curves were generally elastic and had minor residual slip after unloading at each load step. As the applied load approached failure, slip increased and larger residual slips were observed.

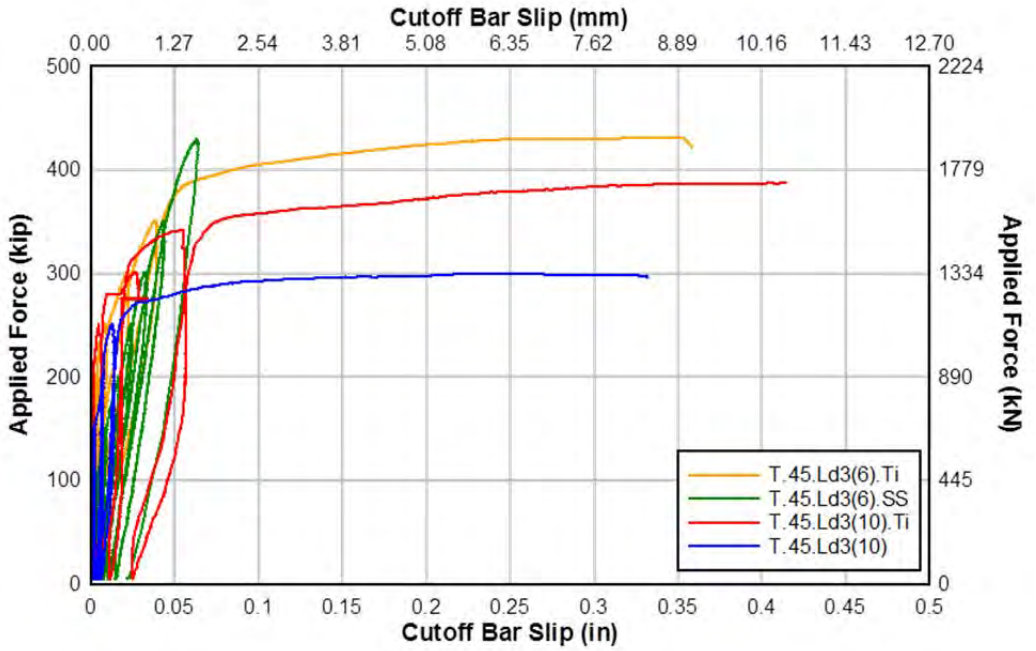


Figure 4.10: Anchorage slip response of west flexural cutoff bars in T-specimens.

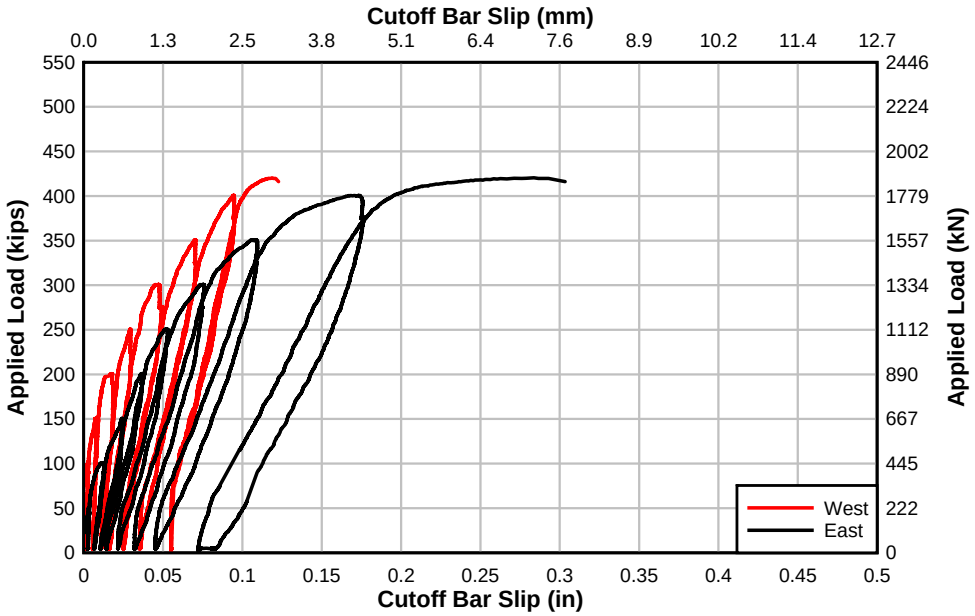


Figure 4.11: Specimen IT.45.Ld3(10).Ti load-cutoff bar slip response.

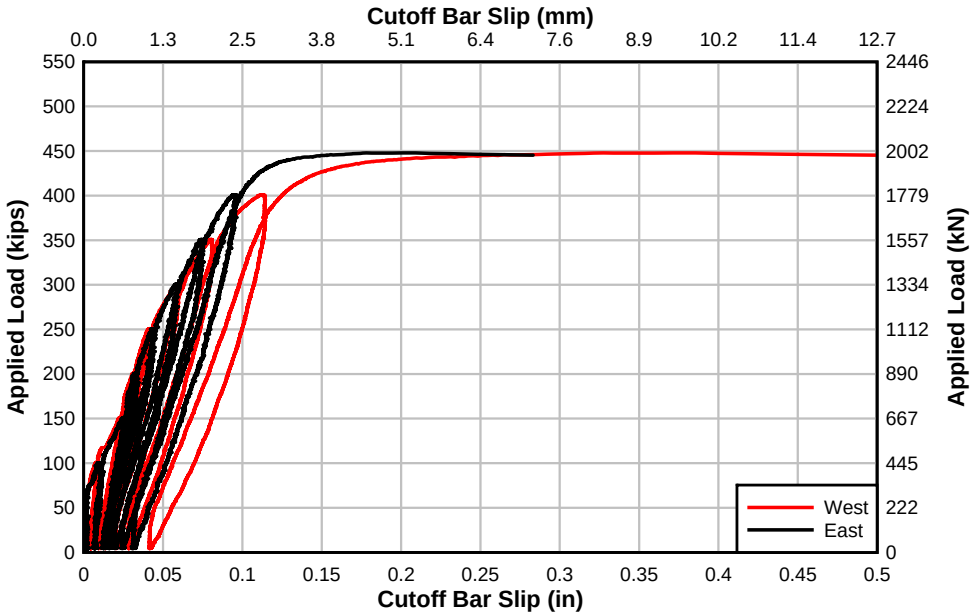


Figure 4.12: Specimen IT.45.Ld3(6).Ti load-cutoff bar slip response.

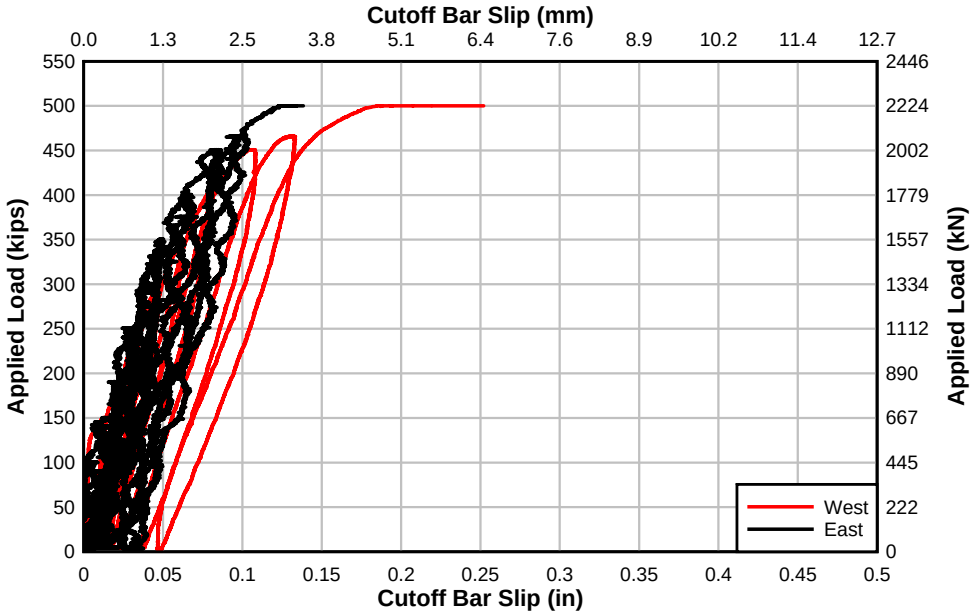


Figure 4.13: Specimen IT.45.Ld3(6).SS load-cutoff bar slip response.

Since the cutoff reinforcing steel bars were not anchored and detailed to modern engineering design practice, all specimens experienced some degree of anchorage slip. However, only specimens T.45.Ld3(10).Ti and IT.45.Ld3(10).Ti failed in a mode dependent on the anchorage or the cutoff reinforcing steel. The titanium alloy and stainless steel NSM bars effectively increased the capacity, delayed the slip of the cutoff reinforcing steel bars until higher loads were achieved, and delayed loss of anchorage for the cutoff reinforcing steel bars. The stainless steel strengthened specimens exhibited reduced slip compared to the titanium alloy strengthened

specimens and this was again attributed to the increased stiffness of the NSM stainless steel bars, which attracted additional force.

### 4.1.4 Slip Strain Behavior in Girder Specimens

Slip-strain responses were determined for the cutoff flexural reinforcing steel bars. Changes in strain along the cutoff bar, specifically from the end of the bar to the preformed diagonal crack, indicated how quickly the #11 (36M) bar developed stress. The cutoff reinforcing steel bar slip reduced significantly between the 45o performed diagonal crack and midspan of the specimens with NSM materials. Increases in bar strain indicate that the steel reinforcing bar was becoming well anchored. Locations along the span designated as “Cut 4,” “Cut 5,” and “Cut 6” corresponded to the intersection of the preformed diagonal crack, and 7 in. (178 mm) and 14 in. (356 mm) from the crack towards the end of the cutoff reinforcing steel bar. The measured slip strain response of the NSM strengthened T-specimens are shown in Figures 4.14 to 4.16.

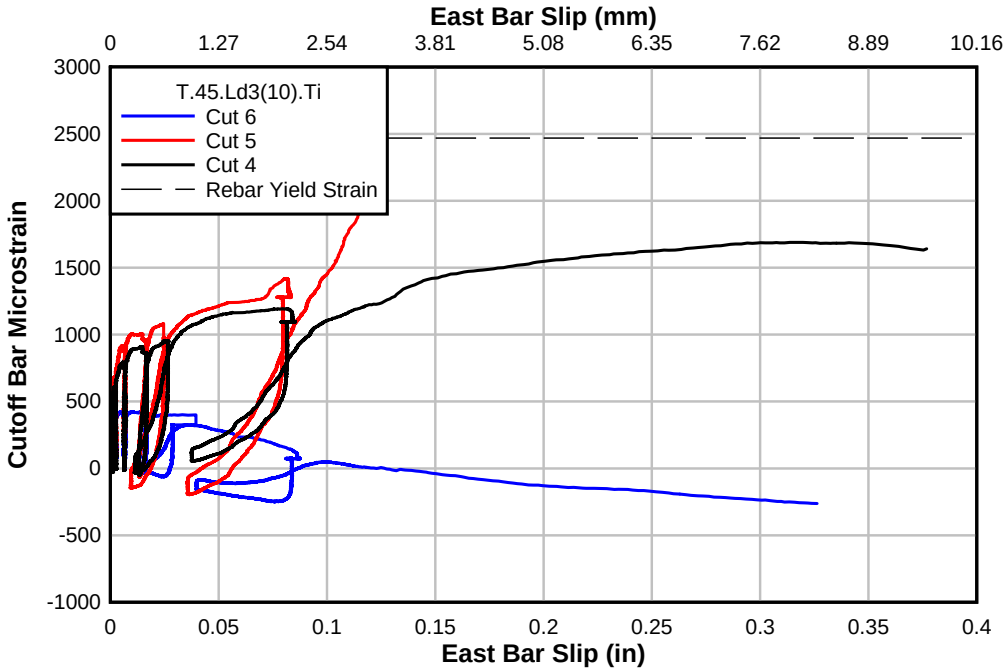


Figure 4.14: T.45.Ld3(10).Ti cutoff reinforcing steel bar strain vs slip.

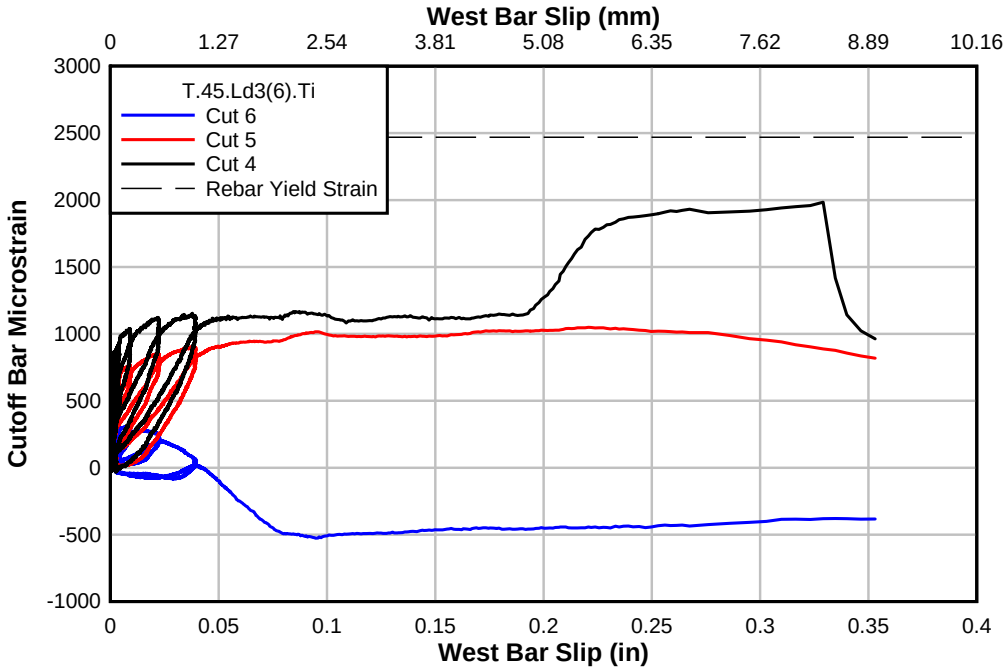


Figure 4.15: T.45.Ld3(6).Ti cutoff reinforcing steel bar strain vs slip.

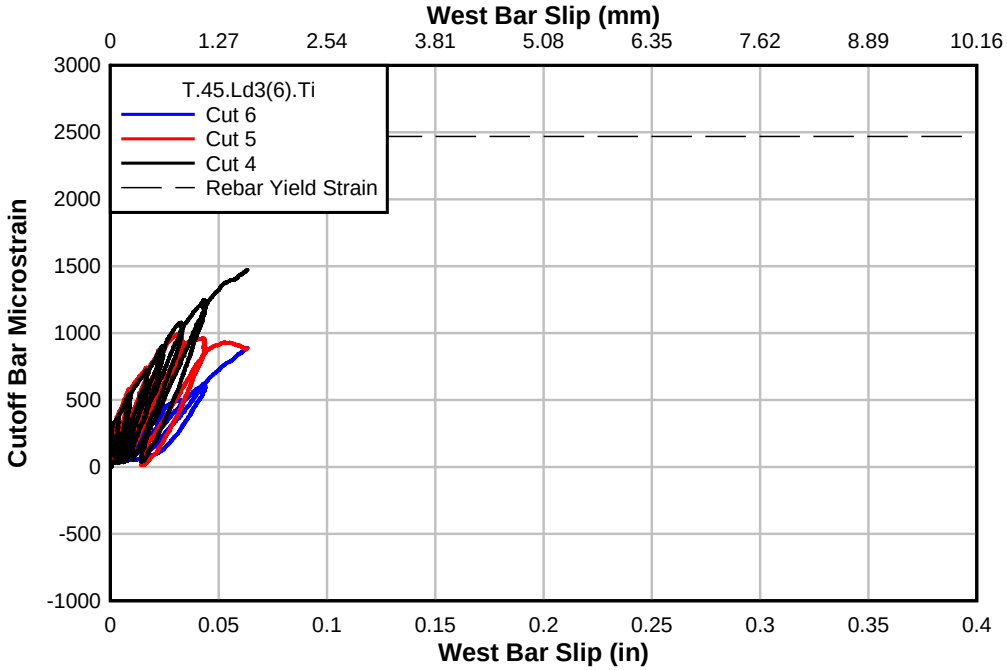


Figure 4.16: T.45.Ld3(6).SS cutoff reinforcing steel bar strain vs slip.

In specimen T.45.Ld3(10).Ti and T.45.Ld3(6).Ti the strain decreased at “Cut 6” due to loss of bond. This limited the strains at “Cut 4” and “Cut 5.” The specimens strengthened with NSM-titanium alloy bars had several cracks intersect the bar between strain gages at “Cut 5” and “Cut 4.” This cracking created an unbonded length producing similar strains between “Cut 4” and “Cut 5.” The stainless steel NSM specimen, T.45.Ld3(6).SS, exhibited less cutoff reinforcing

steel bar slip than the other specimens. The strains were also seen to increase farther away from the termination of the cutoff reinforcing steel bar for this specimen. For all T-specimens, “Cut 6” had small strains, and “Cuts 4” and “5” had an average value of 1000 microstrain. This showed that the stress in the cutoff reinforcing steel bar was approximately 29 ksi (200 MPa), almost half of the nominal yield stress just 14 in. (356 mm) from the end of the bar. Consequently, the development length of a Gr. 60 (Gr. 420) #11 (M36) bar may be closer to half the expected value from using ACI 318.

Critical instrumentation on the cutoff flexural steel bars for the IT specimens were similarly located along the 20.4 in. (516 mm), (1/3 development length) dimension past the preformed diagonal crack. The strain gages were 20.4, 13.4, and 6.4 in. (518, 340, and 163 mm) from the end of the cutoff bar and were labeled as “Cut 4, 5, and 6”, respectively. “Cut 4” was located at the preformed crack intersection. The strain-slip response is shown in Figures 4.17 to 4.19 for each of the specimens with preformed diagonal cracks. The response curves are labeled “initial slip” at points where the strain reversed due to slip in the cutoff bar. The strain reversals were caused by the lowered bond between the reinforcing bar and the surrounding concrete as the flexural steel cutoff bar slipped.

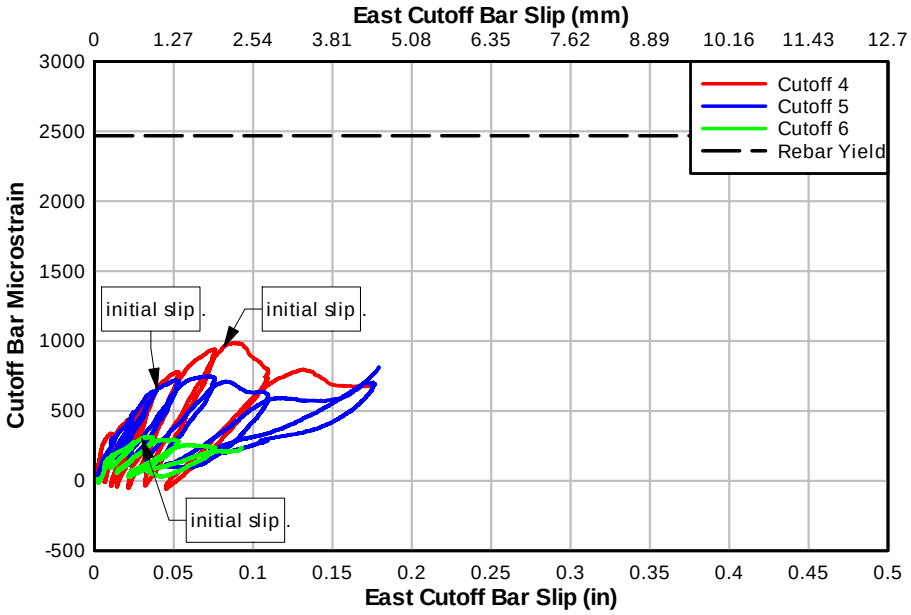


Figure 4.17: Specimen IT.45.Ld3(10).Ti cutoff bar strain vs slip.

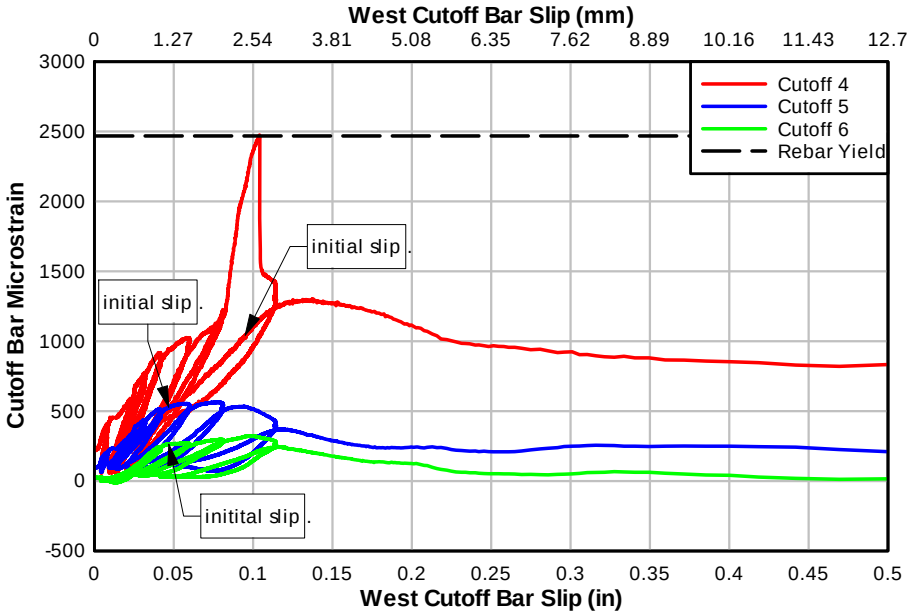


Figure 4.18: Specimen IT.45.Ld3(6).Ti cutoff bar strain vs slip.

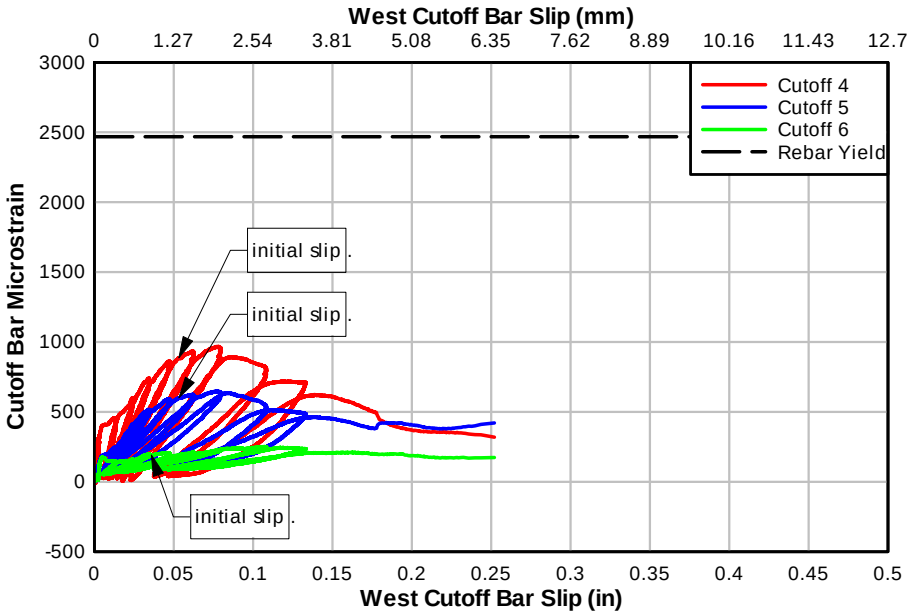


Figure 4.19: Specimen IT.45.Ld3(6).SS cutoff bar strain vs slip.

### 4.1.5 Material Strains in Girder Specimens

The instrumentation plan allowed monitoring of strains in different reinforcing bars on one quarter of the specimens. The instrumented bars included the cutoff and hooked reinforcing steel bars and NSM bars. This section reports example strain responses for each instrumented bar and cross section for specimen T.45.Ld3(6).Ti and IT.45.Ld3(6).Ti. The locations for the strain sensors are shown in Figures 4.20 and 4.21 for the T and IT specimens, respectively. Results for other specimens are shown in Appendices A and B.

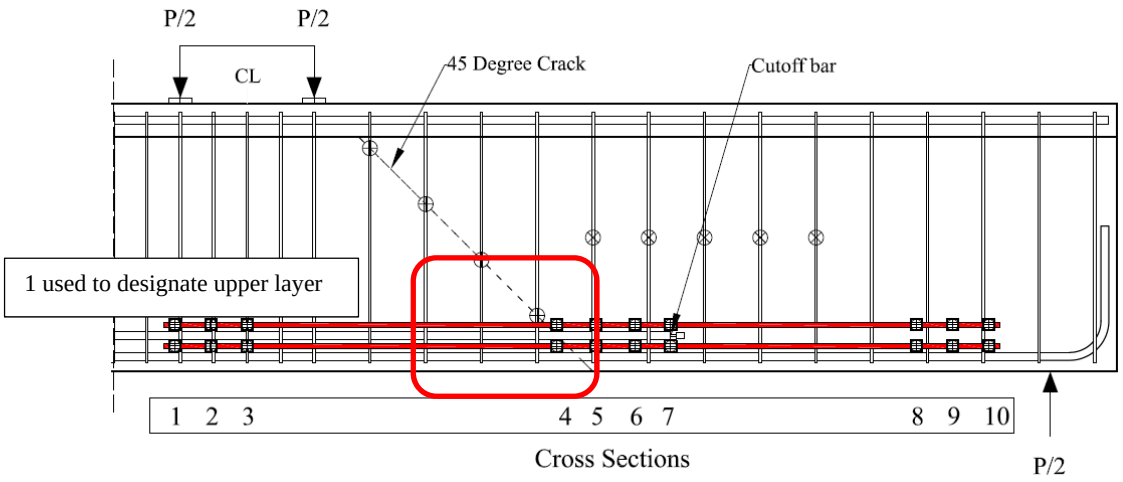


Figure 4.20: Labeling convention of cross sections in typical T-specimen.

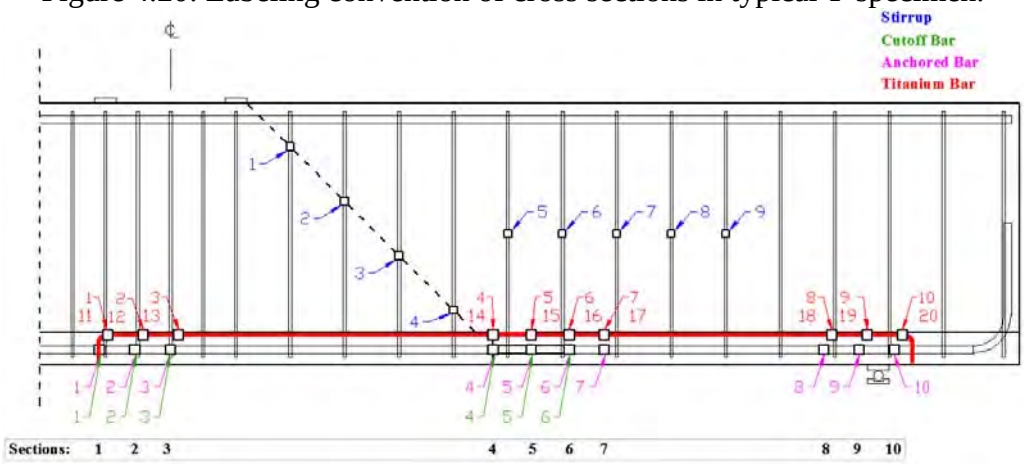


Figure 4.21: Labeling convention of cross sections in typical IT-specimen.

### *4.1.5.1 Strains at Cross Sections Along the Length of the Specimens*

Hook and cutoff steel reinforcing bars, and NSM bar strains were plotted at each instrumented cross section for specimen T.45.Ld3(6).Ti in Figures 4.22 to 4.25 and IT.45.Ld3(10).Ti in Figures 4.25 to 4.29. Yield strain for the longitudinal reinforcing bars and the NSM titanium alloy bars are shown as reference lines in the figures. These comparisons illustrate the interaction between the NSM bar and developing cutoff steel reinforcing bar. The experimental results showed that the internal steel reinforcing bars and NSM bar strains were compatible until concrete cracking and cutoff bar slip occurred. At higher loads the strains in the different reinforcing bars were not fully compatible due to cracking, debonding, and slip.

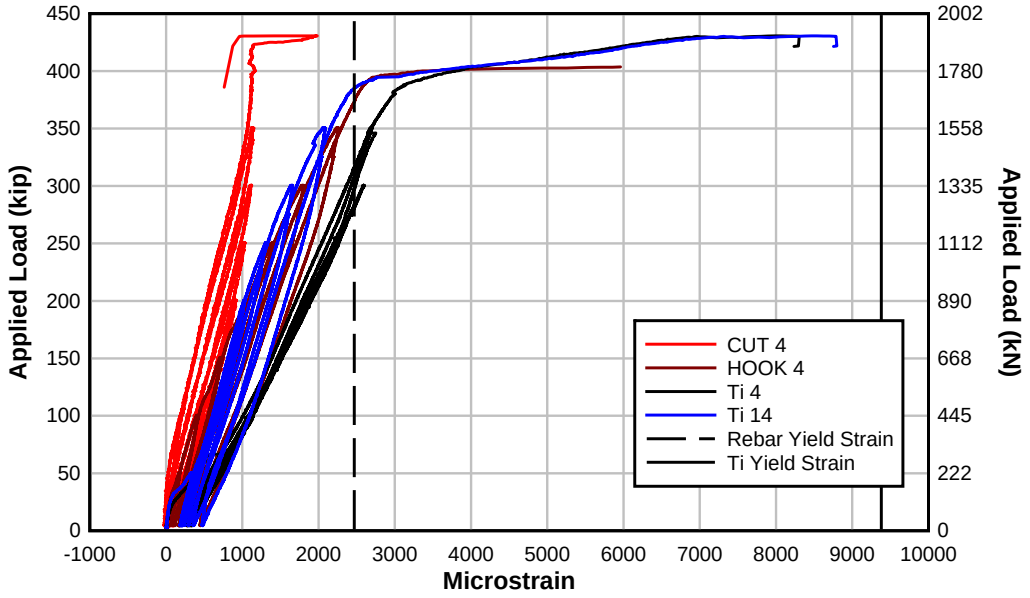


Figure 4.22: Specimen T.45.Ld3(6).Ti load-flexural bar strain (Section 4 at preformed diagonal crack).

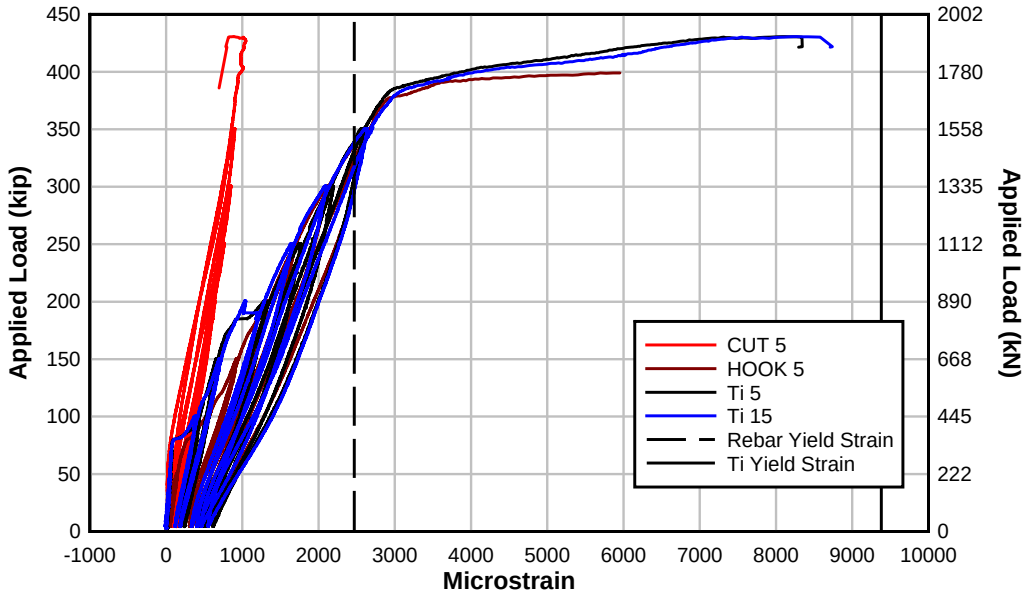


Figure 4.23: Specimen T.45.Ld3(6).Ti load-flexural bar strain (Section 5).

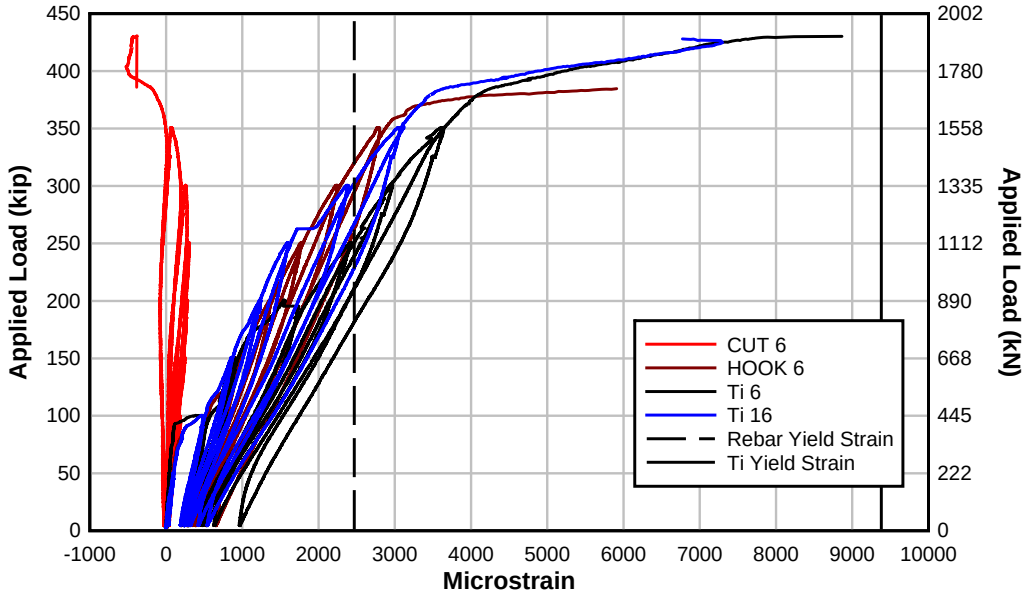


Figure 4.24: Specimen T.45.Ld3(6).Ti load-flexural bar strain (Section 5).

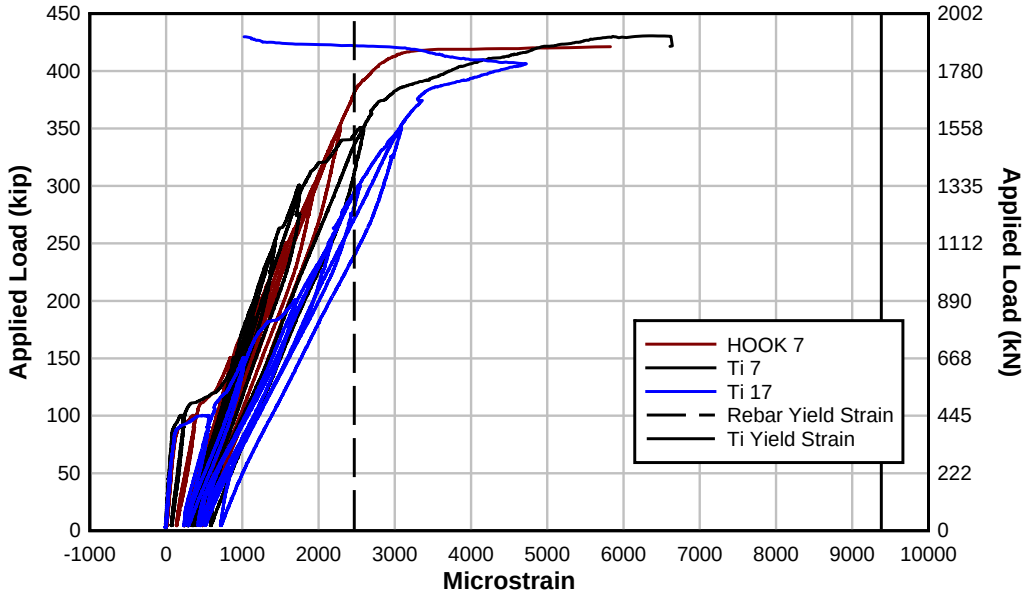


Figure 4.25: Specimen T.45.Ld3(6).Ti load-flexural bar strain (Section 7 end of cutoff).

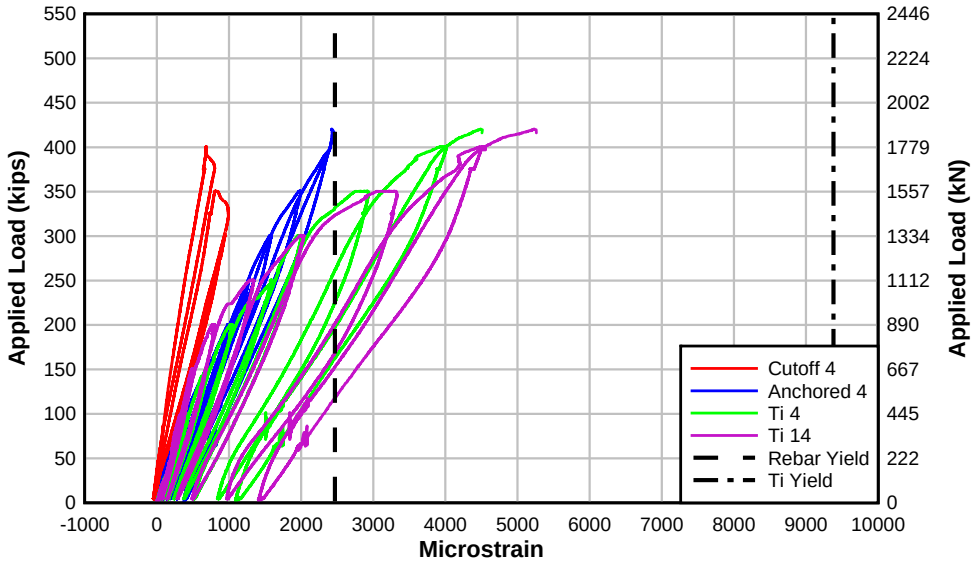


**Figure 4.26– Specimen IT.45.Ld3(10).Ti load-flexural bar strain (Section 4 at preformed crack).**

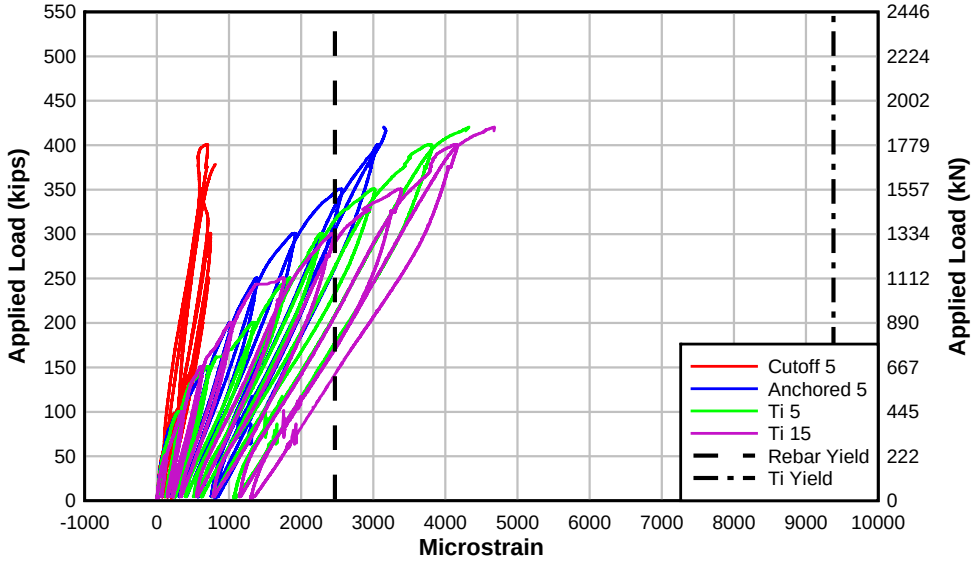


Figure 4.27: Specimen IT.45.Ld3(10).Ti load-flexural bar strain (Section 5).

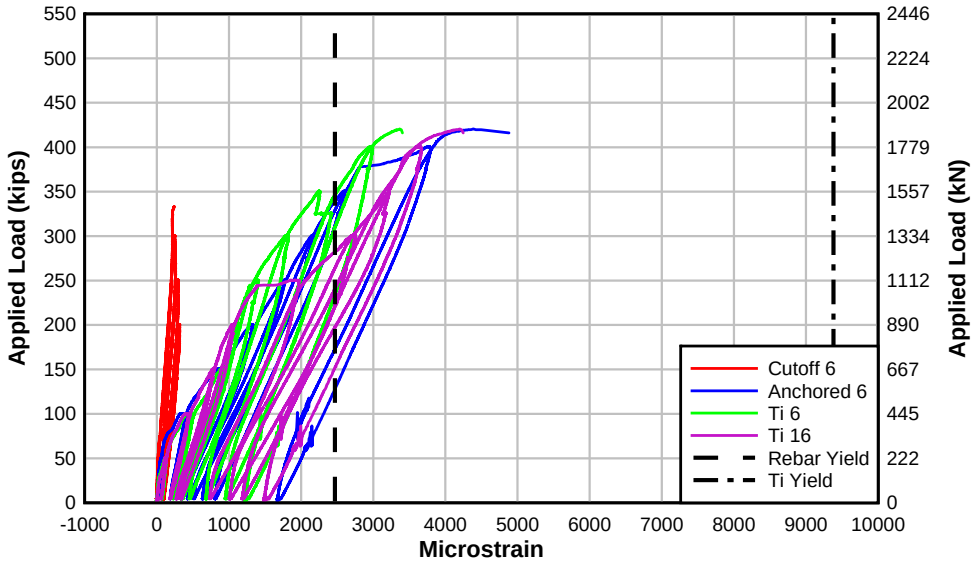


Figure 4.28: Specimen IT.45.Ld3(10).Ti load-flexural bar strain (Section 6).

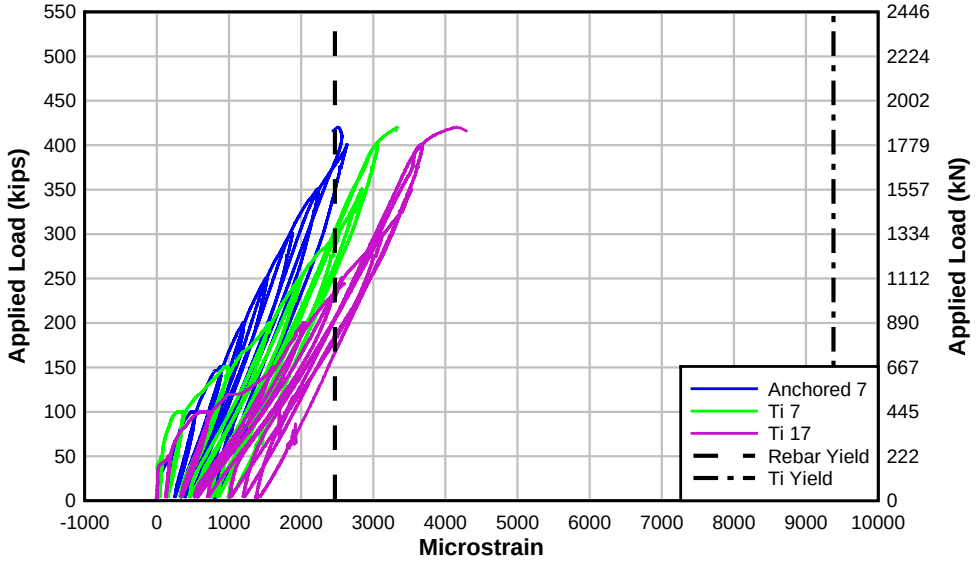


Figure 4.29: Specimen IT.45.Ld3(10).Ti load-flexural bar strain (Section 7).

All materials exhibited similar strain magnitudes (strain compatibility) until the second load interval which produced concrete cracking. After several load cycles, strain reversal was observed in the cutoff steel reinforcing bar which indicated slip. The cutoff reinforcing steel bars achieved about approximately 1000 microstrain or about half of the yield strain. In sections 4, 5, 6, and 7 the hooked reinforcing steel bars were yielding and contributed the majority of the flexural tension capacity at that point. While the strains in the NSM titanium alloy bars track with the hooked reinforcing steel, the force carried by the NSM titanium alloy bars is about half that of the reinforcing steel due to the lower modulus of elasticity for titanium. The NSM titanium alloy bars did not exhibit yielding

at the strain gage locations but may have yielded locally at crack locations prior to failure. Also, a number of strain gages were damaged as the beam approached capacity.

Stirrups crossing the diagonal crack reached yield as seen in Figure 4.30 and most of the mid-height stirrups exhibited strains above yield in specimen T.45.Ld3(6).Ti as seen in Figure 4.31.

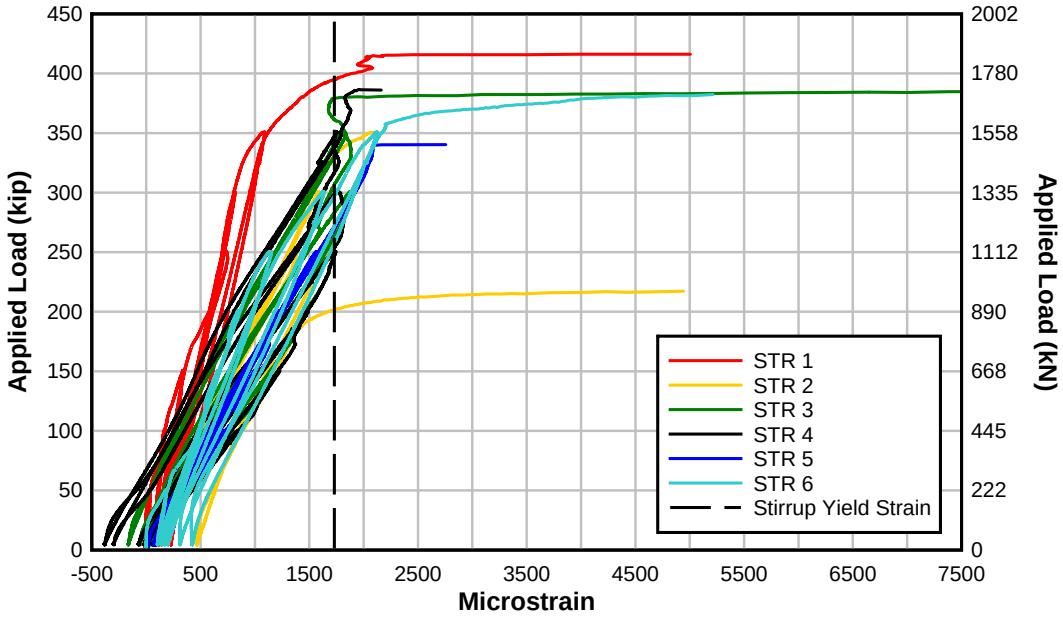


Figure 4.30: Stirrup strains along the preformed diagonal crack on specimen T.45.Ld3(6).Ti.

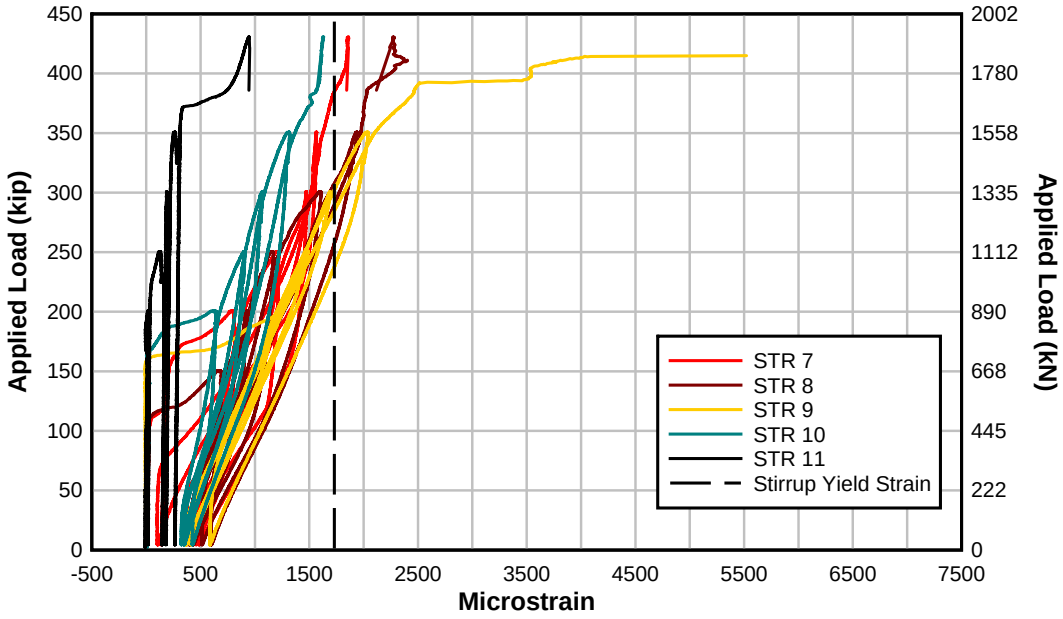


Figure 4.31: Strain in stirrups at mid-height in specimen T.45.Ld3(6).Ti.

### 4.1.6 Tensile forces in Reinforcing Steel and NSM Bars within Girder Specimens

The NSM retrofit design approach is to increase the available flexural tensile capacity over the length of the specimen where demands would otherwise exceed capacity. This section presents the measured flexural tension forces in the reinforcing steel and NSM bars at each instrumented section of the example specimen. Strains measured in the reinforcing steel and NSM materials were transformed into the experimentally measured tensile force in each bar, $T_{exp}$, as:

$$T_{exp} = A_x E_x \varepsilon_x \quad (4.1)$$

where $A_x$ is the cross sectional area of bar $x$, $E_x$ is the material modulus of elasticity, and $\varepsilon_x$ is the measured strain in the bar. The individual bar forces in the hook and cutoff reinforcing steel and the NSM bars were multiplied by the number of similar bars and summed into the total flexural tension force. The analysis was done for each of the referenced sections shown previously. The flexural tensile forces at 50 or 100 kip increments are presented in the subsequent figures and the measured strains were bounded to yield and zero.

The total tension forces from the reinforcing steel and NSM materials for the T-strengthened specimens are shown in Figures 4.32 through 4.34 and for IT specimens in Figures 4.35 to 4.38. In some specimens, some of the strain gages were damaged prior to achieving the peak load, creating abnormally low tensile forces that were not possible to maintain equilibrium in the section. The outlier data points were omitted from the curve but are still shown as square box symbols.

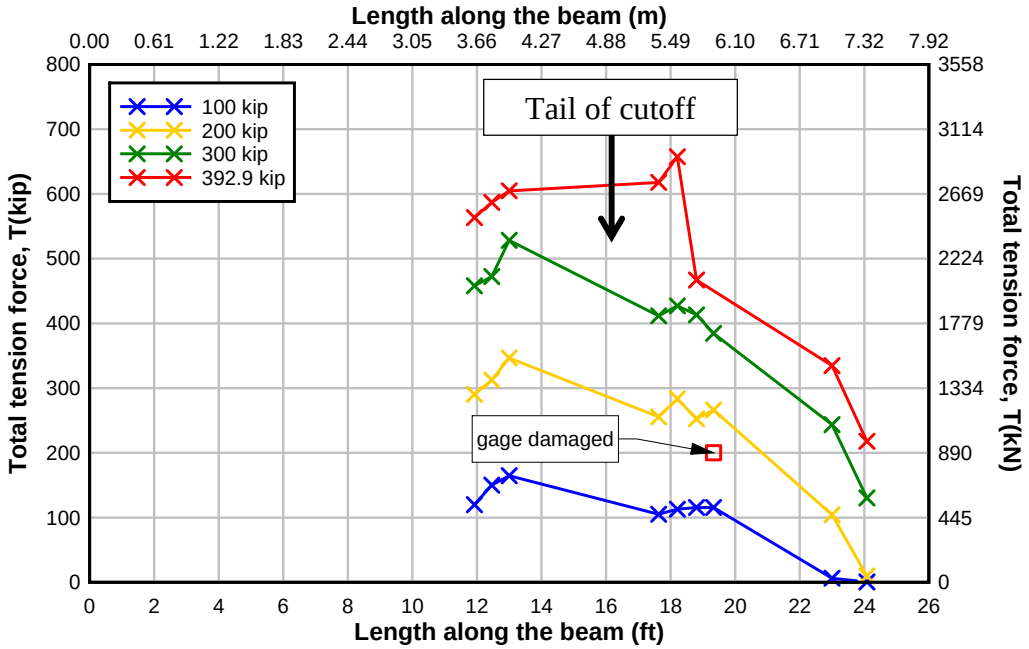


Figure 4.32: Specimen T.45.Ld3(10).Ti total tension force in all reinforcement along beam.

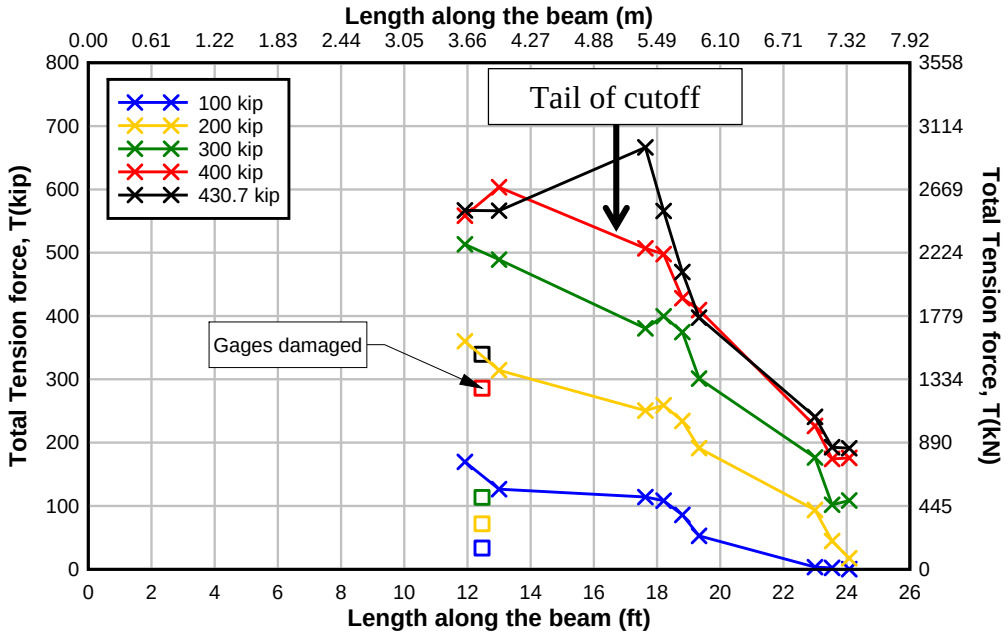


Figure 4.33: Specimen T.45.Ld3(6).Ti total tension force in all reinforcement along beam.

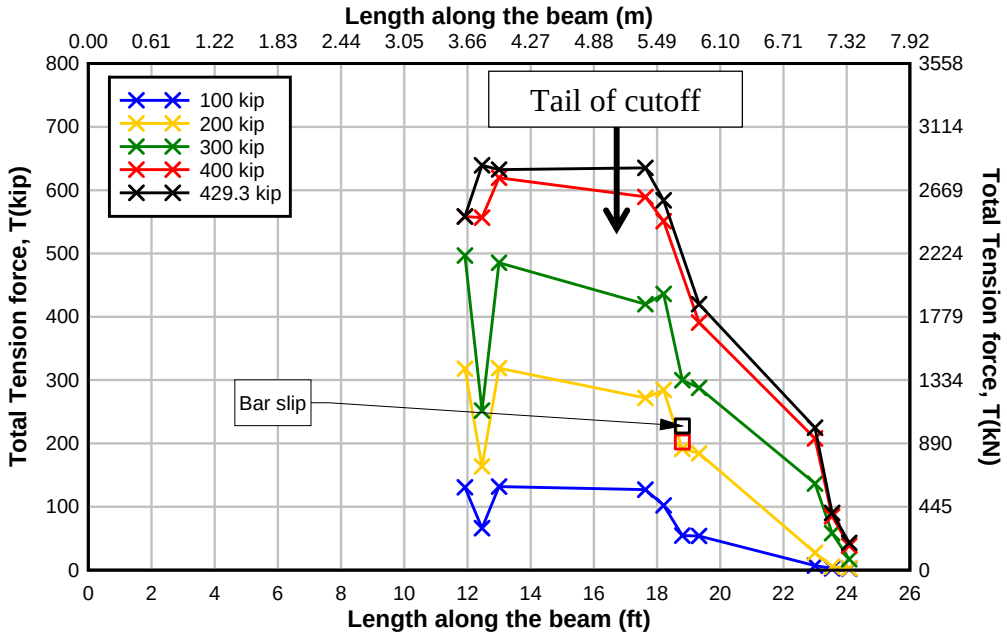


Figure 4.34: Specimen T.45.Ld3(6).SS total tension force in all reinforcement along beam.

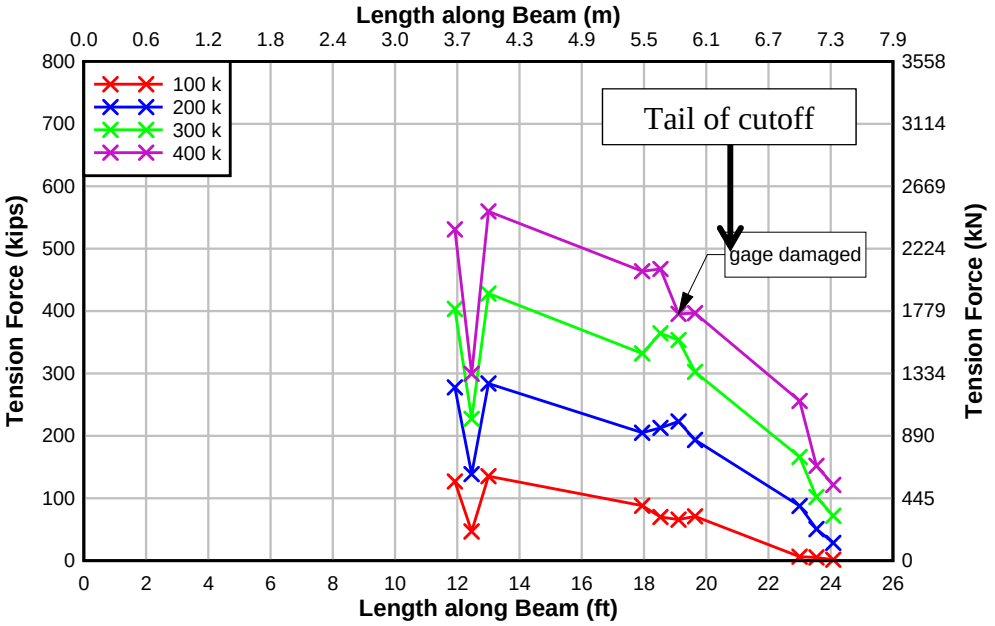


Figure 4.35: Specimen IT.45.Ld3(10).Ti total tension force in all reinforcement along beam.

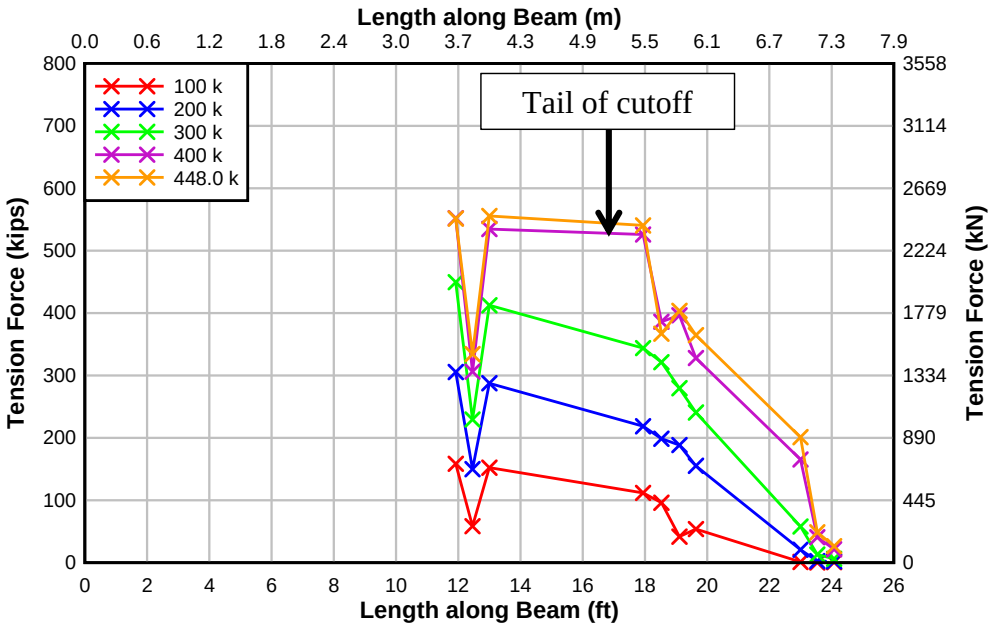


Figure 4.36: Specimen IT.45.Ld3(6).Ti total tension force in all reinforcement along beam.

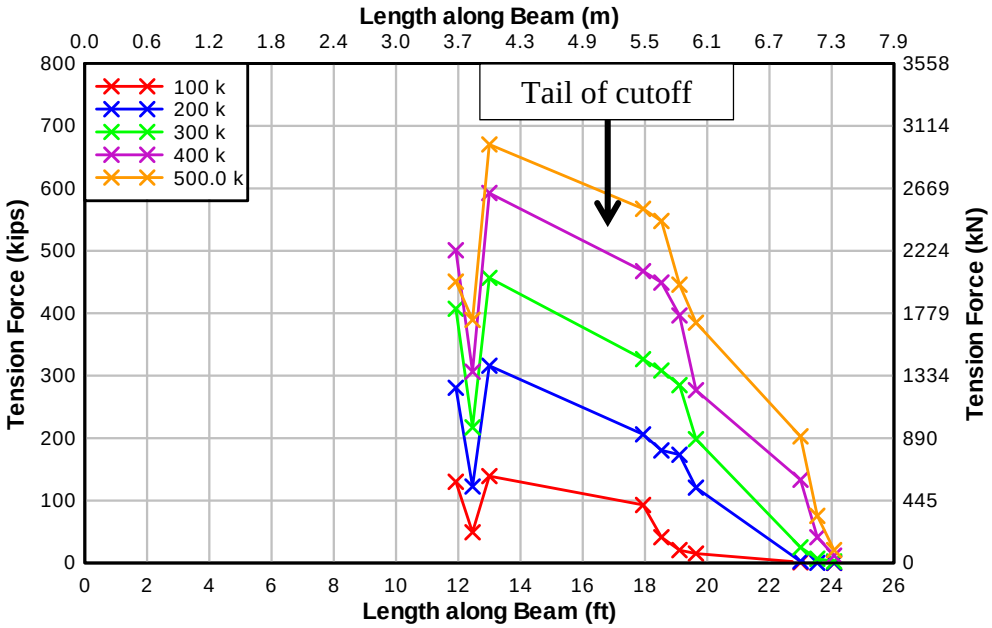


Figure 4.37: Specimen IT.45.Ld3(6).SS total tension force in all reinforcement along beam.

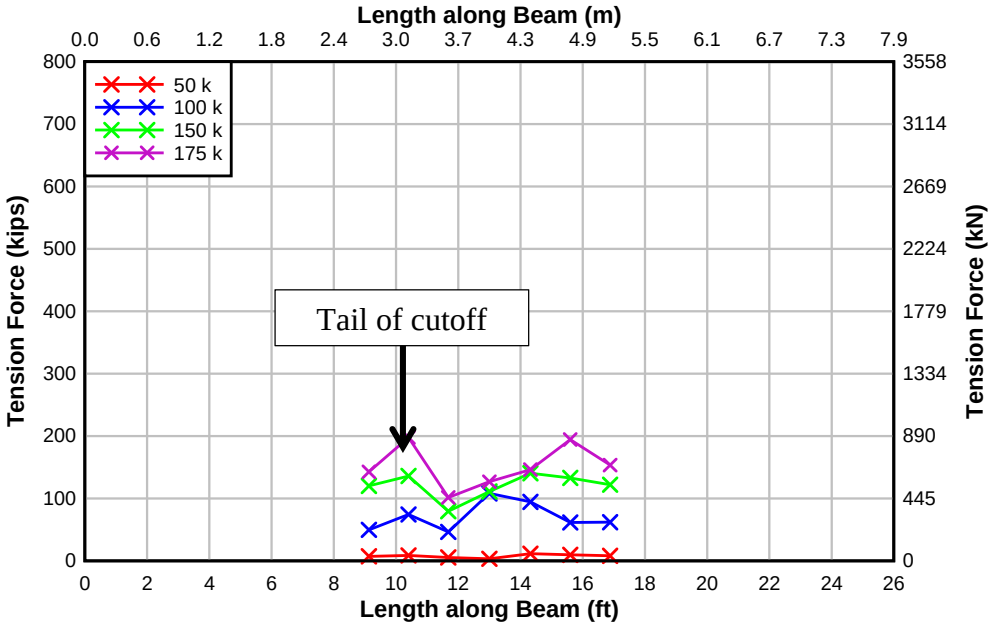


Figure 4.38: Specimen IT.0.0(6).Ti total tension force in all reinforcement along beam.

The tension forces in the specimens increased as the load increased and there were clearly increased flexural demands located around the preformed diagonal cracks, as would be predicted by Equation 2.3. During the last load cycle, tension forces peaked at the preformed diagonal crack location for the T-specimens, while the maximums were located near midspan for the IT specimens.

In all specimens, the tensile forces at maximum load were similar from midspan to the preformed diagonal crack. After the termination of the cutoff bar, the tensile forces decreased due to

reduced moment and more vertically oriented diagonal cracks that produce less demand in the bars.

#### *4.1.6.1 Maximum Measured Reinforcing Steel and NSM Bar Tension Forces*

The following bar charts show the tensile contributions of the internal reinforcing steel and the NSM materials. Sections 1 through 3 are located at midspan of the specimen and Sections 8 through 10 are located at the termination of the NSM material near the support. Damage to some of the strain gages at higher loads was observed and is noted on each figure. The contributions from the steel and NSM materials for specimens T.45.Ld3(10).Ti, T.45.Ld3(6).Ti, and T.45.Ld3(6).SS are shown in Figures 4.39 through 4.41, respectively. The results for specimens IT.45.Ld3(10).Ti, IT.45.Ld3(6).Ti, IT.45.Ld3(6).SS, and IT.0.0(6).Ti are shown in Figures 4.42 to 4.45, respectively. The results are shown just prior to failure or for the maximum load increment achieved prior to failure when sufficient sensor data were available to determine the forces in the bars.

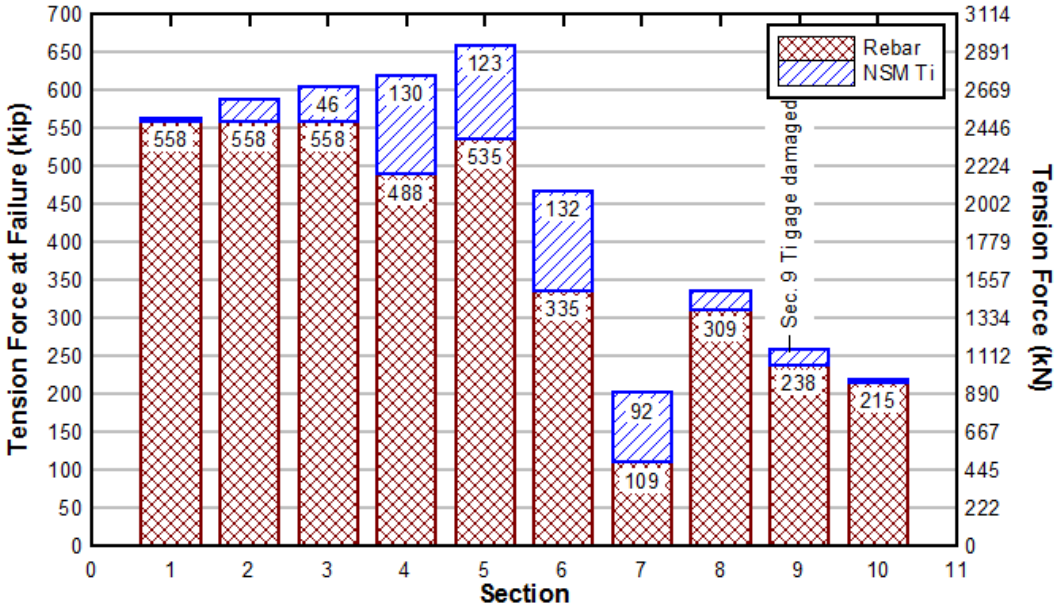


Figure 4.39: Specimen T.45.Ld3(10).Ti maximum tension force contributions at instrumented sections just prior to failure at 392.9 kips (1747 kN).

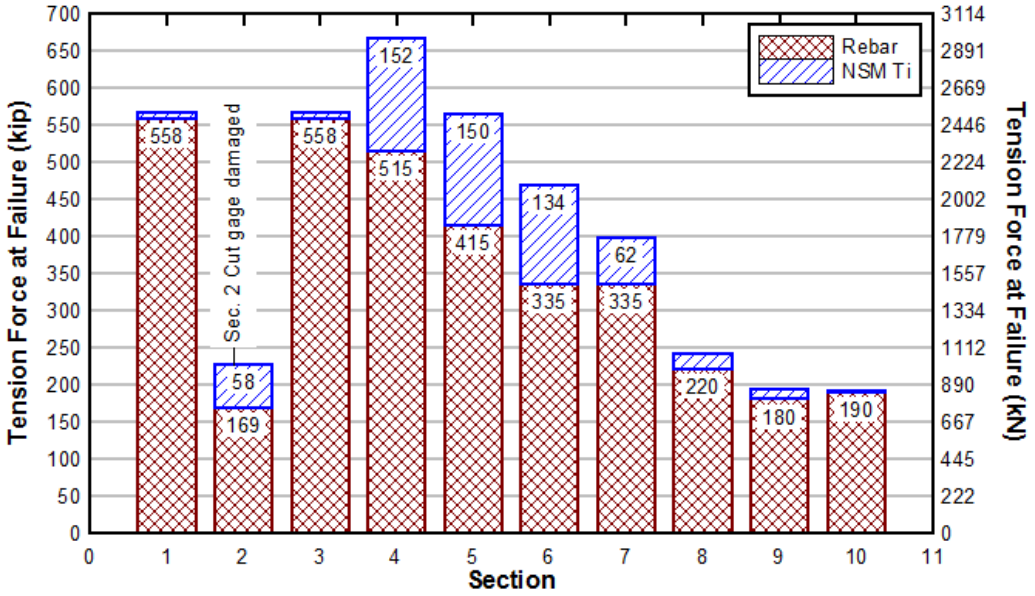


Figure 4.40: Specimen T.45.Ld3(6).Ti maximum tension force contributions at instrumented sections just prior to failure at 430.7 kips (1916 kN).

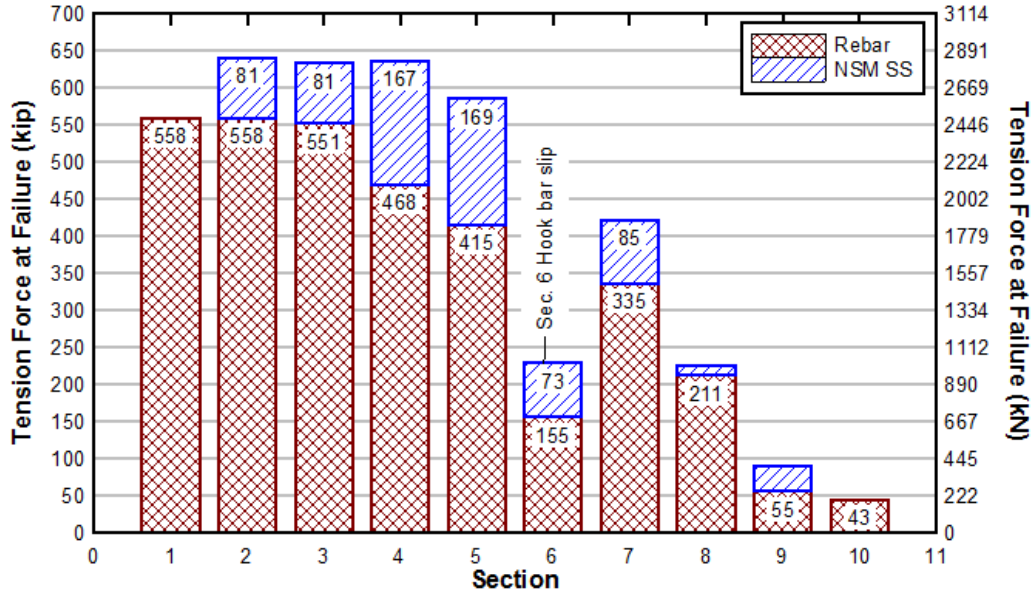


Figure 4.41: Specimen T.45.Ld3(6).SS maximum tension force contributions at instrumented sections just prior to failure at 429.3 kips (1909 kN).

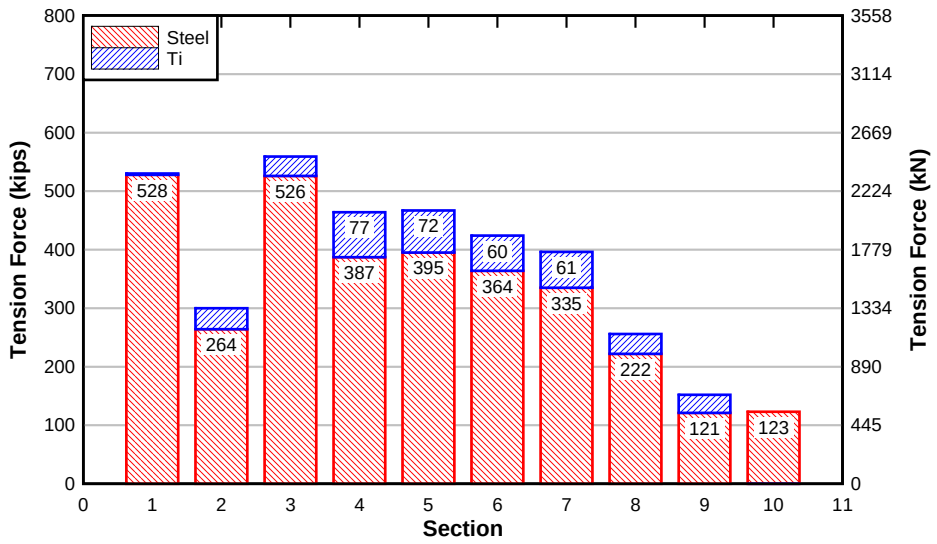


Figure 4.42: Specimen IT.45.Ld3(10).Ti tension force contribution-section at 400 kips (1780 kN).

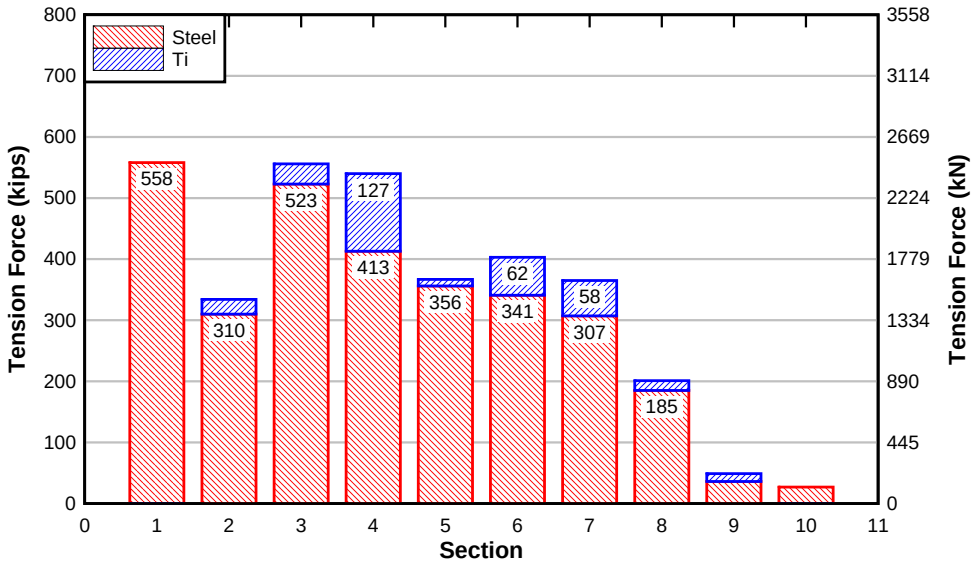


Figure 4.43: Specimen IT.45.Ld3(6) Ti tension force contribution-section just prior to failure.

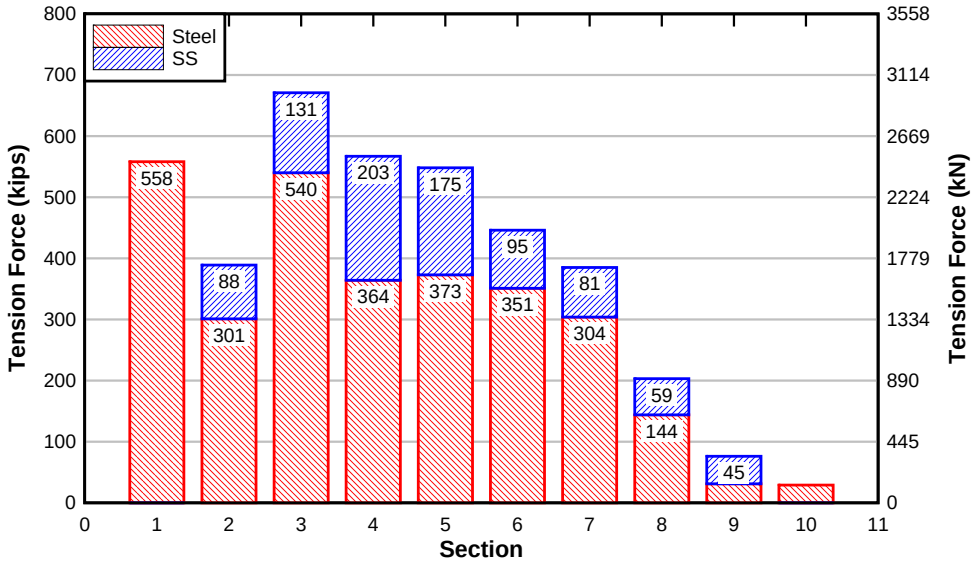


Figure 4.44: Specimen IT.45.Ld3(6).SS tension force contribution-section just prior to failure.

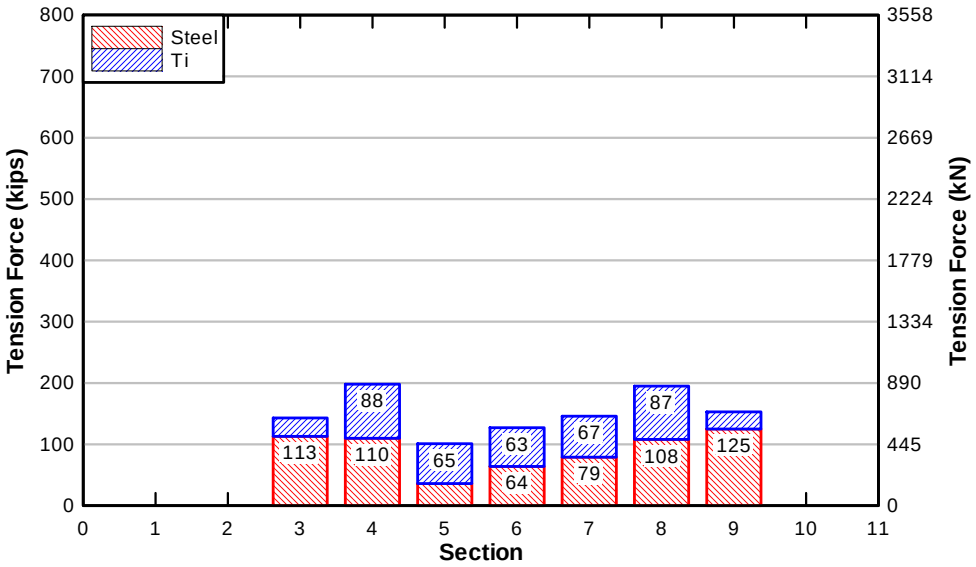


Figure 4.45: Specimen IT.0.0(6).Ti tension force contribution-section at 175 kips (778 kN).

As seen in the figures above, T specimens had higher relative participation from the NSM materials than the IT specimens. Despite using twice the number of bars, the NSM stainless steel strengthened specimen had similar flexural tension contributions to those of the NSM titanium strengthened specimen. For IT specimens, the NSM stainless steel carried higher force than the NSM titanium, while the embedded flexural steel carried the same magnitude of force in the similar IT specimens. This indicates that for the IT configuration, shear lag may play a larger role in developing the forces in the NSM materials (titanium bars were placed only in the flanges while stainless steel bars were placed within the flanges and the web). In each retrofitted specimen, the relative contribution of the NSM materials was largest in Sections 4, 5, and 6 (length from

preformed crack to end of cutoff reinforcing steel bar). The demands in the NSM materials at the termination of the NSM bars (at midspan and close to the support) were low.

### 4.1.7 Bond Stresses in Girder Specimens

Bond stresses were calculated for each of the specimens using three or more consecutive strain gages along the length of a bar of interest from the preformed diagonal crack to the end of the cutoff bar. The average bond stress, $\mu_{avg}$, over an incremental length of reinforcement was calculated as:

$$\mu_{avg} = \frac{\Delta f_s d_b}{4\Delta l} \qquad [4.2]$$

where $\Delta f_s$ is the change in the bar stress, $\Delta l$ is the length between the strain gages, and $d_b$ is the bar diameter. The mean average bond stress, $\overline{\mu}_{avg}$, for the cutoff reinforcing steel bars, the fully anchored reinforcing steel bars, and the NSM bars were taken as the mean of the incremental average bond stress measurements along the instrumented sections of bars. The peak bond stress $\mu_{max}$, of any bar was taken as the maximum incremental average bond stress along the section. Critical bond stresses for all specimens except specimen IT.0.0(6).Ti were located near the cutoff bars in Sections 3 to 7. The critical section for bond stresses in specimen IT.0.0(6).Ti was located near midspan along the development length of the steel. Bond stresses at failure were estimated for the applicable cutoff reinforcing steel bars, fully anchored reinforcing steel bars, and NSM bars and are reported in Table 4.2.

**Table 4.2: Summary of largest measured bond stresses at critical section**

| Specimen | Cutoff Bar | | Anchored Bar | | NSM Bars | | |
|---|---|---|---|---|---|---|---|
| | $\overline{\mu}_{avg}$ (psi) [MPa] | $\mu_{max}$ (psi) [MPa] | $\overline{\mu}_{avg}$ (psi) [MPa] | $\mu_{max}$ (psi) [MPa] | Bar ! | $\overline{\mu}_{avg}$ (psi [MPa] | $\mu_{max}$ (psi) [MPa] |
| T.45.Ld3(10).Ti | 802 [5.52] | 858 [5.90] | 0.000 [0.00] | 0.000 [0.00] | U | 450 [3.09] | 1057 [7.28] |
| | | | | | L | 359 [2.47] | 889 [6.12] |
| T.45.Ld3(6).Ti | 552 [3.80] | 1212 [8.35] | 335 [2.31] | 697 [4.80] | U | 262 [1.80] | 392 [2.70] |
| | | | | | L | 116 [0.79] | 187 [1.28] |
| T.45.Ld3(6).SS | 761 [5.24] | 1422 [9.78] | - - | - - | U | 142 [0.97] | 278 [1.91] |
| | | | | | L | 667 [4.59] | 1457 [10.03] |
| IT.45.Ld3(10).Ti | 466* [3.21] | 735 [5.07] | 24 [0.17] | 73 [0.51] | 1 | 132 [0.91] | 326 [2.25] |
| | | | | | 2 | 123 [0.83] | 188 [1.30] |
| IT.45.Ld3(6).Ti | 424 [2.92] | 898 [6.19] | 164 [1.13] | 324 [2.23] | 1 | 1097 [7.56] | 2254 [15.5] |
| | | | | | 2 | n/a n/a | n/a n/a |
| IT.45.Ld3(6).SS | 263 [1.81] | 362 [2.50] | 122 [0.84] | 365 [2.52] | 1 | 304 [2.10] | 488 [3.36] |
| | | | | | 2 | 504 [3.47] | 1478 [10.2] |
| IT.0.0(6).Ti | **Cutoff Bar 1** | | **Cutoff Bar 2** | | 1 | 165* [1.14] | 421* [2.90] |
| | 158 [1.09] | 415 [2.86] | 156 [1.08] | 416 [2.87] | | | |
| | | | | | 2 | 326* [2.25] | 648* [4.47] |

*taken at lower load because of strain gages were lost prior to failure
! U is Upper and L is Lower layer of steel

The cutoff steel reinforcing bars exhibited higher bond stresses than the hooked and NSM reinforcement. This indicated significant stress transfer between the concrete and cutoff steel reinforcing bars in the termination region. The bond stresses in the hooked steel reinforcing bars were lower than the cutoff bars at the same locations because they were adequately anchored and as shown from the material strain plots, the hooked steel reinforcing bars were at or near yield in

this region. The titanium NSM reinforcement exhibited lower bond stresses than the stainless steel NSM reinforcement at similar load levels. Comparison with the bond stresses reported by Triska and Goodall *(Triska and Goodall 2010)* showed that the NSM bars reduced the magnitude of the bond stress in the embedded flexural steel cutoff bars.

## 4.2 COMPONENT TEST BOND STRESS RESULTS

This section describes the results of six bond length specimens. Three (3) specimens were tested with a 4 in. (102 mm) bond length and three (3) with a 12 in. (305 mm) bond length. The average bond stress and bar slip responses observed from the experiments are reported.

### 4.2.1 Component Bond Stress Test: 4 in. (102 mm) Specimens

The failure surface of the 4 in. (102 mm) long embedded specimens was the concrete-epoxy interface. The surrounding concrete showed diagonal cracks initiating from the pulled (or loaded) end of the bar. The cracks were typical of bursting stresses and eventually progressed to the stress-free end of the bar (mid-block). illustrates the cracking at failure and a detail of the concrete epoxy failure. Figure 4.46


Figure 4.46: Bond stress specimen with 4 in. (102 mm) bond length at failure.

The applied load-slip responses for each 4 in. (102 mm) bond length specimen are shown in Figure 4.47. The slip of the NSM titanium bar was measured at the stress-free end of the bar at mid-block. Since the observed failure surface was at the epoxy-concrete interface, bond stress was calculated along the bonded groove surface as in Equation (4.3):

$$\mu_{avggroove} = \frac{\Delta T}{3 d_g L} \tag{4.3}$$

where $\Delta T$ is the change of force along the bar, taken as the actuator load, $d_g$ is the depth of the groove taken nominally as 1 in. (25.4 mm), $L$ is the bonded length, taken as 4 in. (102 mm).

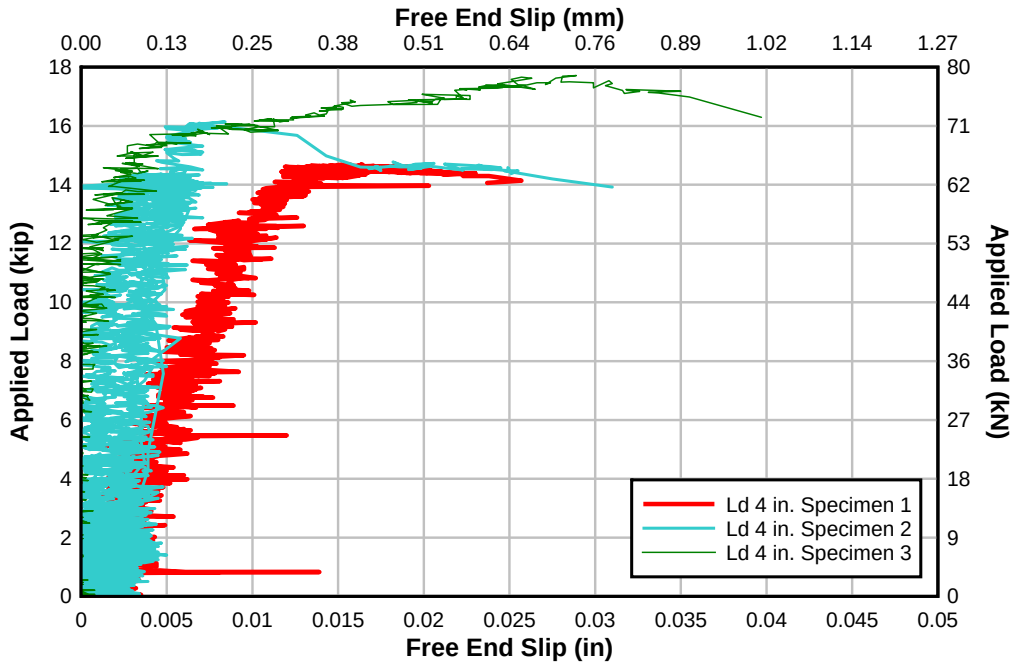


Figure 4.47: Load-slip response of 4 in. (102 mm) bond length specimen.

The bar slip versus load response exhibited minimal bar slip until failure. Specimen 1 exhibited more bar end slip due to more extensive concrete cracking in the specimen. All failures were abrupt. Bond stresses computed using the concrete-epoxy failure surface (Equation (4.3)), were less than those using Equation (2.1) because the surface area of the bar-epoxy interface was smaller than that of the concrete-epoxy interface. The mean and maximum average bond stresses are reported in Table 4.3.

**Table 4.3: Bond stresses for 4 in. (102 mm) bond length specimens of titanium alloy bars.**

| Specimen | Maximum $\mu_{avg}$ Groove (ksi) [MPa] | Mean $\mu_{avg}$ Groove (ksi) [MPa] | Maximum $\mu_{avg}$ Bar (ksi) [MPa] | Mean $\mu_{avg}$ Bar (ksi) [MPa] | Embedded End Slip (in) [mm] |
|---|---|---|---|---|---|
| Ld 4 in. 1 | 1.305 | 1.437 [9.90] | 1.899 | 2.091 [14.4] | 0.016 |
| | [8.99] | | [13.08] | | [0.40] |
| Ld 4 in. 2 | 1.434 | | 2.086 | | 0.008 |
| | [9.88] | | [14.37] | | [0.21] |
| Ld 4 in. 3 | 1.574 | | 2.290 | | 0.029 |
| | [10.84] | | [15.78] | | [0.71] |

Throughout the bond length tests the maximum NSM titanium bar stress achieved was around 60 ksi (414 MPa), which is less than half the yield stress of the NSM titanium bar. The 4 in. bond length specimen results indicate that the development length of a straight NSM titanium alloy bar is greater than 4 in. (51 mm) and if linearly extrapolated would be approximately 8 in. (102 mm).

### 4.2.2 Component Bond Stress Tests: 12 in. (305 mm) Specimens

The intent of the 12 in. (305 mm) NSM titanium bar embedment length was to measure the active bond length and to further investigate the bond stresses along the embedment length. Since the 4 in. (102 mm) specimens did not reach the yield stress of the NSM titanium bars, a longer embedment of 12 in. (305 mm) was selected. The specimens were instrumented with three strain gages spaced at 3 in. (76.2 mm) intervals along the bonded length of the NSM titanium alloy bars. An average maximum actuator load of 16.3 kips (72.5 kN) was reached for the three 12 in. (305 mm) embedment tests. The average slip at peak load was 0.0035 in. (0.089 mm). When approaching the maximum load, the load-end slip displacement response softened. The titanium-epoxy and epoxy-concrete interfaces remained intact until near failure. The strength of the specimen became dependent on the concrete and internal reinforcing steel within the concrete block. This failure condition is shown in Figure 4.48. As seen in this figure, the failure is controlled by the strength of the block rather than the epoxy bonded interfaces. The free-end bar slip of the titanium versus applied load for each test is shown in Figure 4.49.

Figure 4.48: Bond stress test specimens with 12 in. bond length at failure (left) and detail of remaining concrete (right).

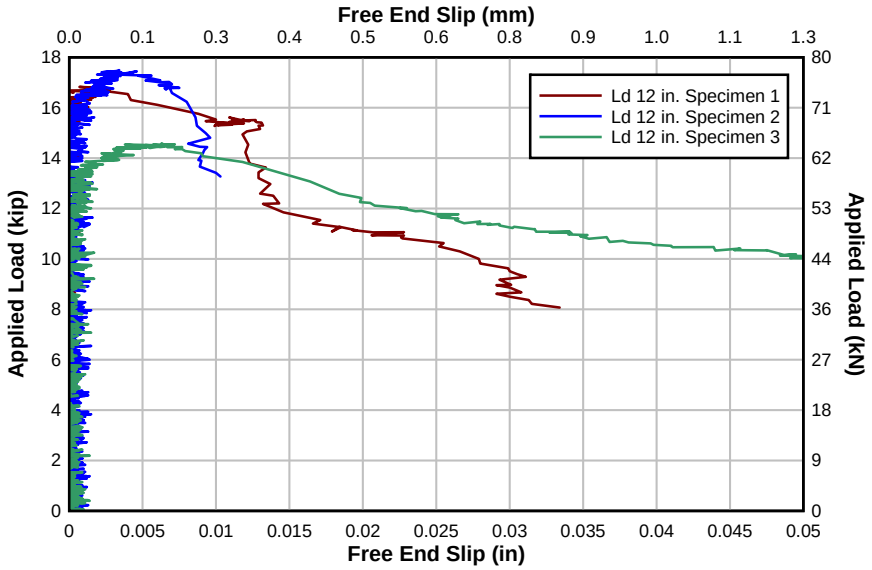


Figure 4.49: Load-slip response of 12 in. (305 mm) bond length specimen.

As seen in Figure 4.49, the embedded stress-free end did not slip until near failure loads. The load slip curves from the 12 in. (304 mm) embedment length were much stiffer than those from the 4 in. (102 mm) embedment length. The maximum average applied load in the 12 in. (304 mm) tests are almost identical to those of the 4 in. (102 mm) tests but with less bar slip. These similar maximum loads indicate that the material properties and geometry of the concrete blocks were the limiting factors rather than the bonded length of the NSM titanium.

Failure occurred in the concrete around the groove and the 12 in. (305 mm) bond length specimens did not achieve the yielding load for the NSM titanium alloy bars. The observed cracking angle in the concrete was approximated to 37° with a failure depth equal to the depth of the groove (1 in. (25.4 mm)). This indicates that the controlling parameter for NSM bars will be the concrete interface. Reliance on concrete tensile strength at the surface will limit the magnitude of stress that can be developed by NSM materials. The addition of mechanical anchorages is necessary to make full use of the material strength and the reason hooked ends were used in the present research study.

Strains at 3 in. (76.2 mm) intervals along the embedded bars were monitored and are shown at various load levels in Figure 4.50. The point at length 0 is representative of strain in the bar from the applied load. The point at 12 in. (305 mm) is the free end of the NSM titanium bar located at mid-block.

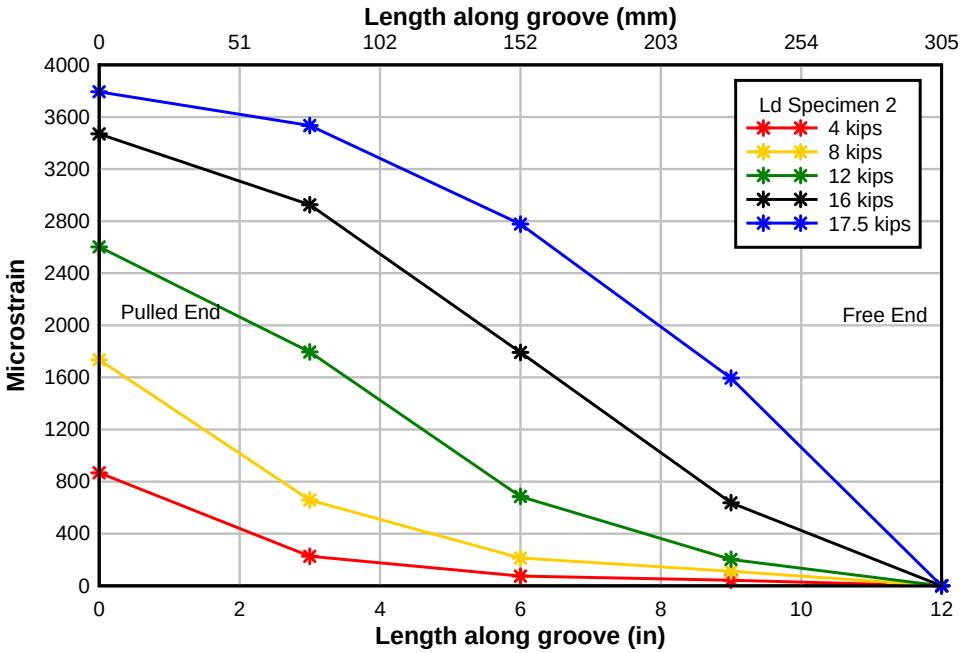


Figure 4.50: Variation in strains along 12 in. (305 mm) bond length specimen of NSM titanium alloy bar.

Using methods described previously to compute bond stresses from the strain gage data, the average bond stresses along the bar were determined. The stress in the loaded end of the bar was known directly from the actuator load cell and this was used to compute the mean average bond stress over the embedded 12 in. (305 mm) length. The maximum average bond stress was taken

from the strain gradient observed from the strain gages along the bar. The mean and maximum average bond stresses are shown in Table 4.4.

**Table 4.4: Bond test results for 12 in. embedment length.**

| Specimen | Load (kip) [kN] | Maximum $\mu_{avg}$ Bar (psi) [MPa] | Mean $\mu_{avg}$ Bar (psi) [MPa] |
|---|---|---|---|
| Ld 12 in. 1 | 16.7 | 980 | 802 [5.53] |
| | [74.4] | [6.75] | |
| Ld 12 in. 2 | 17.5 | 754 | |
| | [77.8] | [5.20] | |
| Ld 12 in. 3 | 14.4 | 673 | |
| | [64.2] | [4.64] | |

It is common in bond or development length tests to achieve higher bond stresses than those observed in a full-scale beams or girders. From the bond tests, the NSM titanium alloy bars exhibited bond stresses twice that of the full-scale T girders and eight times that of the IT-specimens.

## 4.3 TITANIUM PULLOUT RESULTS

Tests were performed on five different titanium surface treatments to assess the role of the surface treatment on the bond and anchorage of the bars. The stress-strain curves for the titanium alloy bars were shown in Figure 4.51. The titanium alloy bars did not have a well-defined yield plateau and the 0.2% offset was used to determine the yield values. The yield stress and ultimate stress values for each titanium surface treatment are summarized in Table 4.5. The material properties were similar for all five different surface treatments.

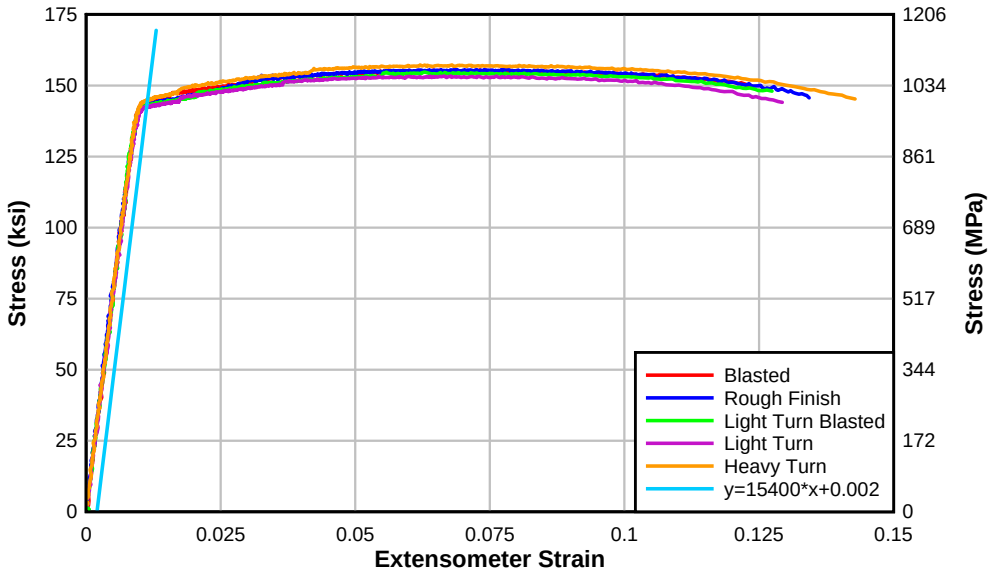


Figure 4.51: Stress-strain curves for titanium alloy bars with various surface treatments.

**Table 4.5: Titanium surface roughness tensile testing summary.**

| Surface Finish | 0.2% Offset Yield Stress (ksi) [MPa] | Ultimate Stress (ksi) [MPa] |
|---|---|---|
| Blasted | 144.5 [996] | 155.5 [1072] |
| Rough Finish | 143.8 [991] | 155.6 [1073] |
| Blasted Light Turn | 143.2 [987] | 154.7 [1067] |
| Light Turn | 142.4 ]982] | 153.4 [1058] |
| Heavy Turn | 144.6 [997] | 157.2 [1084] |

Pullout tests were then performed on the titanium alloy bars having five different surface treatments, on four bars containing bulb end samples, and on three additional bars having the "heavy turn" pattern that was used for the greater specimens. These tests were used to assess relative differences in bond along the different surface treatments. From the applied loads, average bond stresses were calculated using Equation (4.2). Average bond stresses versus pullout displacement are shown from Figures 4.52 to 4.54.

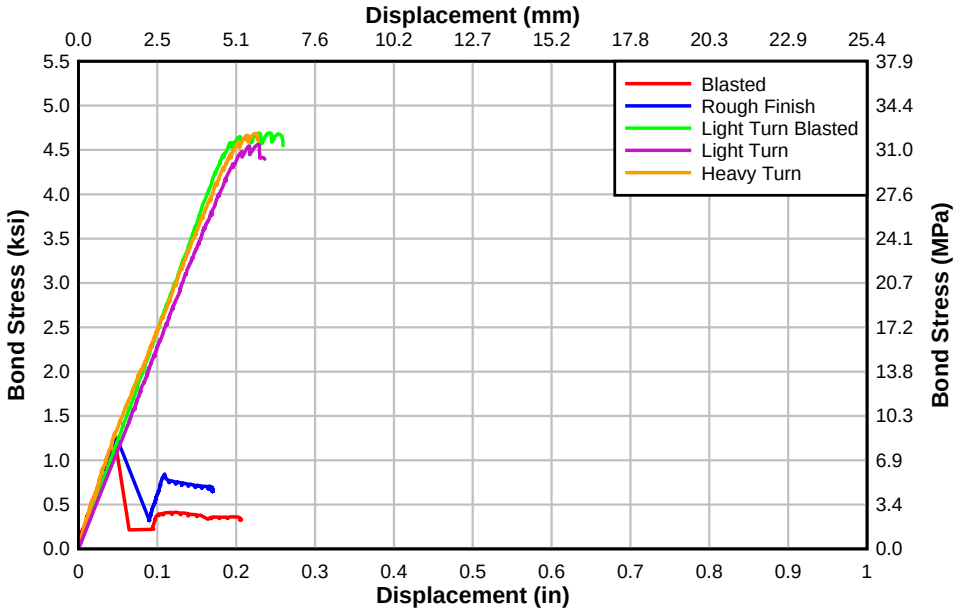


Figure 4.52: Bond stresses from pullout tests of titanium alloy bars with alternative surface treatments.

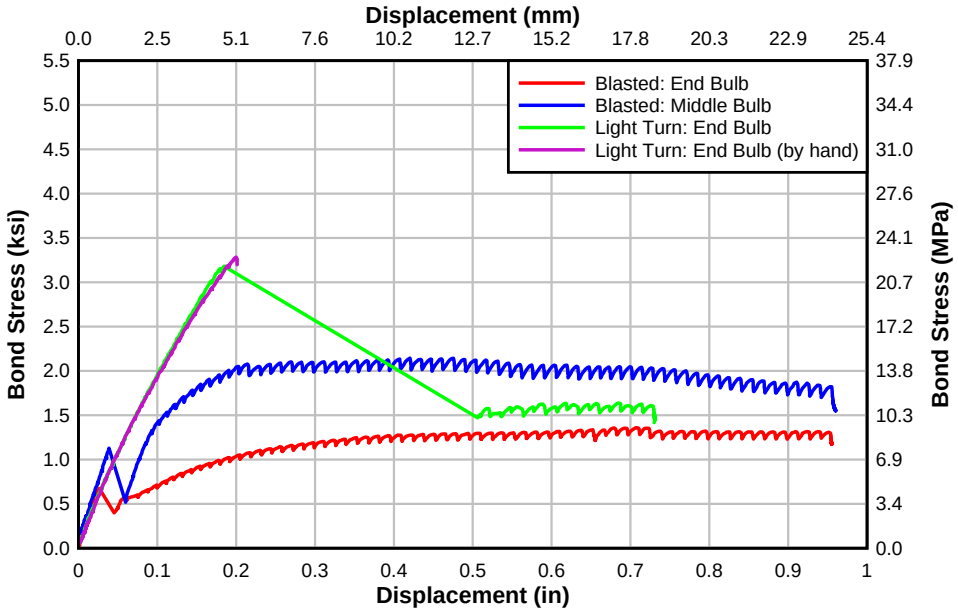


Figure 4.53: Bond stresses from pullout tests of titanium alloy bars with alternative bulbed end treatments.

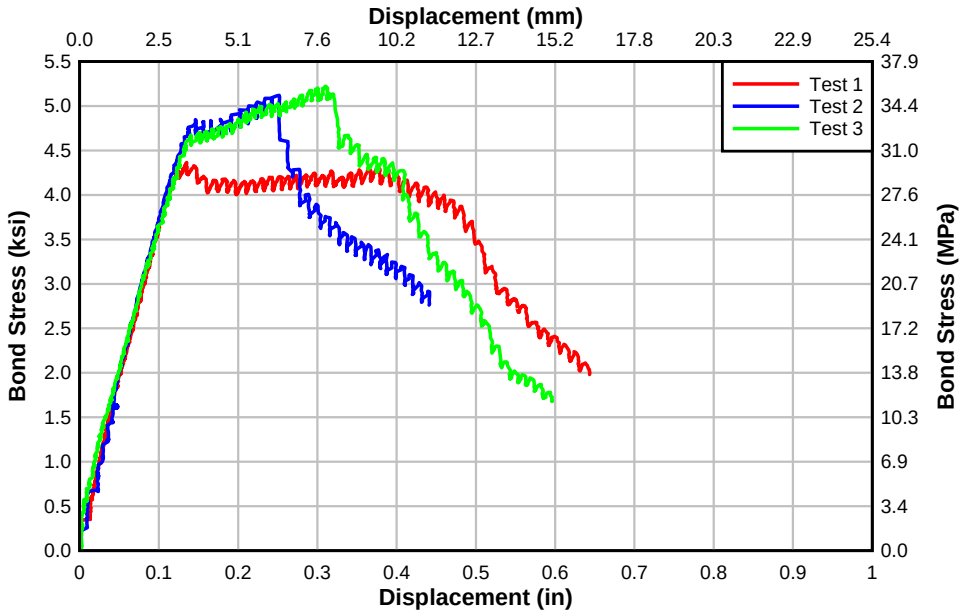


Figure 4.54: Bond stresses from pullout tests of titanium alloy bars with "heavy turn" surface treatment.

The blasted and surface roughened titanium alloy bars failed along the epoxy-titanium interface. Once the bars lost adhesion to the epoxy they were pulled through the epoxy and exhibited friction behavior. The team alloy bars with the turn surface were able to achieve much higher loads. The titanium alloy bars with special bulbed ends (embedded in the hole) showed similar results to the blasted finishes. None of the bulb end specimens were able to achieve bond stresses in the range of the heavy turned bars without the bulbs. The heavy turn bars were able to achieve the yield stress of the titanium alloy bars. Based on the tensile and pullout test results, the heavy turn titanium alloy bars were selected as the NSM titanium material for retrofitting the full-scale specimens.

## 4.4 HOOK DUCTILITY TESTS

The titanium alloy bars used for the hook ductility tests came from a different material heat than the titanium alloy bars used for the full-scale girder tests and the tensile and pullout tests described previously. Thus, tensile tests were performed for the titanium alloy bars used in the hook tests. Tensile test results are shown in Figure 4.55. The yield stresses were found using the 0.2% offset method. Average of three tests resulted in a yield stress of 144.7 ksi (998 MPa), an ultimate stress of 157.2 ksi (1084 MPa), and an ultimate elongation of 14%. The yield and elongation properties were nearly identical to the titanium alloy bars used in the full-scale girder tests.

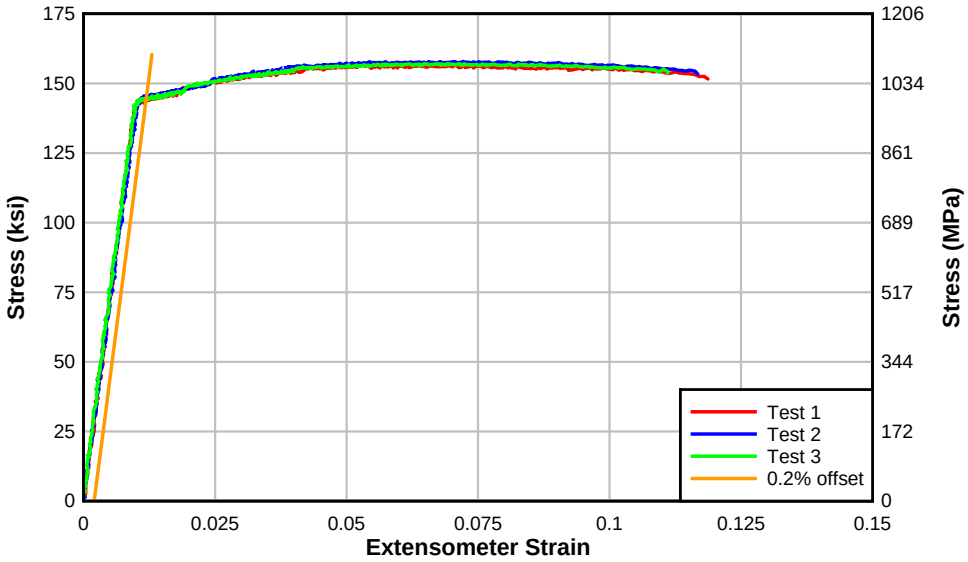


Figure 4.55: Stress-strain curves for titanium alloy bars used for hook ductility tests.

In total, 12 samples were fabricated and tested. Three sets of (3) replicates were heated to 900 ˚F (482 ˚C) and bent around 2 in. (51 mm), 3 in. (76 mm), and 4.5 in. (114 mm) diameter bending pins, respectively. An additional three samples were heated to 1250 ˚F (677 ˚C) and bent around the 2 in. (51 mm) diameter bending pin.

The first two samples of each group of three were tested without any modifications. Of these, each of the 2 in. (51 mm) hooks fractured in the center of the 180˚ bend and the 3 in. (76 mm) and 5 in. (127 mm) hooks fractured at the top or bottom bearing point location just outside the plate fixture. The third specimen in each group had the inside bend ground manually using a die grinder to smooth out the bend. These removed the stress concentrations in the corners of the bars to enable them to achieve higher loads and additional deformation. These specimens are designated with “ground” in the load-deformation figures.

For each of the hooks bent at 900 ˚F (482 ˚C), the third specimen was modified before testing. On these specimens, the deformations were removed by grinding at the previously observed fracture locations to remove any stress concentrations in the bend. The modified hooks were then tested. The results shifted the failure locations with the 2 in. (51 mm) hook fracturing at the bearing plate location, the 3 in. (76 mm) hook fracturing at the center of the 180˚ bend, and the 5 in. (127 mm) hook fracturing at the bearing point location, but the overall load and displacement were greatly increased. For the third test of the 2 in. (51 mm) and 3 in. (76 mm) hooks, the horizontal movement of the bend of the hook toward the fixture during straightening was measured using a laser extensometer to quantify the geometry change during the test. This showed that the hook eccentricity decreases by about 0.25 in. (6 mm) as the hook was pulled in tension, thereby decreasing the amount of bending relative to the axial load in the bars as the test progressed.

The first test of the 2 in. (51 mm) hooks bent at 1250 ˚F (677 ˚C) had a large load of approximately 0.6 kips applied accidentally prior to the test. This accounts for the large difference in the slope for the specimen. The displacement results for each set of tests are

summarized from Figure 4.56 to Figure 4.59. A summary of the test results is shown in Table 4.6.

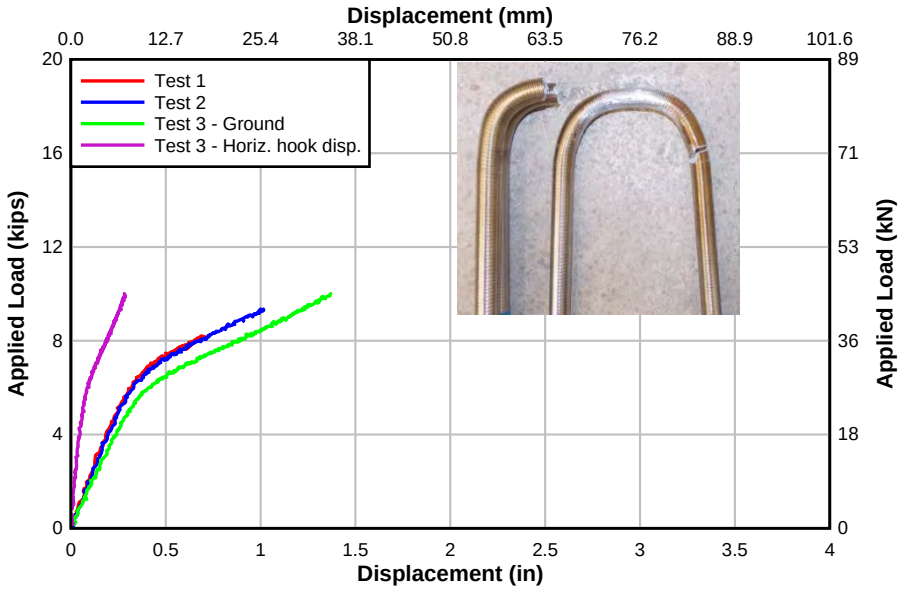


Figure 4.56: 2 in. (51 mm) hooks bent at 900 ˚F (482 ˚C).

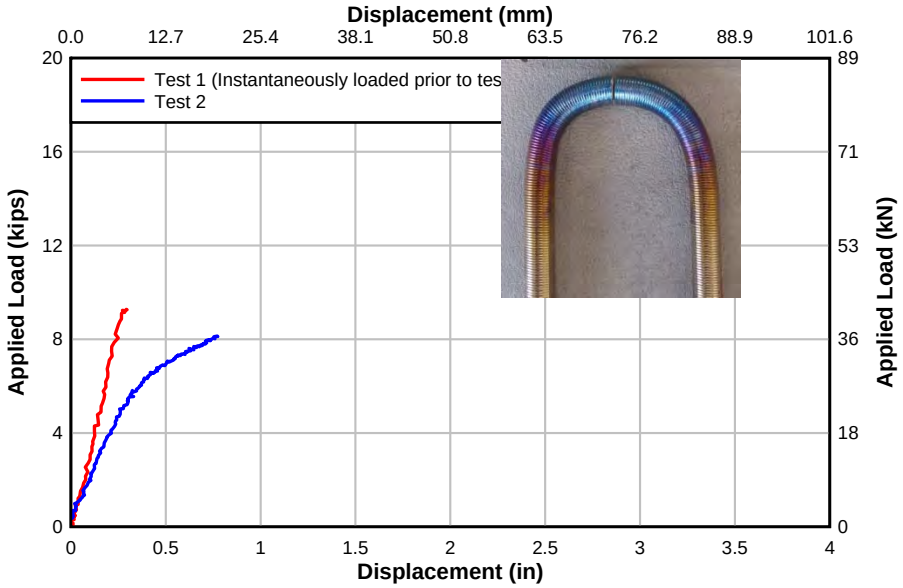


Figure 4.57: 2 in. (51 mm) hooks bent at 1250 ˚F (677 ˚C).

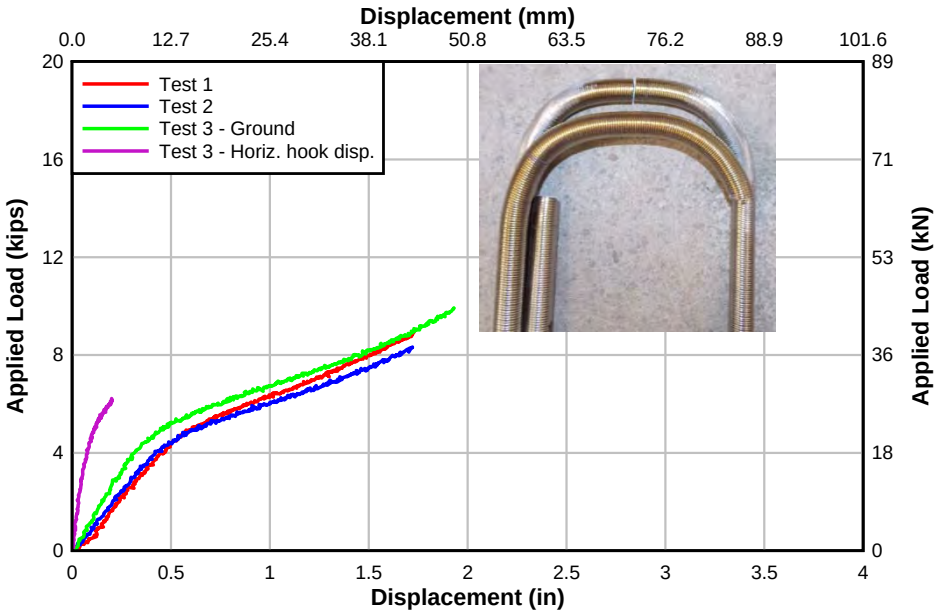


Figure 4.58: 3 in. (76 mm) hooks bent at 900 ˚F (482 ˚C).

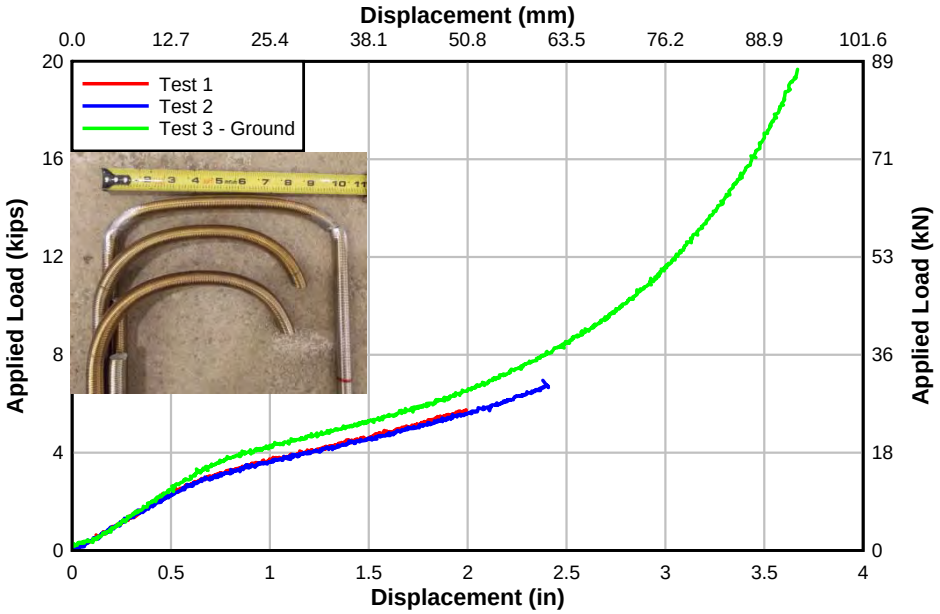


Figure 4.59: 5 in. (127 mm) hooks bent at 900 ˚F (482 ˚C).

**Table 4.6: Summary of 180˚ hook ductility tests.**

| Specimen | Test | $P_{max}$ (kips) [kN] | Max. Disp. (in.) [mm] | Failure Location |
|---|---|---|---|---|
| 2 in. (51 mm) 900 ˚F (482 ˚C) | 1 | 8.20 [36.5] | 0.69 [17.5] | hook center |
| | 2 | 9.35 [41.6] | 1.10 [28.0] | hook center |
| | 3 | 10.0 [44.5] | 1.37 [34.8] | bearing point |
| 2 in. (51 mm) 1250 ˚F (677 ˚C) | 1 | 9.28 [41.3] | 0.292 [7.4] | hook center |
| | 2 | 8.14 [36.2] | 0.772 [18.3] | hook center |
| 3 in. (76 mm) 900 ˚F (482 ˚C) | 1 | 8.95 [39.8] | 1.73 [43.9] | bearing point |
| | 2 | 8.33 [37.1] | 1.72 [43.7] | bearing point |
| | 3 | 9.92 [44.1] | 1.93 [49.0] | hook center |
| 5 in. (127 mm) 900 ˚F (482 ˚C) | 1 | 5.75 [25.6] | 1.99 [48.8] | bearing point |
| | 2 | 6.95 [30.9] | 2.38 [60.5] | bearing point |
| | 3 | 19.7 [87.5] | 3.67 [93.2] | bearing point |

To assess whether the hook failures were occurring elastically or inelastically, the plastic moment capacity of the titanium alloy bars, $M_p$, was calculated as:

$$M_p = zf_y \tag{4.5}$$

where $z$ is the plastic section modulus, taken as $z = 1.33r^3$, with $r$ equal to the radius of the bar, and $f_y$ is the titanium alloy yield strength. The applied load necessary to achieve the plastic moment, $P_{plastic}$, was calculated using:

$$P_{plastic} = \frac{2M_p}{e} \tag{4.6}$$

where $e$ is the distance from the bearing plate to the outside of the hook based on the initial geometry of the setup. From the test results, the maximum surface stress in the bar if it remained elastic, $\sigma$, at failure was calculated as:

$$\sigma = \frac{P_{\max}}{A} + \left(\frac{P_{\max} e}{2}\right)\frac{1}{S} \tag{4.6}$$

where $P_{max}$ is the maximum load achieved at failure, $A$ is the area of the bar, and $S$ is the section modulus of bar. The summary of these calculations are shown in Table 4.7. The inside bend at the point of inflection was plastic at failure for all the hooks as seen from the comparison of $P_{max}$ to $P_{plastic}$. All fractures (before grinding) occurred at approximately the same load, but were greater than the load required to produce the plastic bending moment capacity of the titanium alloy bars, and indicated that fracture occurred well into the inelastic range. The removal of surface deformations within the high stress regions can significantly increase deformation and strength.

**Table 4.7: Summary of initial eccentricities, plastic loads, and combined titanium alloy stresses (bending and axial) from hook ductility tests.**

| Specimen | Test | $P_{max}$ (kips) [kN] | e (in.) [mm] | $P_{plastic}$ (kips) [kN] | Stress, σ (ksi) [MPa] |
|---|---|---|---|---|---|
| 2 in. (51 mm) 900 ˚F (482 ˚C) | 1 | 8.20 [36.5] | 2.0 [50.8] | 5.61 [25.0] | 386 [2661] |
| | 2 | 9.35 [41.6] | | | 430 [3034] |
| | 3 | 10.0 [44.5] | | | 471 [3247] |
| 2 in. (51 mm) 1250 ˚F (677 ˚C) | 1 | 9.28 [41.3] | 2.0 [50.8] | 5.61 [25.0] | 437 [3009] |
| | 2 | 8.14 [36.2] | | | 383 [2639] |
| 3 in. (76 mm) 900 ˚F (482 ˚C) | 1 | 8.95 [39.8] | 2.5 [63.5] | 4.49 [20.0] | 519 [3577] |
| | 2 | 8.33 [37.1] | | | 483 [3329] |
| | 3 | 9.92 [44.1] | | | 575 [3963] |
| 5 in. (127 mm) 900 ˚F (482 ˚C) | 1 | 5.75 [25.6] | 3.5 [88.9] | 3.21 [14.3] | 459 [3164] |
| | 2 | 6.95 [30.9] | | | 555 [3825] |
| | 3 | 19.7 [87.5] | | | 1570 [10824] |

# 5.0 ANALYTICAL METHODS

This chapter describes the analytical methods used to compare experimental findings, design specifications, and other past experiments found in the literature. The primary methods of analysis were Response 2000 (*Bentz 2000*), the AASHTO-LRFD, and ACI 318-11 design specifications. Flexural strength predictions were determined using Response 2000 (R2K) and AASHTO-LRFD specifications. The development lengths of straight and hooked steel reinforcing bars were compared between AASHTO and ACI design specifications. The experimentally measured flexural tension forces in the reinforcing materials were compared with the predicted forces using Response 2000, AASHTO, and ACI. The overall response and bond stress of the strengthened specimens were compared to archival tests from Higgins *(Higgins 2004)* and Triska and Goodall *(Triska and Goodall 2010)*. Lastly, a design methodology is presented using an equivalent area of steel method and ACI 440 specifications.

## 5.1 PREDICTED SHEAR AND MOMENT CAPACITIES

The following section discusses the shear and moment capacities of the strengthened test specimens determined according to AASHTO and ACI methods. The predicted capacities were compared to the predictions from R2K. Analyses were performed for each specimen at critical sections along the span considering combined shear-moment interactions.

The specimen base strength was first computed without considering the presence of NSM materials. The specimen strengths (either diagonal-tension controlled or flexurally controlled) were translated into a corresponding applied shear to produce failure at the controlling critical section. Four (4) critical sections along the span were evaluated: 1) the termination of the cutoff reinforcing steel (corresponding approximately to a 33 degree crack extending from the edge of the load plate), 2) the intersection of the precast diagonal crack with the centroid of the internal flexural steel (approximately 1/3 the development length of the cutoff steel), 3) a location approximately $d_v$ (distance from the center of the compression block to the centroid of steel) from the edge of the loading plate near midspan, and 4) at midspan (flexural failure). The correct moment-to-shear ratios at each of the three sections were used in the analyses. The M/V ratios in the T specimens were 7.5:1 (critical section 3), 7.2:1 (critical section 2) and 5.5:1 (critical section 1) for T specimens and 6.3:1 (critical section 3), 5.9:1 (critical section 2) and 4.19:1 (critical section 1) for IT specimens. A diagonal-tension failure was presumed to occur at a distance at least $d_v$ away from the load point. Therefore, a M/V larger ratio than 7.5:1 or 6.3:1(the ratio of the 45 degree crack) was not considered. The shear and flexural strengths were also computed according to the AASHTO provisions at the same critical sections. The simplified ACI approach was not used because it fails to consider moment–shear interactions in the strength calculation. To model the developing cutoff flexural reinforcing steel in the analyses, an equivalent area of reinforcing steel was used having the same yield stress as the #11 (36M) cutoff reinforcing steel bars. The ACI development length of the straight #11 (36M) bar was calculated for each specimen based on the experimentally determined material properties (see following section) and used to determine the equivalent area of the flexural cutoff bar in the model. Except for the #4 (13M) deck steel, all reinforcing bars were included in the R2K model. The #4 deck steel was

considered for specimen IT.0.0(6).Ti. The material inputs corresponded to the measured day-of-test material properties for each specimen. The specimen base strengths are shown in Table 5.1a and 5.1b. As seen in these tables, without NSM, all specimens would fail at a location $d_v$ from the loading plates. If all five (5) #11 bars were fully anchored along the span, then the failure could be either flexural at midspan (for specimens with 6 in. stirrup spacing) or shear-flexure at $d_v$ from the loading plates. Because none of the base specimens has five (5) fully anchored #11 reinforcing bars along the span, the failure would be controlled by shear-flexure at $d_v$.

The analyses were repeated considering the NSM materials applied to the specimens. The analyses with the NSM materials assumed that they were fully anchored and could develop their full strength. The predicted specimen capacities and the controlling actuator load are also shown in Table 5.2a and 5.2b, for AASHTO-LRFD and R2K, respectively.

**Table 5.1a: Analytically predicted capacities for all specimens *without* NSM using AASHTO-LRFD.**

| Specimen ID | Moment Capacity for 5 #11's (kip-ft) [kN-m] | Shear to Reach Moment Capacity for 5 #11's (kips) [kN] | Shear Capacity @ dv for 3 #11's + 2 partial #11's (kips) [kN] | Shear Capacity @ dv for 5 #11's (kips) [kN] |
|---|---|---|---|---|
| T.45.Ld3(10).Ti | 1822.9 | 165.7 | 140.8 | 168.2 |
| | [2471] | [737] | [626] | [748] |
| T.45.Ld3(6).Ti | 1823.0 | 165.7 | 154.4 | 188.2 |
| | [2472] | [737] | [687] | [837] |
| T.45.Ld3(6).SS | 1822.0 | 165.6 | 151.7 | 188.2 |
| | [2470] | [737] | [675] | [837] |
| IT.45.Ld3(10).Ti | 2083.5 | 212.0 | 173.9 | 182.1 |
| | [2825] | [943] | [774] | [810] |
| IT.45.Ld3(6).Ti | 2083.5 | 212.0 | 194.0 | 230.0 |
| | [2825] | [943] | [863] | [1023] |
| IT.45.Ld3(6).SS | 2083.4 | 211.9 | 192.9 | 228.6 |
| | [2825] | [943] | [858] | [1017] |
| IT.0.0(6).Ti* | 867.8 | - | - | - |
| | [1176] | | | |

*Moment at midspan.

**Table 5.1b: Analytically predicted capacities for all specimens *without* NSM using R2K.**

| Specimen ID | Moment Capacity for 5 #11's (kip-ft) [kN-m] | Shear to Reach Moment Capacity for 5 #11's (kips) [kN] | Shear Capacity @ dv for 3 #11's + 2 partial #11's (kips) [kN] | Shear Capacity @ dv for 5 #11's (kips) [kN] |
|---|---|---|---|---|
| T.45.Ld3(10).Ti | 2415.4 | 219.6 | 149.1 | 180.7 |
| | [3275] | [977] | [663] | [804] |
| T.45.Ld3(6).Ti | 2400.0 | 218.2 | 166.0 | 196.6 |
| | [3254] | [970] | [738] | [874] |
| T.45.Ld3(6).SS | 2380.7 | 216.4 | 163.1 | 196.3 |
| | [3228] | [963] | [725] | [873] |
| IT.45.Ld3(10).Ti | 2380.0 | 242.1 | 177.8 | 193.2 |
| | [3227] | [1077] | [791] | [859] |
| IT.45.Ld3(6).Ti | 2369.3 | 241.0 | 206.1 | 249.8 |
| | [3212] | [1072] | [917] | [1111] |
| IT.45.Ld3(6).SS | 2367.8 | 240.9 | 205.4 | 250.6 |
| | [3210] | [1071] | [914] | [1115] |
| IT.0.0(6).Ti* | 967.0 | | | |
| | [1311] | | | |

*Moment at midspan.

**Table 5.2a: Analytically predicted capacities for all specimens *with* NSM using AASHTO-LRFD.**

| Specimen ID | Shear at #11 End of Cutoff (kips) [kN] | Shear at Pre-formed Crack (kips) [kN] | Shear at $d_v$ from Load Plate (kips) [kN] | Controlling Shear (kips) [kN] | Experiment Shear (kips) [kN] | Experiment/ Predicted |
|---|---|---|---|---|---|---|
| T.45.Ld3(10).Ti | 170.3 | 167.7 | 167.2 | 165.7! | 200.0 | 1.21 |
| | [758] | [746] | [744] | [737] | [890] | |
| T.45.Ld3(6).Ti | 212.6 | 207.6 | 207.1 | 165.7! | 216.4 | 1.31 |
| | [946] | [923] | [921] | [737] | [963] | |
| T.45.Ld3(6).SS | 211.8 | 206.4 | 205.6 | 165.6! | 215.7 | 1.30 |
| | [942] | [918] | [915] | [737] | [959] | |
| IT.45.Ld3(10).Ti | 185.4 | 182.9 | 182.7 | 182.7 | 213.8 | 1.17 |
| | [825] | [814] | [813] | [813] | [951] | |
| IT.45.Ld3(6).Ti | 234.3 | 230.6 | 230.0 | 212.0! | 224.0 | 1.06 |
| | [1042] | [1026] | [1023] | [943] | [996] | |
| IT.45.Ld3(6).SS | 239.7 | 232.6 | 231.1 | 211.9! | 250.0 | 1.18 |
| | [1066] | [1034] | [1028] | [943] | [1112] | |
| IT.0.0(6).Ti* | | | | *867.8 kip-ft | *951.0 kip-ft | 1.10 |
| | | | | [1176 kN-m] | [1289 kN-m] | |

! Controlled by flexure from Table 5.1a *Moment at midspan.

**Table 5.2b: Analytically predicted capacities for all specimens *with* NSM using R2K.**

| Specimen ID | Shear at #11 End of Cutoff (kips) [kN] | Shear at Pre-formed Crack (kips) [kN] | Shear at $d_v$ from Load Plate (kips) [kN] | Controlling Shear (kips) [kN] | Experiment Shear (kips) [kN] | Experiment/ Predicted |
|---|---|---|---|---|---|---|
| T.45.Ld3(10).Ti | 198.2 | 197.7 | 197.1 | 197.1 | 200.0 | 1.01 |
| | [757.67] | [745.87] | [743.87] | [877] | [890] | |
| T.45.Ld3(6).Ti | 241.9 | 238.5 | 237.0 | 218.2! | 216.4 | 0.99 |
| | [945.64] | [923.40] | [921.18] | [970] | [963] | |
| T.45.Ld3(6).SS | 234.3 | 223.7 | 222.5 | 216.4! | 215.7 | 1.00 |
| | [942.09] | [918.07] | [914.51] | [963] | [959] | |
| IT.45.Ld3(10).Ti | 210.6 | 198.5 | 197.1 | 197.1 | 213.8 | 1.08 |
| | [824.78] | [813.70] | [812.87] | [877] | [951] | |
| IT.45.Ld3(6).Ti | 262.5 | 257.4 | 257.2 | 241.0! | 224.0 | 0.93 |
| | [1042.23] | [1025.74] | [1022.88] | [1072] | [996] | |
| IT.45.Ld3(6).SS | 272.9 | 265.6 | 262.2 | 240.9! | 250.0 | 1.04 |
| | [1066.23] | [1034.43] | [1028.10] | [1071] | [1112] | |
| IT.0.0(6).Ti* | | | | 967.0 kip-ft | 951.0 kip-ft | 0.98 |
| | | | | [1311] kN-m | [1289] kN-m | |

! Controlled by flexure from Table 5.1b *Moment at midspan.

As seen in Table 5.2a, the AASHTO-LRFD predicted strengths were conservative for all cases including T and IT specimens. The NSM strengthened specimens achieved capacities above the AASHTO predicted nominal flexural strength assuming that all five (5) of the #11 steel reinforcing bars were well anchored over the entire span. This was the intent of the retrofit approach. As seen in Table 5.2a, R2K reasonably predicted the capacity for all NSM strengthened T-specimens, and accurately predicted both the diagonal-tension and flexural failures. These indicate that the T specimens, which have transverse steel acting across the splitting plane can allow the titanium and stainless steel NSM to achieve their material strength. The IT specimens were not as well predicted. For the IT specimens with NSM titanium alloy bars, the predicted strength for the specimen with 10 in. stirrup spacing was conservative but the predicted strength for the specimen with 6 in. stirrup spacing was not conservative. With higher amounts of transverse steel, the specimens carry higher loads. Higher loads result in increased demands in the flexural steel. If the internal cutoff bars slip and cause splitting of the relatively thin deck (as was observed on one flange of specimen IT.45.Ld3(6).Ti), then the NSM bars bonded to the deck soffit are adversely affected by the surrounding concrete spalling and

cracking. The specimen IT.45.Ld3(6).SS with stainless steel NSM bars had bars located in both the deck soffit and stem. Placement of bars in the web for the fairly narrow flange width used in the specimens was advantageous because it was not adversely affected by cracking and splitting of the deck after slip of the cutoff flexural steel bars. In addition, the larger number of bars with higher modulus provided more stiffness than the similar titanium alloy specimen and thus exhibited higher strength and deformation capacity. From these observations, when strengthening negative moment regions, the full material strength of the NSM materials may not necessarily be achieved when bonded only to the deck soffit for narrow effective flange widths. NSM should be applied to both the soffit of the deck and in the stem for negative moment strengthening.

As seen in Table 5.1a and 5.1b, all the base specimens (without NSM) would have failed in diagonal-tension at the location $d_v$ from the loading plate within the region of the cutoff #11 flexural reinforcing steel bars. Comparing the experimentally observed failure loads, it was observed that the NSM materials significantly increased the strength of the base specimens as shown in Table 5.3.

**Table 5.3: Strength increases achieved by NSM compared to base specimens.**

| Specimen ID | Experiment (kips) [kN] | R2K Predicted Limiting Shear Capacity of Base Specimen (kips) [kN] | Percent Increase in Strength Using R2K | AASHTO Predicted Limiting Shear Capacity of Base Specimen (kips) [kN] | Percent Increase in Strength Using AASHTO |
|---|---|---|---|---|---|
| T.45.Ld3(10).Ti | 200.0 [890] | 149.1 [663] | 34.1% | 140.8 [626] | 42.1% |
| T.45.Ld3(6).Ti | 216.4 [963] | 166.0 [738] | 30.4% | 154.4 [687] | 40.2% |
| T.45.Ld3(6).SS | 215.7 [959] | 163.1 [725] | 32.3% | 151.7 [675] | 42.2% |
| IT.45.Ld3(10).Ti | 213.8 [951] | 177.8 [791] | 20.2% | 173.9 [774] | 22.9% |
| IT.45.Ld3(6).Ti | 224.0 [996] | 206.1 [917] | 8.7% | 194.0 [863] | 15.5% |
| IT.45.Ld3(6).SS | 250.0 [1112] | 205.4 [914] | 21.7% | 192.9 [858] | 29.6% |
| IT.0.0(6).Ti* | 951.0 kip-ft [1289] kN-m | 413.5 [560.60] | 130.0% | 275.5 [373.51] | 245.2% |

## 5.2 COMPARISON OF FLEXURAL TENSION CAPACITY

Flexural tension capacity was a key component of the experimental design. As discussed previously, the flexural tension capacities and demands were compared for the specimens with NSM bars. Analyses were performed for the AASHTO, ACI, and R2K methods using the measured day-of-test material properties. To assess the flexural tension capacity, the minimum development lengths of the different internal reinforcing steel bars were predicted using the AASHTO and ACI design methodologies. The detailed development length equation (Eq. [2.20]) in ACI was used rather than the simplified approach. The predicted straight bar development lengths were computed for each specimen using the actual material properties for the steel and concrete and are reported in Table 5.4. The detailed ACI development length equation for straight bars provides shorter development lengths than that of AASHTO.

**Table 5.4: Comparison of minimum specified development length for straight and hooked #11 (36M) steel reinforcing bars.**

| Specimen ID | $f_y$ (ksi) [MPa] | $f'_c$ (ksi) [MPa] | ACI $l_d$ (in.) [mm] | AASHTO $l_d$ (in.) [mm] |
|---|---|---|---|---|
| T.45.Ld3(10).Ti | 71.6 [494] | 3.712 [25.6] | 62.6 [1590] | 72.7 [1846] |
| T.45.Ld3(6).Ti | | 3.823 [26.4] | 51.8 [1316] | 71.4 [1814] |
| T.45.Ld3(6).SS | | 3.206 [22.1] | 56.6 [1437] | 78.0 [1980] |
| IT.45.Ld3(10).Ti | | 4056 [28.0] | 59.4 [1509] | 69.3 [1760] |
| IT.45.Ld3(6).Ti | | 3734 [25.7] | 57.6 [1463] | 72.3 [1836] |
| IT.45.Ld3(6).SS | | 3525 [24.3] | 59.3 [1506] | 74.4 [1890] |
| IT.0.0(6).Ti | | 3397 [23.4] | 60.4 [1534] | 75.8 [1925] |

The ACI and AASHTO methods were used to compute the flexural tensile force available along the length of the specimens. The flexural tension demand along the length of the specimens was determined by setting the flexural tension demand to the theoretically available resistance at midspan. ACI indirectly accounts for additional demand in the flexural tension forces from the influence of shear by requiring extensions of bars beyond theoretical locations a minimum dimension of the depth of the member. Therefore, the flexural tension demand was shifted horizontally at each location on the span to a dimension equal to *d*. A range of possible diagonal cracks were swept through the span length creating a non-linear flexural tension demand curve for the AASHTO method. The slope of the flexural tension capacity was related to the amount of reinforcing steel being developed based on the lengths shown in Table 5.4. The left side of each

specimen contained stirrup spacing of 6 in. (152.4 mm) and all steel reinforcing bars extended past the support. The right side of the specimens contained the flexural cutoff detail. The location where the demand in the flexural steel is closest to or exceeds the available capacity was the expected location of anchorage failure. NSM materials were installed over the cutoff flexural steel to provide additional flexural reinforcing over the location of the specimens which would otherwise be deficient in tensile capacity. An example of the demand in the flexural steel using AASHTO-LRFD and ACI, which directly accounts for the additional demand due to shear, is shown in Figure 5.1.

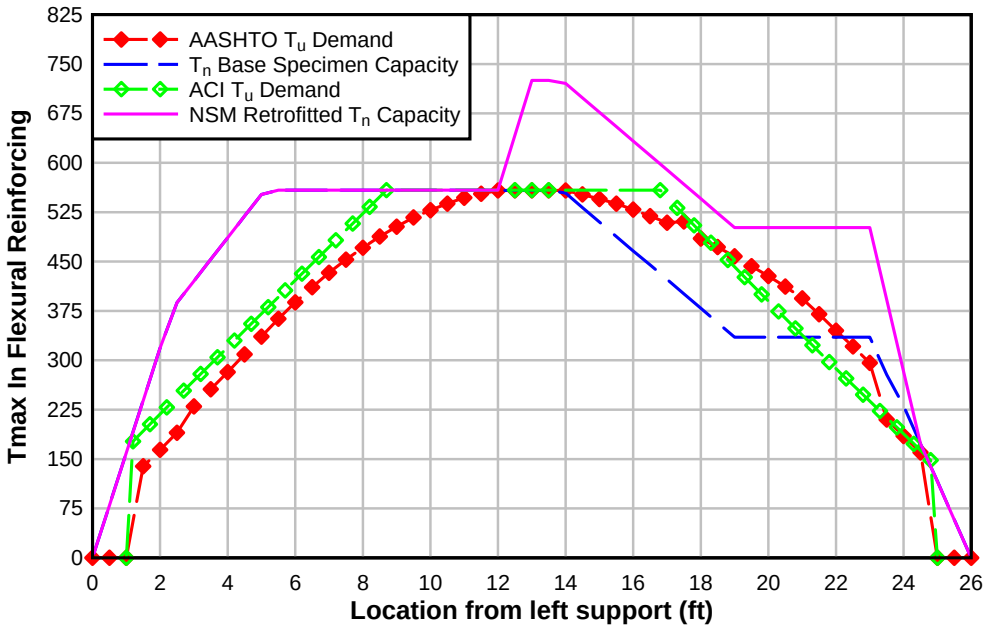


Figure 5.1: Example of ACI and AASHTO predicted flexural tension demands and available capacity along specimen with and without NSM.

As seen here, the ACI demands are slightly larger than the AASHTO approach near midspan because ACI assumes a constant 45$^o$ diagonal crack angle while AASHTO has variable crack angles and would have a more vertical angle where the behavior is flexurally dominated. Also as seen in the figure, the tension deficiency at the cutoff bar location in the base specimen is ameliorated by use of NSM (blue curve changed to purple curve) and the predicted failure location (based on capacity using all the flexural tension steel as fully developed) is expected near midspan at the end of the NSM bars. From these anchorage analyses, flexural failures for all specimens would be predicted at the end of the NSM bars near midspan. This was observed for all specimens except T.45.Ld3(10).Ti which failed in diagonal tension and IT.45.Ld3(6).Ti which exhibited a partial anchorage failure of the cutoff steel reinforcing bar in one flange. The capacities predicted by the shear-moment analysis conducted in the previous section more closely predicted these failures. This confirmed that shear and moment capacities must be evaluated simultaneously with flexural tension capacities to identify critical sections, strength, and controlling failure mode of the member.

Following this approach, for specimens with preformed diagonal cracks, the ACI predicted flexural tensile force available along the length of the specimens relative to the experimentally

measured and AASHTO-LRFD predicted demands were determined and are shown in Figure 5.2 through Figure 5.7. The ACI available force capacity was used because it provided shorter development lengths that are more representative of the actual behavior. AASHTO tension demands were used because they directly consider the additional influence of shear in the presence of diagonal cracking.

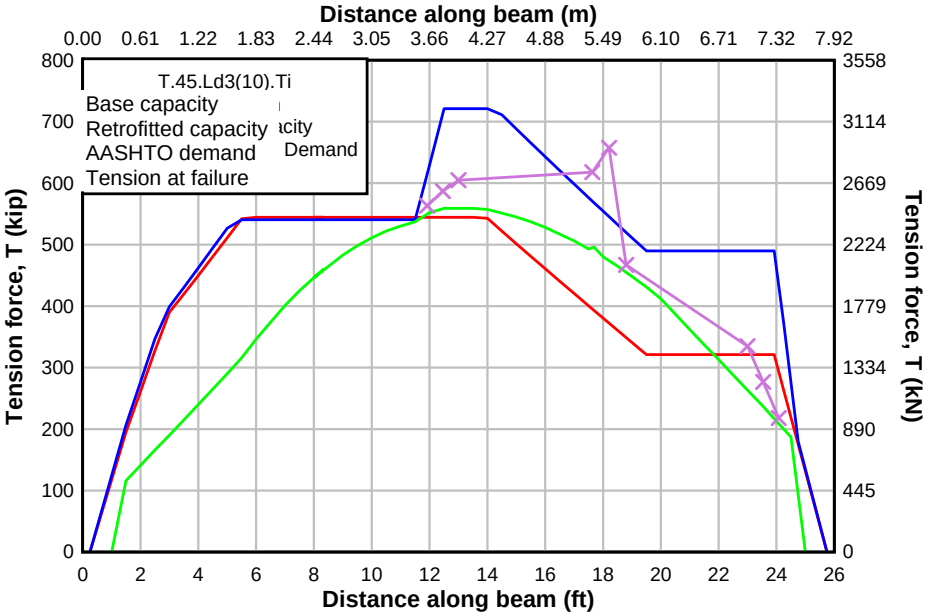


Figure 5.2: Predicted and measured flexural tension force along span for T.45.Ld3(10).Ti.

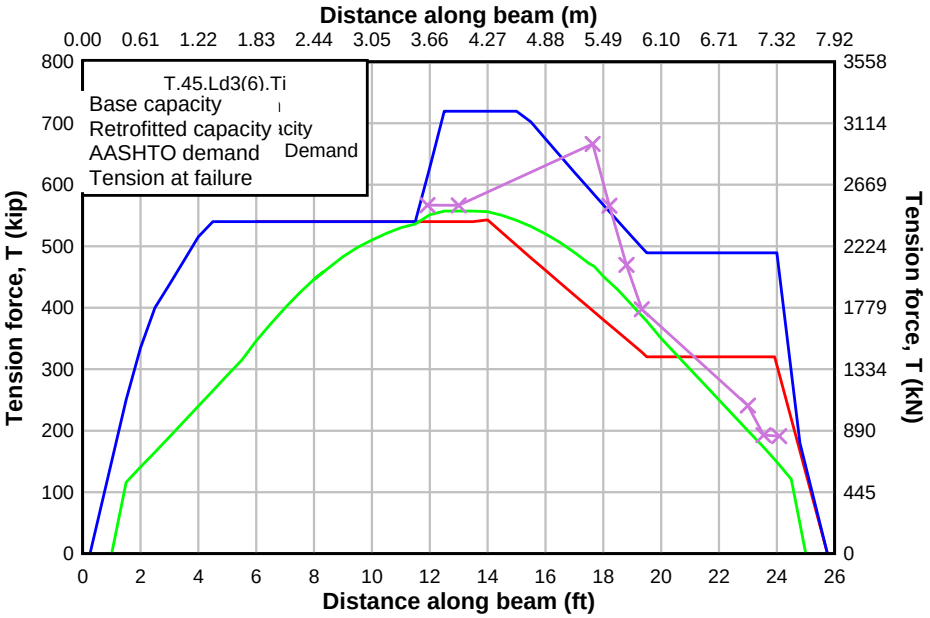


Figure 5.3: Predicted and measured flexural tension force along span for T.45.Ld3(6).Ti.

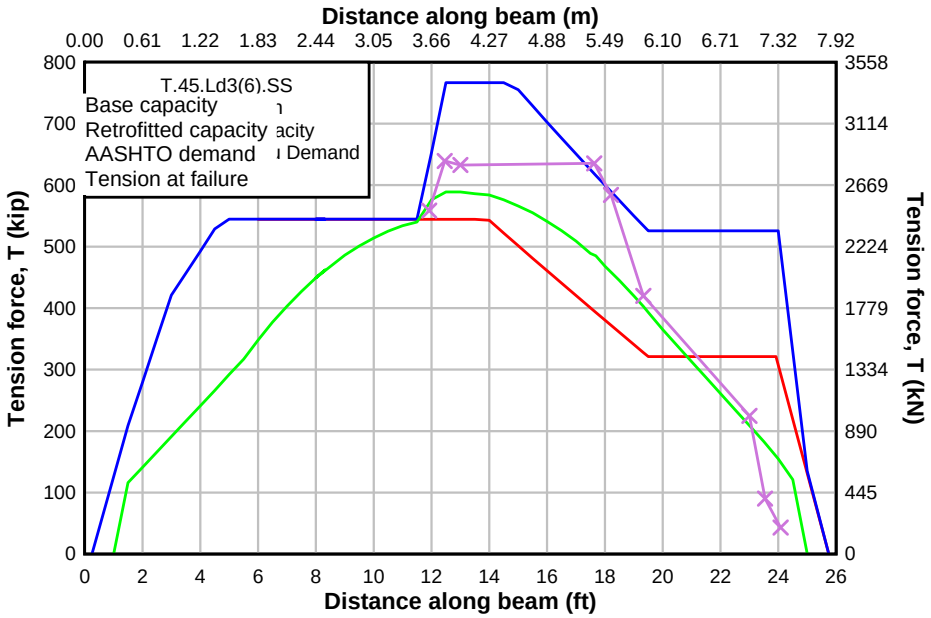


Figure 5.4: Predicted and measured flexural tension force along span for T.45.Ld3(6).SS.

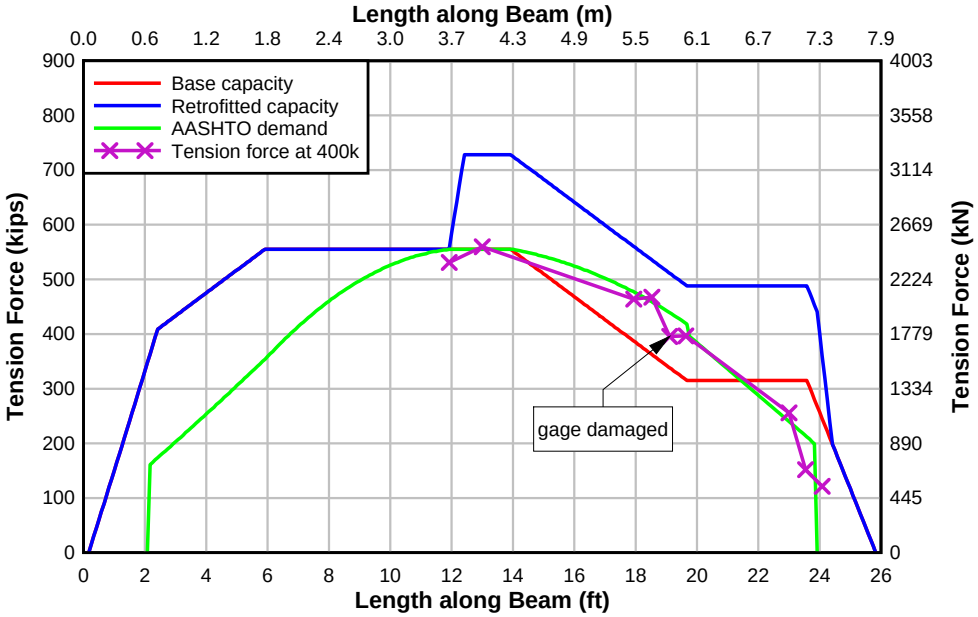


Figure 5.5: Predicted and measured flexural tension force along span for IT.45.Ld3(10).Ti.

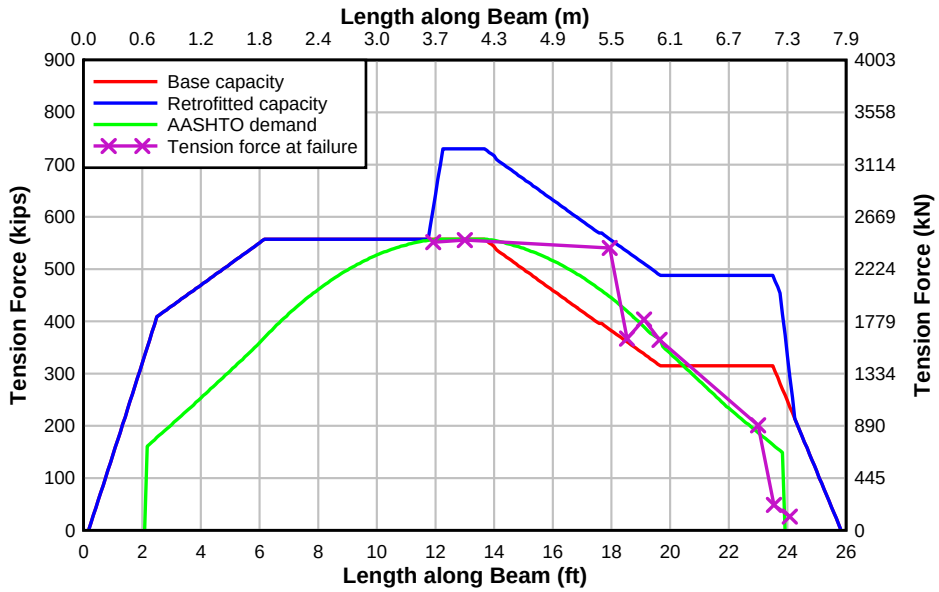


Figure 5.6: Predicted and measured flexural tension force along span for IT.45.Ld3(6).Ti.

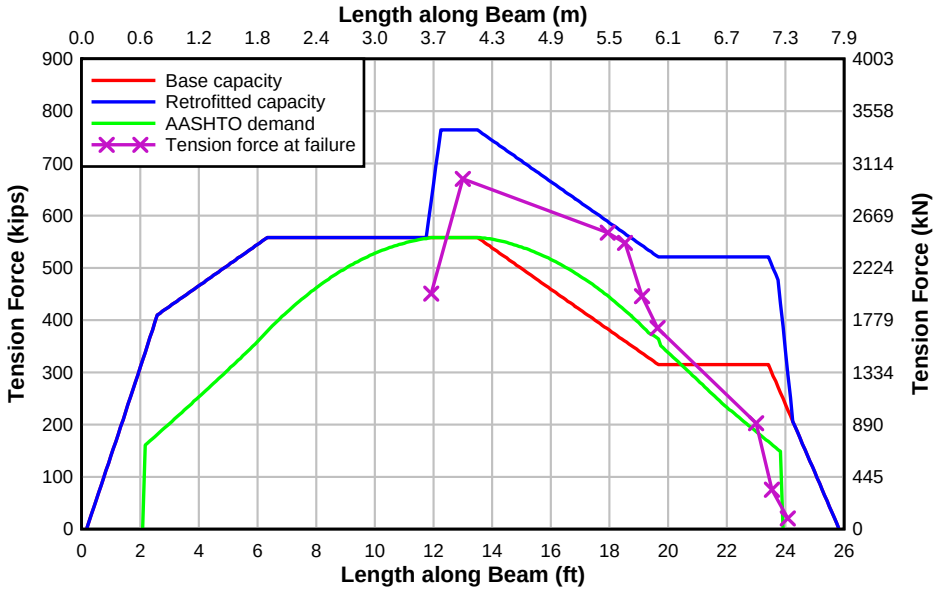


Figure 5.7: AASHTO flexural tension resultant along length of specimen IT.45.Ld3(6).SS.

R2K was also used to predict the tension demands in the specimens at loads very near failure. R2K predictions were compared with the experimentally measured flexural tension forces near failure in Figure 5.8 through Figure 5.13 for specimens with preformed diagonal cracks. Strain gages were often damaged prior to achieving failure. Where sensor data were obviously compromised, they were omitted from the curve, but reported as a data point in the figures shown below.

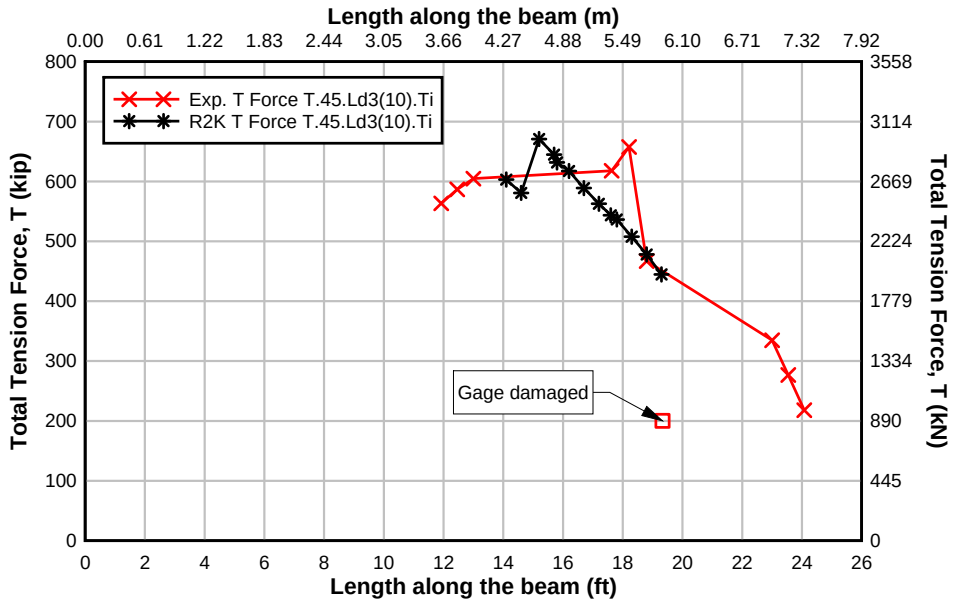


Figure 5.8: Total experimental and R2K predicted tension force resultant for specimen T.45.Ld3(10).Ti.

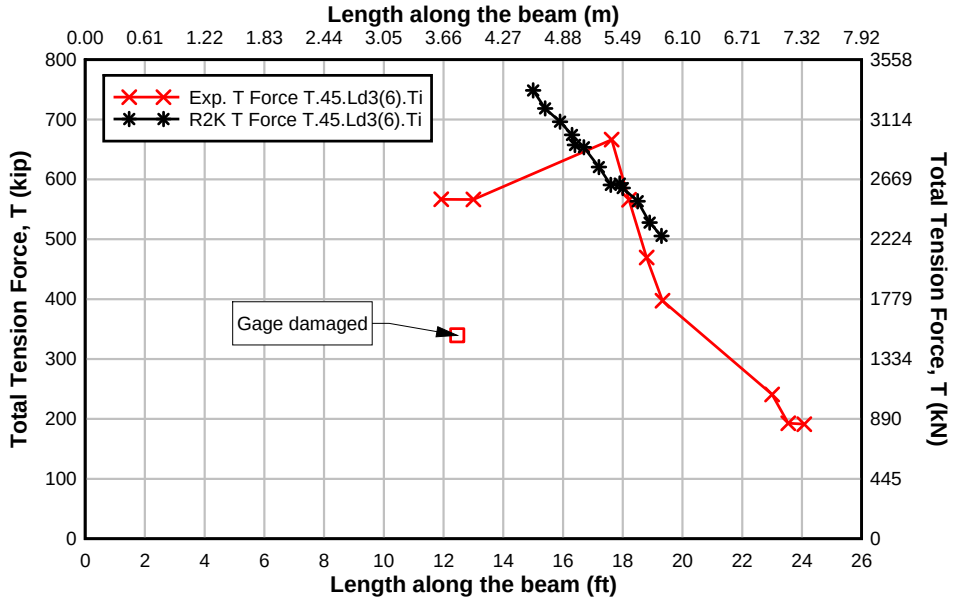


Figure 5.9: Total experimental and R2K predicted tension force resultant for specimen T.45.Ld3(6).Ti.

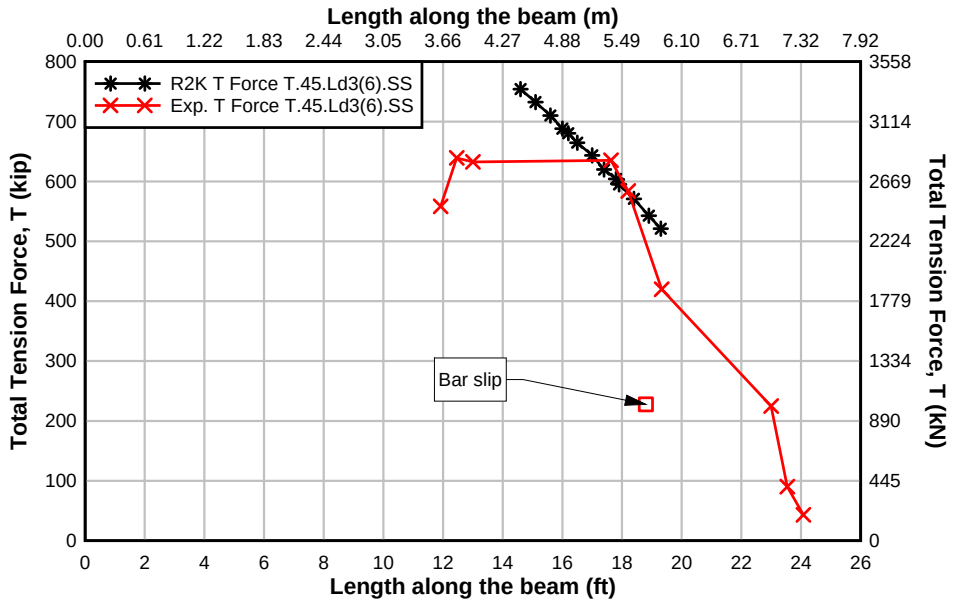


Figure 5.10: Total experimental and R2K predicted tension force resultant for specimen T.45.Ld3(6).SS.

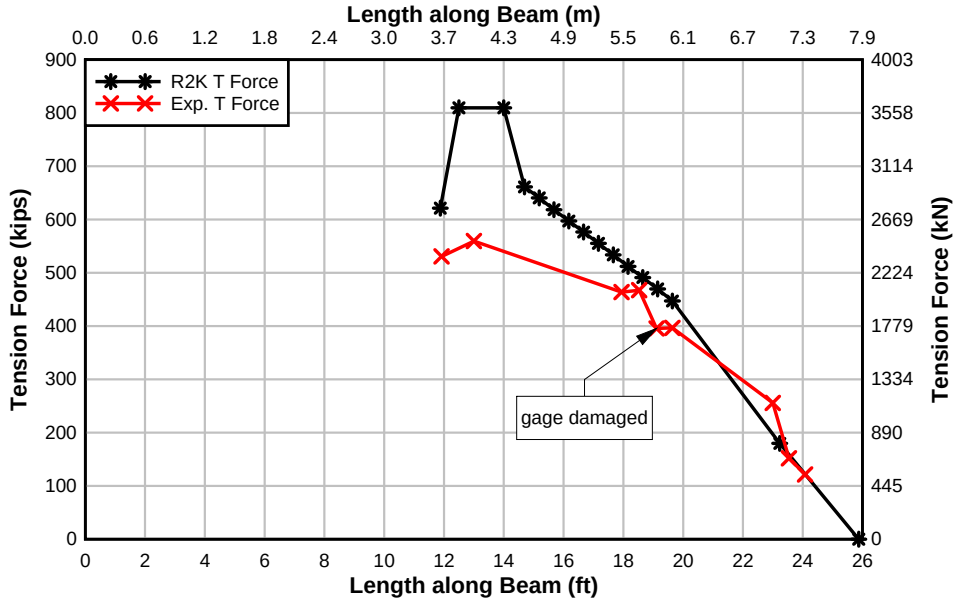


Figure 5.11: Total experimental and R2K predicted tension force resultant for specimen IT.45.Ld3(10).Ti.

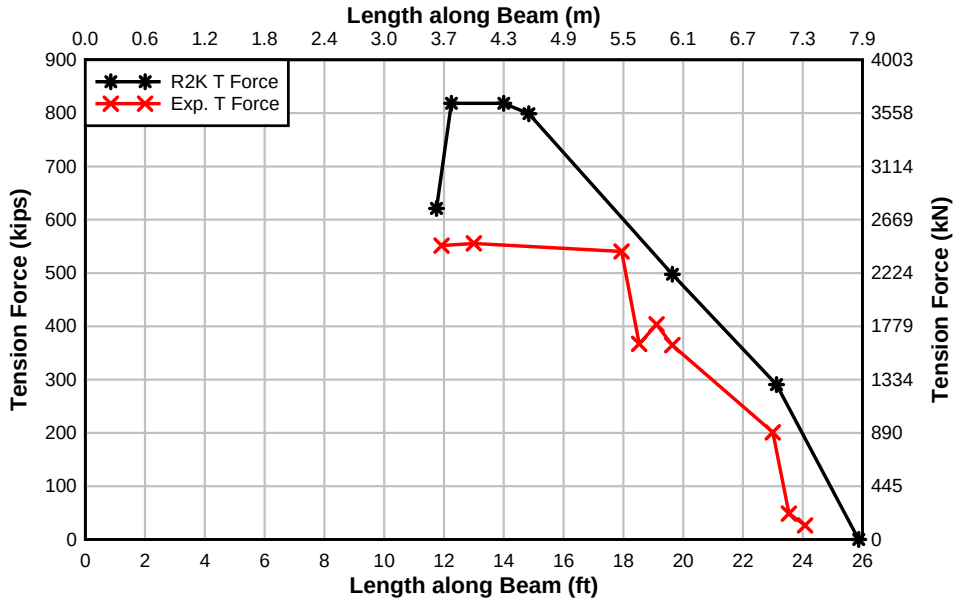


Figure 5.12: Total experimental and R2K predicted tension force resultant for specimen IT.45.Ld3(6).Ti.

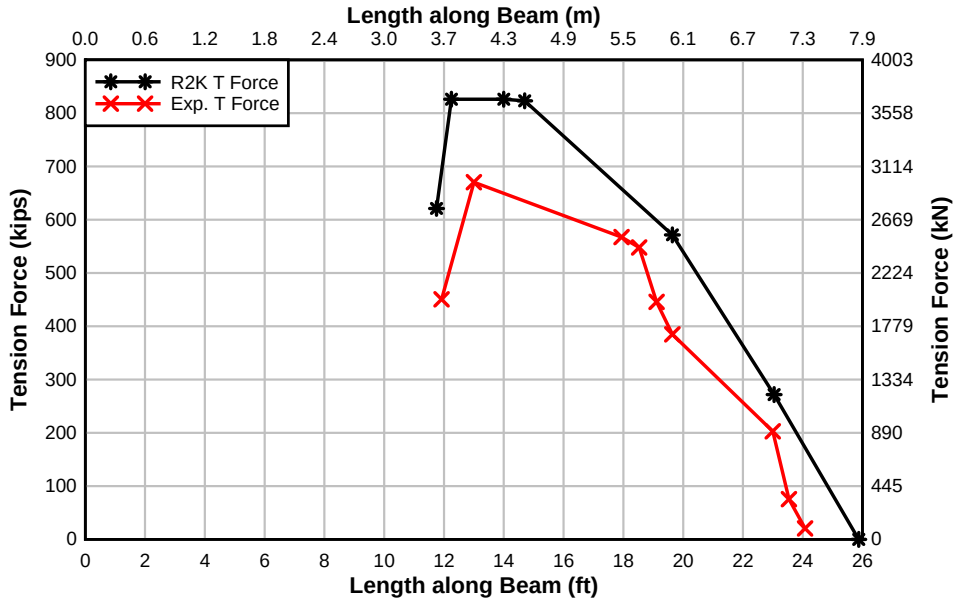


Figure 5.13: Total experimental and R2K predicted tension force resultant for specimen IT.45.Ld3(6).SS.

For all specimens, the experimentally measured flexural tension demands along the span corresponded reasonably well to those predicted from R2K. The IT specimens showed lower measured forces in the critical regions than those predicted by R2K while the T-specimens showed forces slightly above those predicted. The AASHTO and ACI flexural tension capacities also correlated well with the R2K predictions for all specimens, as seen previously. The R2K predictions incorporate strain hardening into the reinforcing materials, producing slightly higher

flexural tension forces than those from the design specifications. Variability in material properties, geometry, and strain measurements contributed to some additional uncertainty in the experimentally measured flexural tension forces for the specimens. However, the trend and magnitudes of the experimental data were similar to those predicted.

## 5.3 CONTRIBUTION OF NSM BARS AS EQUIVALENT AREA OF REINFORCING STEEL

Generally, when evaluating the flexural capacity of a reinforced concrete section, the strength increases as the area of flexural reinforcing steel increases. However, above a certain threshold of flexural steel, the member capacity plateaus because it becomes dependent on the diagonal-tension strength of the section. This behavior is illustrated in Figure 5.14 through Figure 5.24. This section describes the NSM strengthening in terms of an equivalent area of reinforcing steel. Once the required area of reinforcing steel is found at the critical section, the area of steel can be transformed into an equivalent NSM strength.

The loads versus area of steel responses were computed using the specific specimen geometry and measured material properties. The cutoff reinforcing steel bar area was increased from 0 to 1.56 $in^2$ (1006 $mm^2$) for each #11 (36M) bar. Then, the five flexural steel reinforcing bars were grouped into one area of steel located at distance $d_s$ from the top of the section. The combined area of steel was then increased incrementally to 20 $in^2$ (129 $cm^2$) of steel. The yield strength of the equivalent reinforcing steel was set as 71.7 ksi (494 MPa). Each point along each curve was evaluated for the same moment-to-shear ratio. The moment-to-shear ratios (M:V) chosen were 5.67:1, corresponding approximately $d_v$ away from the loading point, and 7.52:1, corresponding to the failure location. Choosing a moment-to-shear ratio $d_v$ away from the loading point provided a common location for comparison between specimens. The predicted and experimentally measured failure loads for the specimens are shown in the figures for reference. Other relevant reference lines are also included for the NSM strengthened specimens.

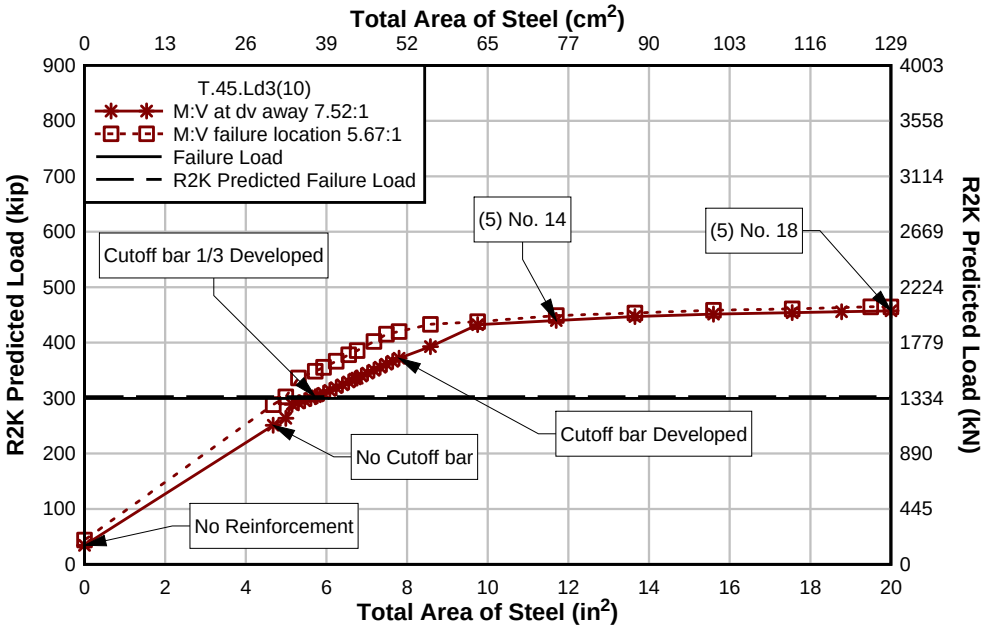


Figure 5.14: Specimen T.45.Ld3(10) predicted load for increasing area of equivalent flexural reinforcing steel area.

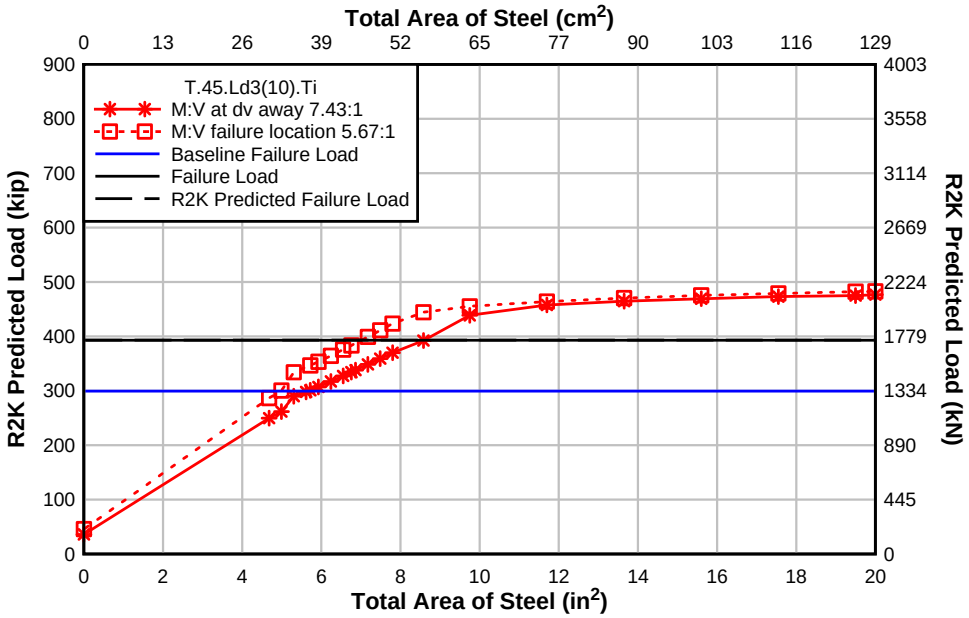


Figure 5.15: Specimen T.45.Ld3(10).Ti predicted load for increasing area of equivalent flexural reinforcing steel area.

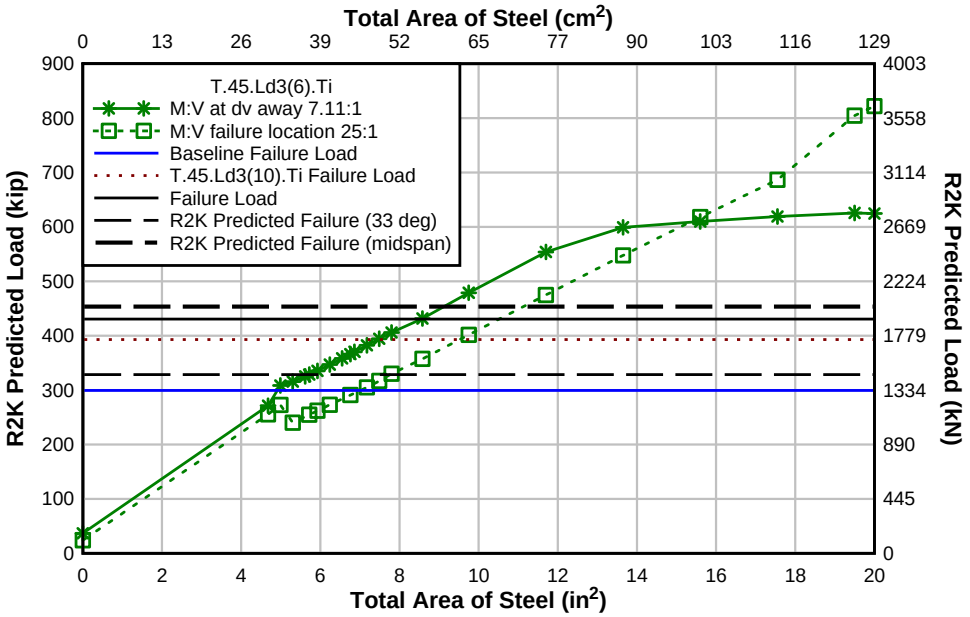


Figure 5.16: Specimen T.45.Ld3(6).Ti predicted load for increasing area of equivalent flexural reinforcing steel area.

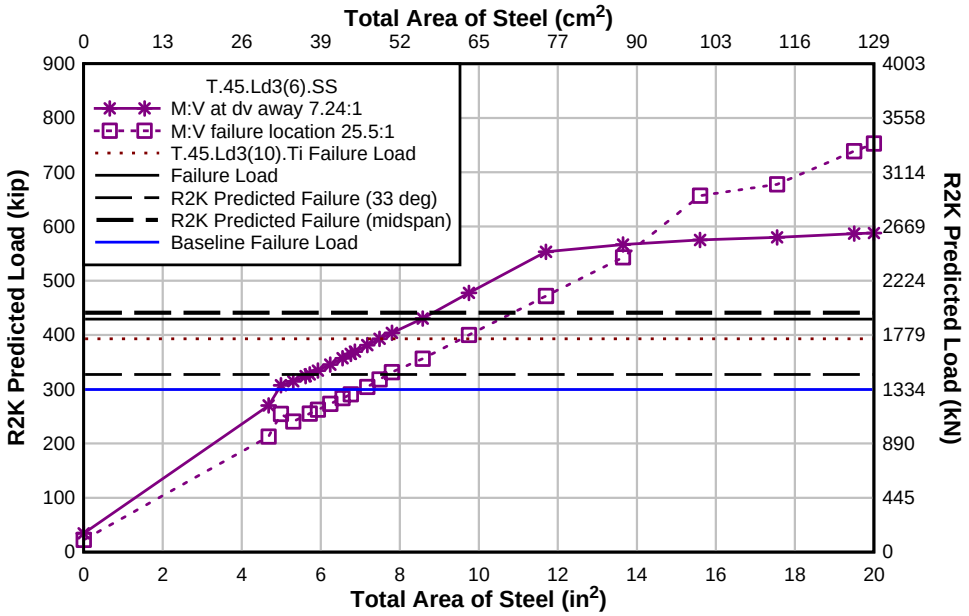


Figure 5.17: Specimen T.45.Ld3(6).SS predicted load for increasing area of equivalent flexural reinforcing steel area.

For the T-specimens, T.45.Ld3(6).Ti and SS failed in flexure near midspan and thus used a larger M:V to predict the section capacity. The flexurally predicted load and area of steel curves were more linear than the curve at $d_v$ away because diagonal-tension did not control strength for the tightly spaced transverse reinforcing steel in these specimens. Using the reference lines, the area of internal reinforcing steel that would provide an equivalent strength as the NSM bars was

determined. The NSM titanium alloy bar strengthened specimen, T.45.Ld3(10).Ti, failed at a load of 430.7 kips (1920 kN) and had an equivalent area of internal reinforcing steel of approximately 8.6 in$^2$ (55.5 cm$^2$). Therefore, installing four NSM titanium bars with a centroid over the cutoff bars was equivalent to increasing the area of steel reinforcing bars by 3.6 in$^2$ (23.2 cm$^2$). This is comparable to adding two #11 (36M) bars as internal reinforcement at $d_v$ away from the loading point. The specimen retrofitted with 8 stainless steel NSM bars, T.45.Ld3(6).SS, provided approximately an additional 2.3 in$^2$ (14.8 cm$^2$) of equivalent area of internal reinforcing steel at $d_v$ away to the baseline specimen.

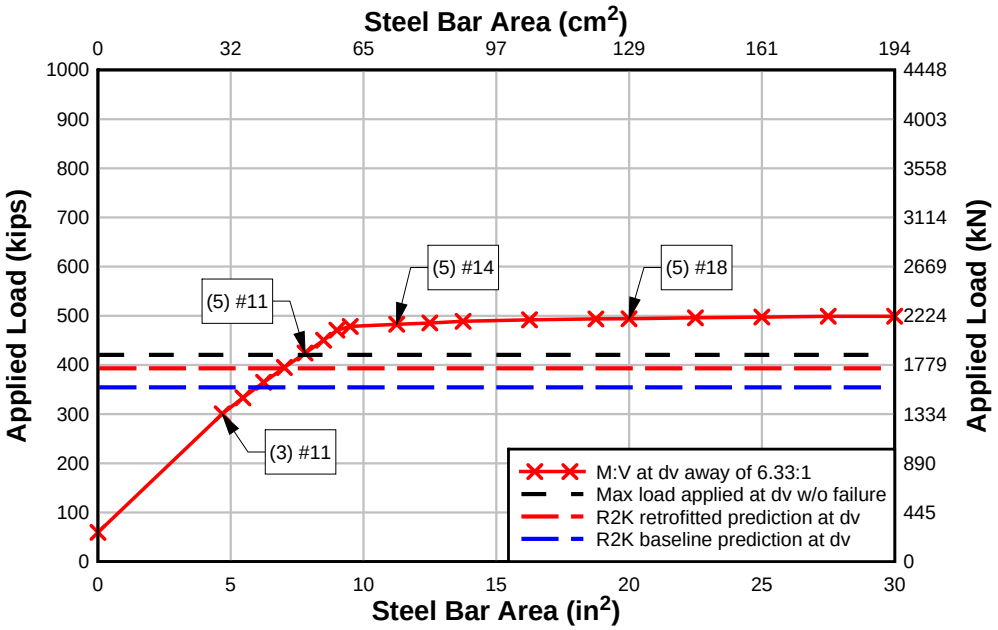


Figure 5.18: Specimen IT.45.Ld3(10).Ti load-bar area at $d_v$ away.

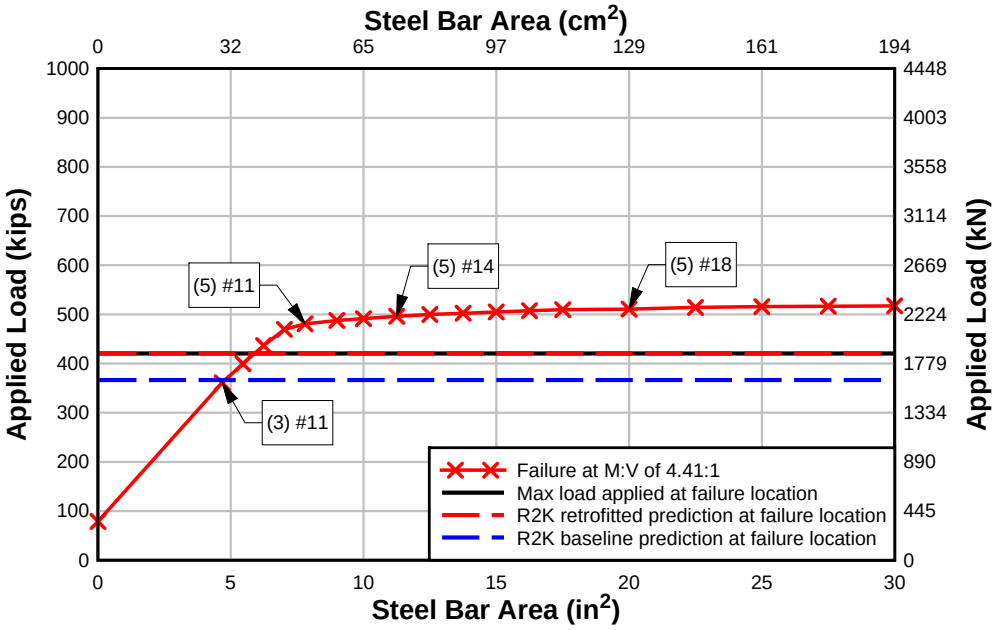


Figure 5.19: Specimen IT.45.Ld3(10).Ti load-bar area at failure location.

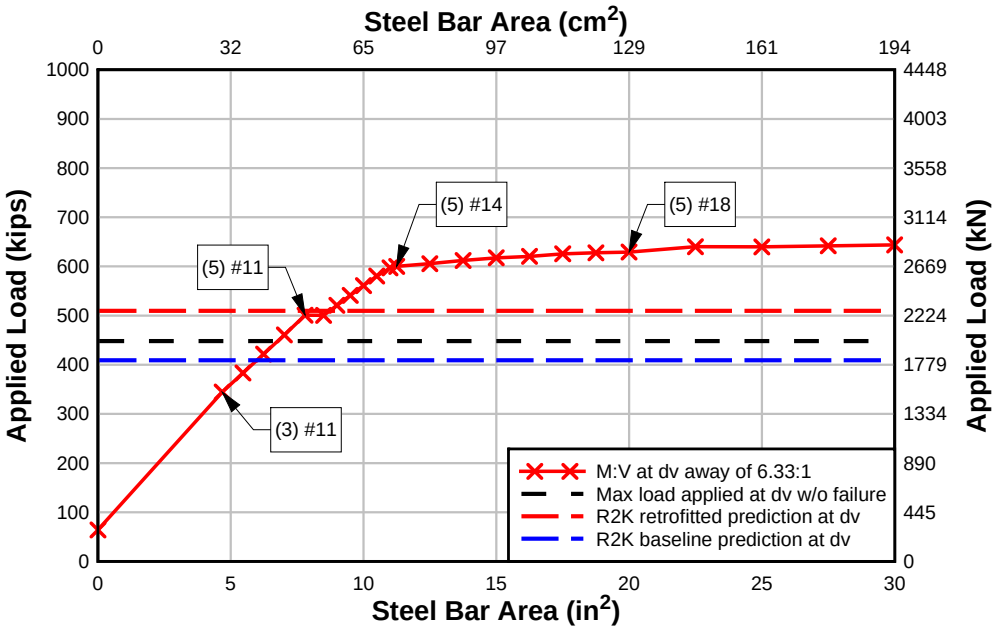


Figure 5.20: Specimen IT.45.Ld3(6).Ti load-bar area at $d_v$ away.

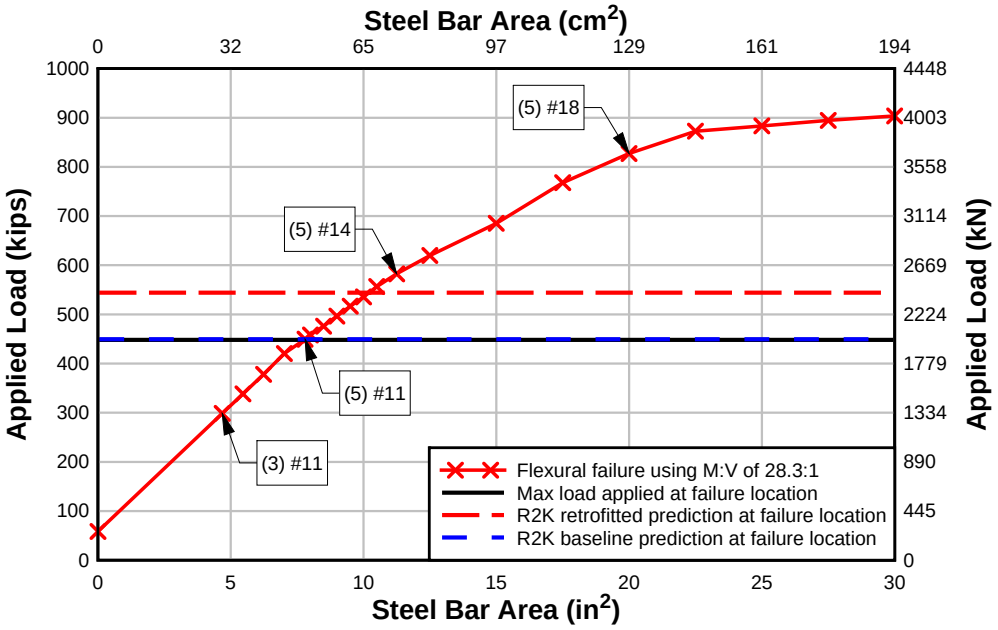


Figure 5.21: Specimen IT.45.Ld3(6).Ti load-bar area at failure location.

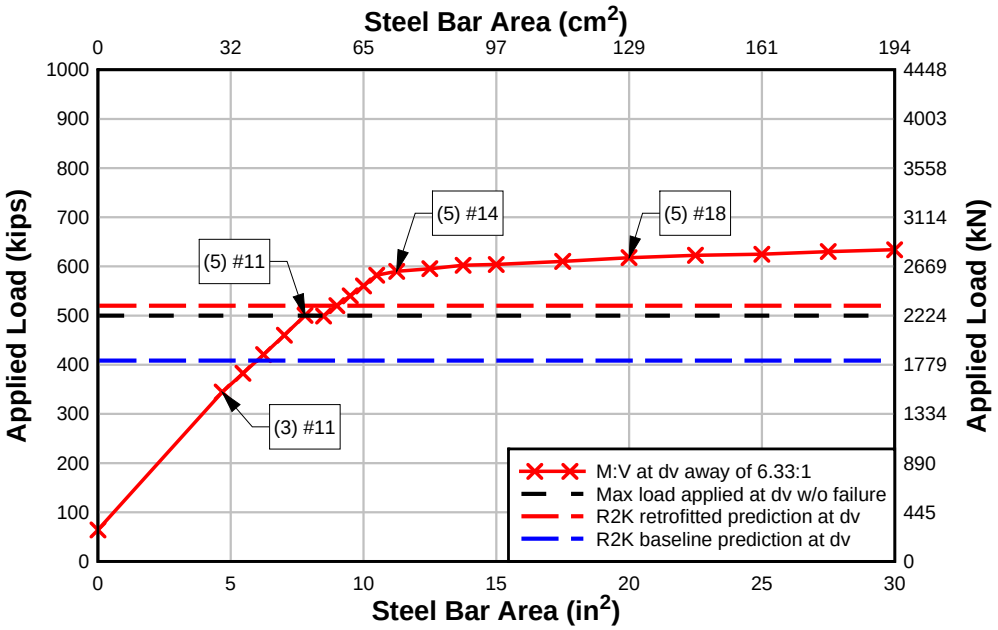


Figure 5.22: Specimen IT.45.Ld3(6).SS load-bar area at $d_v$ away.

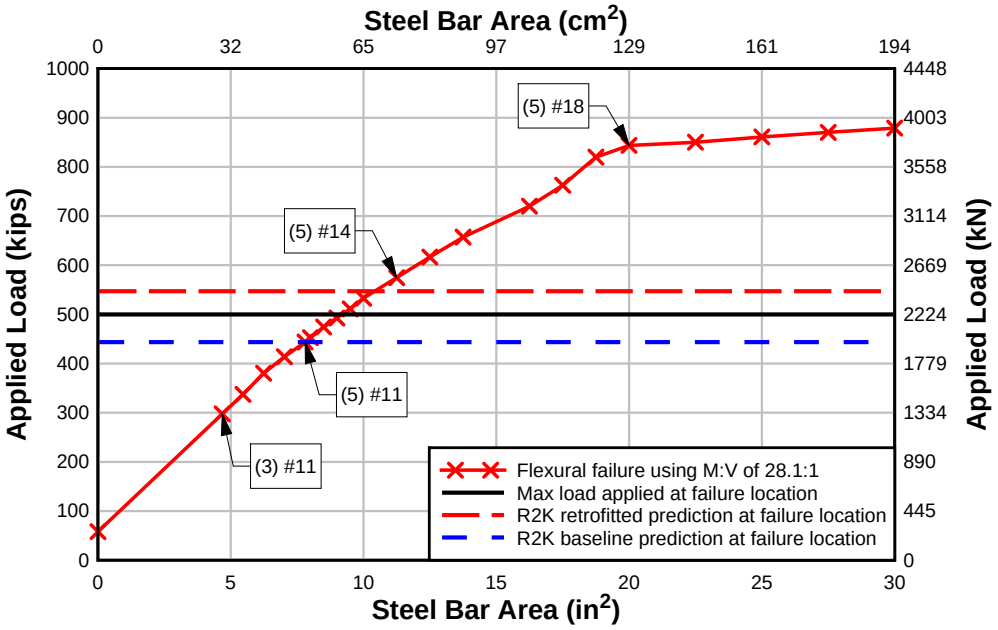


Figure 5.23: Specimen IT.45.Ld3(6).SS load-bar area at failure location.

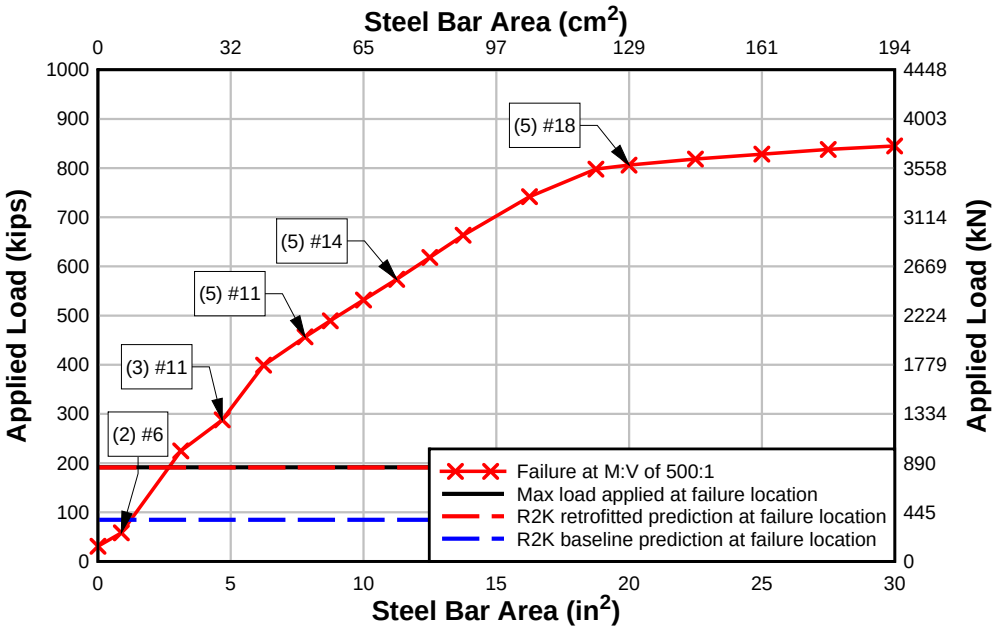


Figure 5.24: Specimen IT.0.0(6).Ti load-bar area at failure location.

From the IT specimen section analyses at $d_v$ away, there was an optimum area of steel around 10 in$^2$ (65 cm$^2$) that could be utilized. Any larger area of equivalent flexural steel would produce only a small increase in the applied load capacity. The change in slope in these curves represents the change in the specimen from flexure to diagonal-tension controlled failure. The section analysis at the failure location for IT.45.Ld3(10).Ti shows a similar trend as that at $d_v$ away. The analyses at the failure locations for the other three specimens indicate that adding steel up to

approximately 20 $in^2$ (129 $cm^2$) will continue to increase the applied load capacity with small changes in the bar area. The change of the point of inflection for these curves indicates that these specimens would be controlled by flexure. In specimen IT.45.Ld3(10).Ti, failure occurred by the end of the cutoff bars. Without any contribution from the cutoff bars, there are only three #11 (M36) bars available to provide strength. The area of steel crossing the applied failure load reference line shows the contribution of the NSM titanium as an equivalent reinforcing steel area of 1.07 $in^2$ (690 $mm^2$). In order to make more efficient use of the NSM bars, additional transverse steel would be required. Specimen IT.45.Ld3(6).Ti failed in flexure at the end of the NSM titanium bars. All 5 of the flexural steel bars were fully developed at this point and the applied failure load reference line crosses at this steel bar area. This intersection shows there was no contribution from the NSM bars at the failure point, but that the addition of the NSM bars was able to allow the specimen to make full use of the internal steel. The NSM bars were able to effectively remediate the cutoff location and allow the section to develop its full strength. The IT.45.Ld3(6).SS specimen shows the partial contribution from the stainless steel bars as the applied load reference line crosses the curve between the retrofitted and baseline predictions. Lastly, the IT.0.0(6).Ti specimen curve at failure shows how much equivalent steel the titanium contributed. The majority of the capacity is due to the NSM titanium alloy bars, with only a small contribution from the #6 (M19) and #4 (M13) bars.

## 5.4 APPLICATION OF ACI 440 DESIGN RECOMMENDATIONS FOR METALLIC NSM MATERIALS

This section considers adapting present design guidance for NSM CFRP to NSM metallics. To demonstrate the design approach, calculations using titanium and stainless steel bars were compared to CFRP bars using ACI 440 guidelines for the T-specimen configuration. Applicable ACI 440 equations are described in Section *2.3.4 ACI 440 Guide for Design for External FRP Systems.*

The environmental factor was neglected in the calculations since the intent of this section is to compare materials with identical exposure types. The yield strain of the metallic materials is listed in the tables for reference. In addition, the maximum strain in the NSM materials was calculated based on the strain diagram assuming strain compatibility. The maximum debonding strain, usually calculated by Equation (2.23), was limited to the maximum debonding strain in the CFRP (taken as 0.0117 in/in). Experimental research has determined the bond of NSM materials is typically limited by the concrete-epoxy interface; therefore, it is not feasible to achieve much greater bond strengths than those achieved by the CFRP NSM at non-termination locations. The effective strain in the NSM materials was the lesser of the debonding strain or strain to achieve concrete crushing calculated in Equation (2.23) and is listed in Table 5.5. Two CFRP bars of the same material but different diameters were chosen for comparison. The smaller 0.5 in. (12.7 mm) diameter bar is more commercially available and would provide a tensile strength similar to the titanium NSM strengthening.

**Table 5.5: ACI 440 NSM stress and strain calculations for alternative materials.**

| NSM Material | # of NSM bars | Bar Dia. (in) [mm] | Yield Strain $\varepsilon_y$ | Max. NSM strain in section ($f_s=f_y$) | Debonding Strain $\varepsilon_{fd}$ | NSM Effective Strain $\varepsilon_{fe}$ | NSM Effective Stress $f_{fe}$ (ksi) [MPa] |
|---|---|---|---|---|---|---|---|
| Titanium | 4 | 0.625 | 0.0094 | 0.0286 | 0.0117* | 0.0117 | 145 |
| | | [15.9] | | | | | [999] |
| Stainless Steel | 8 | 0.625 | 0.0026 | 0.0245 | 0.0117* | 0.0117 | 75 |
| | | [15.9] | | | | | [517] |
| CFRP1 | 4 | 0.625 | - | 0.0159 | 0.0117 | 0.0117 | 210 |
| | | [15.9] | | | | | [1450] |
| CFRP2 | 4 | 0.5 | - | 0.0525 | 0.0117 | 0.0117 | 210 |
| | | [12.7] | | | | | [1450] |

*Debonding strain limited to CFRP debonding strain

In all materials, the effective strain was less than the theoretical maximum strain if the reinforcing steel was at yield. Limiting the debonding strain $\varepsilon_{fd}$ shifted the failure mode of the metallic NSM materials from concrete crushing to debonding of the NSM. Since ACI 440 is predicated on the ultimate strain of a less ductile material, it is not appropriate to design with the ultimate strains of titanium and stainless steel. The titanium and stainless steel NSM materials still reach their yield strength, despite limiting $\varepsilon_{fd}$ to the CFRP debonding strain. The ultimate stress for the CFRP material was 300 ksi (2068 MPa). Due to debonding, only 210 ksi (1447 MPa), or 70% of the material strength is utilized. The larger diameter CFRP bar had identical effective stress and strains to the smaller diameter CFRP bar. Also it is important to note that at the limiting strain of 0.0117, the titanium alloy bars will be above the yield stress and due to the relatively low ultimate to yield strength ratio for the material, the titanium alloy bars are less likely to have a bond failure compared to CFRP.

Section properties including the distance to the neutral axis, curvature, average bond stress, and development length were calculated using ACI 440 and are tabulated in the Table 5.6. The distance to the neutral axis, c, was calculated by iteratively and incorporated the compression steel, the compression flange, and the NSM materials. The average bond stress was calculated using Equation (2.1) and the ACI 440 bond length (Equation (2.22)).

**Table 5.6: ACI 440 predicted neutral axis, curvature, bond, and development length for alternative NSM materials.**

| NSM Material | ACI 440 c (in.) [mm] | Curvature at midspan ψ (1/in.) [1/mm] | Average Bond Stress, $\mu_{avg}$ (ksi) [MPa] | ACI 440 Development Length (in.) [mm] |
|---|---|---|---|---|
| Titanium | 3.91 | 0.000767 | 1.2 | 11.2 |
| | [99.3] | [0.000030] | [8.6] | [285] |
| Stainless Steel | 4.07 | 0.000738 | 4.5 | 5.8 |
| | [103.3] | [0.000029] | [31.1] | [148] |
| CFRP1 | 6.55 | 0.000458 | 1.0 | 16.3 |
| | [166.3] | [0.000018] | [6.9] | [414] |
| CFRP2 | 2.23 | 0.001345 | 1.0 | 26.3 |
| | [56.6] | [0.000053] | [6.9] | [668] |

The curvature of the section, ψ, is related to the neutral axis location, c. The section strengthened with smaller diameter CFRP bars exhibited the highest curvature. The curvature of the metallic NSM materials was similar. After the yielding moment was reached in the metallic NSM strengthened section, the curvature and ductility will increase without a significant increase in moment capacity. The strains increase after the yield strain with minimal strain hardening in the NSM titanium alloy material.

ACI 440 uses an average bond strength of 1.0 ksi (6.89 MPa) which is calibrated to CFRP materials. Limiting the effective strain in the NSM titanium alloy and stainless steel bars to the debonding stress of the CFRP bars decreased the bond stress. The modulus and yield strength of materials affected the ACI 440 calculated bond length. Throughout the experimental program, an active bond length of 6 in. (152.4 mm) was used for the mechanically anchored NSM titanium alloy and stainless steel bars. The ACI 318 hooked development lengths for reinforcing bar are approximately half those of straight-bar development and accordingly, thus hooked NSM bond lengths can be assumed to be shorter than the straight bar bond length calculated by ACI 440.

According to the ACI 440 design methodology, the maximum flexural tensile force provided by the NSM strengthening is equal to the effective stress multiplied by the number and area of the NSM bars. The number of NSM bars equivalent to a nominal Gr. 60 (Gr. 420) #11 (36M) steel reinforcing bar tensile strength is listed in Table 5.7.

**Table 5.7: ACI 440 predicted number of alternative NSM bars required to replace a #11 (36M) steel reinforcing bar.**

| Material | Bar Area ($in^2$) [$mm^2$] | Effective Stress (ksi) [MPa] | Effective Force (kip) [kN] | # of NSM Bars Required |
|---|---|---|---|---|
| Steel | 1.56 | 60 | 93.6 | 1.0 |
| | [1006] | [413] | [416] | |
| Titanium | 0.31 | 145 | 44.95 | 2.1 |
| | [200] | [999] | [200] | |
| Stainless Steel | 0.31 | 75 | 23.25 | 4.0 |
| | [200] | [517] | [103] | |
| CFRP1 | 0.31 | 210 | 65.1 | 1.4 |
| | [200] | [1447] | [290] | |
| CFRP2 | 0.2 | 210 | 42 | 2.2 |
| | [129] | [1447] | [187] | |

To retrofit an inadequate anchorage detail of two Gr. 60 (Gr. 420) #11 (36M) cutoff reinforcing bars requires four #5 (16M) titanium bars, eight #5 (16M) stainless steel bars, over two #5 (16M) CFRP bars, or over four #4 (13M) CFRP bars would be required for an equivalent retrofit. The design methodology used for strengthening the specimens in the experimental program was consistent with these values and achieved the member flexural strength. After limiting the metallic NSM material to a debonding strain, the metallic NSM materials would still be able to achieve yield stress prior predicted failure and further provide deformation capacity in addition to strength. Obtaining the design strength and similar strain values suggest that metallic NSM material can be designed using the ACI 440 methodology and would permit the metallic material yield stress to be used in the calculations.

# 6.0 SUMMARY AND CONCLUSIONS

The objective of this research was to develop methods to strengthen diagonally-cracked RCDGs with poorly detailed flexural cutoff reinforcing steel using metallic NSM materials. To meet this objective, full-scale T and IT specimens were designed, constructed, and tested to failure. Specimens were designed to represent vintage RCDG construction materials and geometric proportions. All specimens had flexural steel reinforcing bars that were cutoff in the flexural tension region. For all but one IT specimen, the cutoff flexural reinforcing steel extended only 1/3 of the nominal design development length past a 45° preformed diagonal crack. The design intent of metallic NSM material was to effectively create an external lap splice thereby providing reinforcing material that could extend the cutoff location and increase the member strength. The NSM material would effectively eliminate the anchorage deficiency common in many vintage RCDGs built in the 1950s. Five specimens were strengthened with NSM titanium alloy bars and two specimens were strengthened with NSM stainless steel reinforcing bars. The NSM bars were terminated with 90° hooks with 6 in. (152 mm) long tails to provide a mechanical anchorage at the ends of the NSM bars. Data were collected to assess global and local structural responses at critical locations along the specimens. The experimental results were compared to ACI 318 and AASHTO-LRFD design specifications as well as a sectional analysis program, Response 2000 (R2K). Comparisons were made with ACI 440 provisions. Conclusions based on the experimental and analytical findings, recommendations, and additional research are discussed in the following sections.

## 6.1 CONCLUSIONS FROM EXPERIMENTS

Based on the experimental observations, the following conclusions are presented. In all specimens, the preformed diagonal crack did not dictate the failure location. In specimens with a lower shear capacity, T.45.Ld3(10).Ti and IT.45.Ld3(10).Ti, the failure location was at the termination of the cutoff steel reinforcing bar due to diagonal tension. Specimens T.45.Ld3(6).Ti and SS failed in flexure just past the termination of the NSM materials near midspan.

All NSM strengthened specimens exhibited increased capacity and ductility compared to an otherwise similar specimens tested by Triska and Goodall *(Triska and Coodall 2010)* without NSM and the predicted member strengths without NSM. The retrofitted specimens displayed distributed cracking around the NSM bars. Longitudinal cracks along the epoxy-concrete interface appeared around the area of the cutoff reinforcing steel bar near failure. A more controlled slip response was achieved in the NSM strengthened specimens. The stainless steel strengthened specimens provided twice the area and twice the stiffness of the titanium alloy bars and provided reduced cutoff bar slip and increased strength.

Strain compatibility between the internal reinforcing steel and NSM reinforcing bars was observed up to first cracking. Localized cracking and reinforcing steel slip produced variations in strains at different sections along the specimens. Strain gages were commonly damaged prior to reaching the maximum load, so the NSM material strains at the moment of failure could not be fully characterized. From the available experimental data, the NSM titanium and stainless steel

bars were close to exhibiting yield at failure for the T-specimens. The strains in the NSM bars for the IT-specimens were observed to be lower than the T-specimens at failure.

Measured flexural tension values peaked at the intersection of the preformed diagonal crack with the cutoff and hooked reinforcing steel. Experimental flexural tension forces between specimens were similar along the length of the specimens and were similar to those predicted by R2K and AASHTO-LRFD.

Average bond stress was calculated immediately after initial slip, where strains in the cutoff reinforcing steel bar reversed. Furthermore, bond stress was also measured after significant slip, and was classified as maximum bond stress. Maximum bond stress was typically observed near failure. The cutoff reinforcing steel bars in the NSM strengthened specimen exhibited reasonably similar bond stress values compared to those found in literature. With increased stirrups and the addition of NSM reinforcement, the transition from initial to maximum bond stress was delayed until larger loads were achieved. Without the NSM reinforcement all the specimens would have failed in diagonal-tension due to anchorage failure of the cutoff reinforcing steel bar and the high bond stresses in the region.

The hook ductility tests of the titanium alloy bars showed that fractures originated at the inside bend of the tight radius hooks used in the present study. The fractures occurred due to sharpening of the surface deformations that formed from the bending process. The fractures occurred after the material reached the plastic limit. Removal of the surface deformations within the hooks allowed the titanium bars to carry much larger loads and have higher ductility.

## 6.2 CONCLUSIONS FROM ANALYTICAL METHODS

Analytical predictions were conducted using R2K as well as the ACI and AASHTO design specifications. To predict the failure mode and location in the specimens, several locations along the span were analyzed to identify the critical section. Key locations at which analyses were conducted included midspan, $d_v$ away from the loading point, and at the end of the cutoff bar. At each section, the diagonal-tension, moment, and flexural tension forces were evaluated.

The specimen strengths were well predicted using available analysis methods that assumed the NSM materials achieved yield stress. To predict the member strength required consideration of the three alternative failure modes: flexure, diagonal-tension, or flexural tension capacity. The AASHTO, ACI, and R2K predicted flexural tension demands were in reasonable agreement with those measured experimentally, particularly at the preformed diagonal crack location. Flexural or diagonal-tension failures were well predicted for the specimens using R2K assuming fully anchored NSM bars except for specimen IT.45.Ld3(6).Ti, which exhibited a partial anchorage failure on one of the deck flanges. The ACI and AASHTO predicted strengths were conservative for all specimens. The NSM strengthened specimens ameliorated or eliminated the flexural tension anchorage deficiency when compared to the design specification strengths (either flexure or diagonal-tension). For all specimens, the NSM bars where able to shift failures to those conservatively predicted as flexural capacity or diagonal-tension capacity using AASHTO or ACI design specifications. Only specimen, IT.45.Ld3(10).Ti exhibited a partial anchorage failure which limited the member capacity, nonetheless it was 10 % above the AASHTO predicted nominal strength.

ACI 440 design guidelines provided an approach for design with metallic NSM. Limiting the strain to the debonding strain for CFRP still allows the yield strength of the titanium alloy and stainless steel NSM materials to be achieved. The groove details and spacing prescribed in ACI 440 were consistent with those used in this experimental program. All specimens were able to achieve the nominal strengths computed by either the AASHTO-LRFD or ACI specifications (for the controlling failure mode of diagonal tension or flexural) for the cross sections with the NSM metallic bars assuming they could achieve yield strength.

## 6.3 RECOMMENDATIONS

The location of existing diagonal cracks was not a definite indicator of the final failure location. Bridge inspectors must look for the presence of chevron cracking around probable cutoff locations and along their development lengths. For negative moment regions, special attention should be directed to visible cracking on the underside of the deck because these cracks develop near the failure. When cracking of this type is observed, the bridge should be evaluated for load posted or strengthened based on the limited reserve capacity and ductility. For negative moment regions, NSM materials should also be placed in the stem as well as in the flange to prevent splitting failure of the relatively thin deck from adversely impacting the NSM bond.

After installation of NSM reinforcing bars for strengthening, during future inspections, bridge inspectors should look for small and distributed cracks at the epoxy-concrete interface along the grooves that may indicate slip of the internal reinforcing steel. Longitudinal cracking of the epoxy along the NSM may indicate near failure conditions.

Titanium alloy bars and stainless steel reinforcing bars provide high strength, ductility, environmental durability, and ability to fabricate mechanical anchorages, which make them suitable for NSM strengthening applications. Based on the experimental results, both titanium alloy bars and stainless steel reinforcing bars were effective for NSM strengthening. The overall member performances were similar and the use of one material over the other may be dictated by project costs or other constraints. Use of titanium alloy bars required approximately half as many bars to achieve the same capacity and ductility as stainless steel strengthened specimen. While the material cost of titanium alloy bars may be greater than stainless steel reinforcing bars, lower construction costs related to concrete cutting, epoxy, and fabrication contribute to the overall lower cost of a titanium NSM strengthening approach. Ultimately, use of NSM titanium alloy bars or stainless steel reinforcing bars could help maintain and improve the operational safety and mobility of the transportation system.

## 6.4 FUTURE RESEARCH

To supplement the research conducted and reported in this report, the following areas are suggested for future work:

- More fully characterize the straight and hooked bond lengths of NSM titanium alloy and stainless steel reinforcing bars.
- Investigate high-cycle fatigue performance of NSM titanium alloy and stainless steel reinforcing bars and the epoxy bond surface to these bars under repeated loading.

- Investigate the potential to use unbonded titanium alloy bars which would eliminate the need for cutting concrete grooves and filling them with epoxy.

- Assess the environmental durability of NSM titanium alloy and stainless steel reinforcing bars bonded in epoxy filled concrete grooves on the surface of a concrete section.

- Investigate alternative bend radii of the hooked details for NSM bars to optimize the hook performance and minimize concrete surface preparations.

- Investigate NSM strengthening of vintage RCDGs exhibiting concrete and reinforcing steel deterioration.

# 7.0 REFERENCES


Abrishami, H., and D. Mitchell. Analysis of Bond Stress Distributions in Pullout Specimens. *Journal of Structural Engineering*, Vol. 122, No. 3, 1996, pp. 255-261.

Al-Mahmoud, F., A. Castel, R. Francois, and C. Tourneur. Anchorage and Tension-Stiffening Effect between Near-Surface-Mounted CFRP. *Cement and Concrete Composites*, Vol. 33, 2011, pp. 346-352.

Al-Mahmoud, F., A. Castel, R. Francois, and C. Tourneur. Strengthening of RC Members with Near-Surface Mounted CFRP Rods. *Composite Structures*, Vol. 91, No. 2, 2009, pp. 138-147. Elsevier. http://www.sciencedirect.com/science/journal/02638223/91/2 Accessed August 1, 2013.

American Association of State Highway Officials (AASHO). *Standard Specifications for Highway Bridges*, 6th Edition, AASHO, Washington, D.C., 1953.

American Association of State Highway Officials (AASHO). *Standard Specifications for Highway Bridges*, 11th Edition, AASHO, Washington, D.C., 1973.

American Association of State Highway and Transportation Officials (AASHTO). *AASHTO LRFD Bridge Design Specifications*, 6th edition with 2013 interims, AASHTO, Washington, D.C., 2012.

American Concrete Institute. *Building Code Requirements for Reinforced Concrete.* ACI Manual of Concrete Practice, Detroit, MI. ACI 318-56,1956.

American Concrete Institute. *Guide for the Design and Construction for Externally Bonded FRP Systems for Strengthening Concrete Structures.* ACI Manual of Concrete Practice, Farmington Hills, MI. ACI 440.2R-08, 2008.

American Concrete Institute. *Building Code Requirements for Structural Concrete* (and Commentary). ACI Manual of Concrete Practice, Farmington Hills, MI, ACI 318-11, 2011.

ASTM A305-50T. Tentative Specifications for Minimum Requirements for the Deformations of Deformed Steel Bars for Concrete Reinforcement. *ASTM International*. 1950.

ASTM A615/A615M-14. Standard Specification for Deformed and Plain Carbon-Steel Bars for Concrete Reinforcement. *ASTM International*, West Conshohocken, PA, 2014.

ASTM B348/B348M-13. Standard Specification for Titanium and Titanium Alloy Bars and Billets. *ASTM International*, West Conshohocken, PA, 2013.

ASTM C39/C39M-13a. Standard Test Method for Compressive Strength of Cylindrical Concrete Specimens. *ASTM International*, West Conshohocken, PA, 2013.

ASTM C496/C496M-11. Standard Test Method for Splitting Tensile Strength of Cylindrical Concrete Specimens. *ASTM International*, West Conshohocken, PA, 2011.

ASTM E8/E8M-13a. Standard Test Methods for Tension Testing of Metallic Materials. *ASTM International*, West Conshohocken, PA, 2013.

Bentz, E. *Response-2000 Reinforced Concrete Sectional Analysis using the Modified Compression Field Theory*. [Computer software]. University of Toronto, Version 1.0.5, Toronto. 2000.

Bournas, D.A., and T.C. Triantafillou. Flexural Strengthening of Reinforced Concrete Columns with Near-Surface-Mounted FRP or Stainless Steel. *American Concrete Institute Structural Journal*, Vol. 106, No. 4, 2009, pp. 495-505

Carpenter Technology Corporation. *Enduramet 32 Stainless Steel* [Material Data Sheet]. 2006. http://www.stainlessrebar.com/docs/CarpenterEnduramet32.PDF. Accessed August 1, 2013.

Castro, H., C. Rodriguez, F.J. Belzunce, and A.F. Canteli. Mechanical Properties and Corrosion Behavior of Stainless Steel Reinforcing Bars. *Journal of Materials Processing Technology*, Vol. 143, No. 144, 2003, pp. 134-137.

Clark, A.P. Bond of Concrete Reinforcing Bars. *Journal of the American Concrete Institute Proceedings*, Vol. 21, No. 3, 1949, pp. 161-84.

Darwin, D. Tension Development Length and Lap Splice Design for Reinforced Concrete Members. *Progress in Structural Engineering and Materials*, Vol. 7, No. 4, 2005, pp. 210-225.

Dawson, M. *Scale Effects on Reinforced Concrete Beams Strengthened for Shear with Discrete Externally Bonded Carbon Fiber-Reinforced Polymer U-Wraps*. Masters Thesis, Oregon State University, Corvallis, OR. 2008.

De Lorenzis, L., A. Nanni, and A. La Tegola. Strengthening of Reinforced Concrete Structures with Near Surface Mounted FRP Rods. International Meeting on Composite Materials Proceedings PLAST: 1-8. 2000.

De Lorenzis, L., and A. Nanni. *Proposed Design Procedure of NSM FRP Reinforcement for Flexural and Shear Strengthening of RC Beams*. Technical Report Bulletin 14: Externally Bonded FRP Reinforcement for RC Structures, 2001, pp. 1-11.

De Lorenzis, L. Anchorage Length of Near-Surface Mounted Fiber-Reinforced Polymer Rods for Concrete Strengthening- Analytical Modeling. *American Concrete Institute Structural Journal*, Vol. 101, No. 3, 2004, pp. 375-386.

De Lorenzis, L., A. Rizzo, and A. La Tegola. A Modified Pull-out Test for Bond of Near-surface Mounted FRP Rods in Concrete. *Composites Part B: Engineering*, Vol. 33, No. 8, 2002, pp. 589-603. Elsevier. http://www.sciencedirect.com/science/article/pii/S1359836802000525. Accessed August 7, 2013.

Doerr, K. *Bond Behavior of Ribbed Reinforcement under Transversal Pressure.* Nonlinear Behavior of Reinforced Concrete Spatial Structures, 1978, pp. 13-24.

Erlin, B. *Embedded Metals and Materials Other than Reinforcing Steel*. Significance of Tests and Properties of Concrete and Concrete-Making Materials STP 169D: 2006, pp. 174-183.

Ferguson, P.M. and J.E. Breen. Lapped Splices for High Strength Reinforcing Bars. *Journal of the American Concrete Institute*, Vol. 62, No. 9, 1965, pp. 1063-1078.

Goodall, J. *Influence of Diagonal Cracks on Negative Moment Flexural Anchorage Performance in Reinforced Concrete Bridge Girders.* Master's Thesis, Oregon State University, Corvallis, OR, 2010.

Google Maps. *Mosier Bridge, Mosier, Oregon* [Street View]. 2014.

Harajli, M.H. Comparison of Bond Strength of Steel Bars in Nominal- and High-Strength Concrete. *Journal of Materials in Civil Engineering*, Vol. 16, No. 4, 2004, pp. 365-374.

Hassan, T., and S. Rizkalla. Investigation of Bond in Concrete Structures Strengthened with Near Surface Mounted Carbon Fiber Reinforced Polymer Strips. *Journal of Composites for Construction*, Vol. 7, No. 3, 2003, pp. 248-257.

Hassan, T., and S. Rizkalla. Bond Mechanism of Near-Surface-Mounted Fiber-Reinforced Polymer Bars for Flexural Strengthening of Concrete Structures. *ACI Structural Journal*, Vol. 101, No. 6, 2004, pp. 830-839.

Higgins, C., T.H. Miller, D.V. Rosowsky, S.C. Yim, T. Potisuk, T.K. Daniels, B.S. Nicolas, M.J. Robelo, A0Y. Lee, and R.W. Forrest. *Assessment Methodology for Diagonally Cracked Reinforced Concrete Deck Girders.* Publication FHWA-OR-RD-05-04. Oregon Department of Transportation and Federal Highway Administration. 2004.

Jeppsson, J., and S. Thelandersson. Behavior of Rinforced Concrete Beams with Loss of Bond at Longitudinal Reinforcement. *Journal of Structural Engineering*, Vol. 129, No. 10, 2003, pp. 1376-1383.

Losberg, A., and P. Olsson. Bond Failure of Deformed Reinforcing Bars Based on the Longitudinal Splitting Effect of Bars. *ACI Journal*, Vol. 76, No. 1, 1979, pp. 5-18.

Lutz, L., and P. Gergely. Mechanics of Bond and Slip of Deformed Bars in Concrete. *ACI Journal*, Vol. 64, No. 11, 1967, pp. 711-721.

Mains, R.M. Measurement of the Distribution of Tensile and Bond Stresses Along Reinforcing Bars. *ACI Journal*, Vol. 23, No 3, 1951, pp. 225-252.

Malvar, L.J. Bond of Reinforcement Under Controlled Confinement. *ACI Materials Journal*, Vol. 89, No. 6, 1992, pp. 593-601.

McLean, D.I., and C.L. Smith. *Noncontact Lap Splices in Bridge Column-Shaft Connections*. Research Report WA-RD 417.1, Washington State Department of Transportation. 1997, pp. 1-44.

Mylrea, T.D. Bond and Anchorage. *Journal of the American Concrete Institute*, Vol. 19, No. 7, 1948, pp. 521-552.

Novidis, D.G., and S.J. Pantazopoulou. Bond tests of Short NSM-FRP and Steel Bar Anchorages. *ASCE Journal of Composites for Construction*, Vol. 12, No. 3, 2008, pp.323-331.

Orangun, C.O., J.E. Breen, and J.O. Jirsa. A Reevaluation of Test Data on Development Length and Splices. *Journal of the American Concrete Institute Proceedings*, Vol. 74, No. 3, 1977, pp. 114-122.

Oregon Department of Transportation. Digital Photograph. 2013.

Oregon Department of Transportation. Type, Size, and Location Narrative, I-84: Mosier WB Connection Bridge. by Devin Connell. Oregon Department of Transportation, Salem, OR. 2013.

Rasheed, H., R. Harrison, R. Peterman, and T. Alkhrdaji. Ductile Strengthening using Externally Bonded and Near Surface Mounted Composite Systems. *Composite Structures*, Vol. 92, No. 10, 2010, pp. 2379-2390.

Reynolds, G.G., and A.W. Beeby. Bond Strength of Deformed Bars. Bond in Concrete: Proceedings of and International Conference, Applied Science Publishers, London, 1982, pp. 434-445.

Rizkalla, S., T. Hassan, and N. Hassan. Design Recommendations for the Use of FRP for Reinforcement and Strengthening of Concrete Structures. *Progress in Structural Engineering and Materials*, Vol. 5, No. 1, 2003, pp. 16-28.

Soroushian, P., K. Choi, G. Park, and F. Aslani. Bond of Deformed Bars to Concrete: Effects of Confinement and Strength of Concrete. *ACI Materials Journal*, Vol. 99 No. 3, 1991, pp. 227-232.

Triska, M.A. *Flexural Steel Anchorage Performance at Diagonal Crack Locations*. Masters Thesis, Oregon State University, Corvallis, OR. 2010.